Theresa Egger, BSc

Design and Implementation of an Optical Communication System between Time-of-Flight Cameras and Embedded Devices

MASTER'S THESIS

to achieve the university degree of

Diplom-Ingenieurin

Master's degree programme: Telematics

submitted to

Graz University of Technology

Supervisor

Ass.Prof. Dipl.-Ing. Dr.techn. Christian Steger

Institute for Technical Informatics (ITI)

Advisor: Ass.Prof. Dipl.-Ing. Dr.techn. Christian Steger
Hannes Plank, MSc (Infineon Technologies Austria AG)

Graz, November 2017

Affidavit

I declare that I have authored this thesis independently, that I have not used other than the declared sources/resources, and that I have explicitly indicated all material which has been quoted either literally or by content from the sources used. The text document uploaded to TUGRAZonline is identical to the present masters thesis.

Date	Signature

Abstract

In recent years, wireless connectivity has become omnipresent and has led to the emergence of the Internet-of-Things (IoT). IoT describes the interconnectivity of various physical devices to exchange data. The most common channel for this type of short-range communication is Radio-Frequency (RF). An increasing number of applications require location-awareness for their devices or desire to at least determine the relative position between communication partners. RF based solutions however show certain deficits. Due to the high density of RF signals coming from various devices such as smart phones etc., interferences and reflections may not just infect the communication channel but severely impair accurate localization.

This thesis presents a novel communication system based on Time-of-Flight technology. An advantage of optical communication with a Time-of-Flight camera is that each pixel is capable of conducting distance measurements and demodulating optical communication signals. When combining such depth measurements with optical communication, it is possible to determine the position of the communication partner in 3D. As the work of Plank et al. shows, this principle can be used to mitigate relay attacks. Another attractive application is indoor positioning, where distance information and a communication possibility are necessary at the same time. For these applications, an optical transceiver is required, enabling a variety of embedded systems to exchange data with a Time-of-Flight camera. Since the optical sending unit of this transceiver allows ToF sensors to detect and localize the device, it can serve as Optical Beacon for the ToF sensors.

The goal of this thesis is to design, implement and proof the feasibility of a bidirectional communication link between Time-of-Flight cameras and such Optical Beacons. This includes the hardware and software design of the Optical Beacon from scratch. The work on the Time-of-Flight communication system accomplished in the OptiSec3D project of Plank et al. is extended to make the ToF camera capable of exchanging data with Optical Beacons.

As the final evaluation shows, a Time-of-Flight sensor is capable of receiving data from the Optical Beacon with a data rate of 6 kbit/s. Since the main purpose of the future location-aware communication link is to localize and identify communication partners, this data rate is more than sufficient for these future purposes. Furthermore, the evaluation shows that it is possible to let ToF sensors transmit data to the Optical Beacon with a rate of 13 kbit/s.

Kurzfassung

In den letzten Jahren wurde die Technologie drahtloser Verbindungen allgegenwärtig und hat zur Entstehung von Internet-of-Things (IoT) geführt. IoT beschreibt die Zusammenschaltung verschiedener physikalischer Geräte um untereinander Daten auszutauschen. Der häufigst verwendete Kanal für diese Art der Kurzstreckenübertragung ist die Hochfrequenz (HF). Immer mehr Anwendungen fordern heutzutage eine Standorterkennung für ihre Geräte, oder möchten zumindest die relative Position zwischen den Kommunikationspartnern bestimmen. HF-basierte Lösungen zeigen hierbei gewisse Probleme. Aufgrund der großen Menge an Geräten, die im hochfrequenten Spektrum arbeiten und kommunizieren, kommt es zu einer sehr hohen Signaldichte in diesem Frequenzbereich. Dadurch können Interferenzen und Überlagerungen auftreten, die sowohl das zur Kommunikation, als auch das zur Datenübertragung verwendete Signal beeinflussen.

Diese Arbeit präsentiert ein neues Kommunikationssystem, das auf Time-of-Flight Technologie beruht. Die Verwendung einer Time-of-Flight Kamera für dieses System bringt den Vorteil, dass der Bildsensor Tiefenwerte für die gemessene Umgebung liefert. Wenn man diese Tiefendaten mit optischer Kommunikation kombiniert, ist es möglich, die Position der Kommunikationspartner in 3D zu bestimmen. Wie die Arbeit von Plank et al. zeigt, können dadurch Relay Attacken abgeschwächt werden. Eine weitere interessante Anwendungsmöglichkeit ist eine Indoor-Positionsbestimmung, wobei Tiefeninformationen und eine Kommunikationsmöglichkeit zur selben Zeit benötigt werden. Für diese Applikationen wird ein optischer Transceiver benötigt, der es einer Vielzahl von eingebetteten Systemen erlauben sollte, Daten mit der Time-of-Flight Kamera auszutauschen. Dieser Transceiver wird in dieser Arbeit als Optical Beacon bezeichnet.

Das Ziel dieser Arbeit sind das Design, die Implementierung und der Beweis der Machbarkeit einer bidirektionalen Kommunikation zwischen Time-of-Flight Kameras und solch Optical Beacons. Dies inkludiert die Hardware- und Softwareentwicklung des Optical Beacons, die von Grund auf durchgeführt wird. Die grundlegende Arbeit des OptiSec3D Projekts von Plank et al. zu Time-of-Flight Kommunikation wird erweitert, um der Kamera Datenaustausch mit Optical Beacons zu ermöglichen.

Wie die Endresultate zeigen, wird eine Datenrate von 6 kbit/s in die Kommunikationsrichtung vom Optical Beacon zur Time-of-Flight Kamera erreicht. Da der Hauptzweck der künftigen, positionsbewussten Kommunikation die Lokalisierung und Identifizierung des Kommunikationspartners ist, ist diese Datenrate für diese Zwecke mehr als ausreichend. Weiters zeigen die Ergebnisse, dass es möglich ist, ToF Sensoren Daten mit 13 kbit/s zu Optical Beacons übertragen zu lassen.

Danksagung

Diese Masterarbeit wurde am Institut für Technische Informatik an der Technischen Universität Graz durchgeführt. Der praktische Teil der Arbeit wurde bei Infineon Technologies Austria AG in Graz entwickelt. Zu allererst möchte ich mich bei all jenen bedanken, die am Entwicklungsprozess dieser Arbeit beteiligt waren.

Ich möchte mich für die Bemühungen und die Unterstützung meines Betreuers Ass.Prof. Dipl.-Ing. Dr.techn. Christian Steger bedanken. Durch seine Beteiligung in Form von hilfreichen Anmerkungen und Richtungsweisungen konnte die Qualität der Arbeit erheblich verbessert werden. Weiters bin ich dankbar für die Unterstützung und Hilfe meines Betreuers MSc. Hannes Plank bei Infineon Technologies. Durch ihn habe ich die Möglichkeit erhalten, eine Masterarbeit in der Thematik Optischer Kommunikation mit Time-of-Flight Technologie durchzuführen. Dank seiner Unterstützung konnte ich die Arbeit zu einem erfolgreichen Abschluss führen.

Weiters möchte ich meinen Freunden und Studienkollegen danken, die mich im Laufe meines Studiums begleitet, ermutigt und unterstützt haben. Die gemeinsam verbrachte Zeit war nicht nur harmonisch, sondern hat mich um neue und intensive Freundschaften bereichert. Besonderer Dank gilt hierbei meinem Freund Sebi, der mich immer ermutigt hat, an mich selbst zu glauben und durch den meine Studienzeit zu einem nicht missen wollenden Lebensabschnitt wurde.

Schließlich möchte ich noch einen großen Dank an meine Familie aussprechen, besonders an meine Eltern, deren emotionale und finanzielle Unterstützung mein Studium erst ermöglicht haben. Dank ihrer Geduld, aufbauenden Worte und vieler Wander- und Kletterausflüge, die für den nötigen Ausgleich und mentale Ausgewogennheit sorgten, konnte ich mein Studium mit großem Erfolg abschließen. Vielen Dank.

Graz, November 2017 Theresa Egger

Contents

Acronyms

ADC . . . . . Analog-to-Digital Converter

APD . . . . . Avalanche Photo Diode

ASF . . . . . Atmel Software Framework

BER . . . . . Bit Error Ratio

CCD . . . . . Charge Coupled Device

DAC . . . . . Digital-to-Analog Converter

DPPM . . . . . Differential Pulse Position Modulation

FDM . . . . . Frequency Division Multiplexing

FPGA . . . . . Field Programmable Gate Array

GPIO . . . . . General Purpose Input/Output

GPS . . . . . Global Positioning System

I^2C . . . . . Inter Integrated Circuit

IoT . . . . . Internet-of-Things

IR . . . . . Infrared

LiFi . . . . . Light Fidelity

MIMO . . . . . Multiple-Input Multiple-Output

MSM . . . . . Multiple-subcarrier Modulation

OCC . . . . . Optical Camera Communication

OCI . . . . . Optical Communication Image Sensor

OOK . . . . . On-off Keying

OWC . . . . . Optical Wireless Communication

PCB . . . . . Printed Circuit Board

PID . . . . . Proportional-Integral-Derivative

PLQPSK . . . . . Quadrature Phase Shift Keying of Pulsed Light

PMD . . . . . Photonic Mixer Device

PMT . . . . . Photo-Multiplier Tube

PPM . . . . . Pulse Position Modulation

PSK . . . . . Phase Shift Keying

QPSK . . . . . Quadature Phase Shift Keying

RF . . . . . Radio Frequency

RFID . . . . . Radio-Frequency Identification

RSS . . . . . Received Signal Strength

RTC . . . . . Real Time Counter

SoC . . . . . System-on-Chip

SPI . . . . . Serial Peripheral Interface

TDM . . . . . Time Division Multiplexing

TDOA . . . . . Time Difference of Arrival

TOA . . . . . Time of Arrival

ToF . . . . . Time-of-Flight

UART . . . . . Universal Asynchronous Receiver Transmitter

UFSOOK . . . . . Undersampled Frequency Shift OOK

UV . . . . . Ultraviolet

V2V . . . . . Vehicle-to-Vehicle

VLC . . . . . Visible Light Communication

WDM . . . . . Wavelength Division Multiplexing

List of Figures

List of Tables

Chapter 1

Introduction

1.1 Motivation

In the last years, the interest in the Internet-of-Things (IoT) has increased enormously. IoT is an expression for the interconnectivity of various physical devices such as embedded devices, sensors, actuators, etc. to collect and exchange information. The area of application ranges from smart home systems through to industrial control to remote health monitoring. Most common technologies which enable IoT for short range are based on radio-frequency (RF) such as BlueTooth or Radio-Frequency Identification (RFID). In this thesis, infrared pulsed light emitted by the illumination unit of a Time of Flight (ToF) camera is considered as a communication channel. In order to enable *things* to communicate with a ToF camera, a simple embedded system, called *Optical Beacon*, is proposed allowing a communication via infrared light to the ToF camera. It should be cheap and simple, so that *things* can be equipped with this Optical Beacon. Thus, a new kind of IoT system based on optical camera communication with ToF cameras is established. In combination with the depth measurement capability of ToF sensors, the communication system allows location-awareness for future applications.

In regard to the fact that the bandwidth of radio frequency is nearly pushed to its limits, other spectra as ultraviolet (UV), infrared (IR) and visible light have gained an increasing interest to replace RF for short-range communication. These frequency ranges bring some important advantages over RF. First, these spectra have a wide bandwidth that is license-free. Moreover, they offer the benefit that they do not interfere with other RF signals since they are placed in another frequency range. This implies that no disturbances to other electrical devices will occur. Beside this, decreasing interferences will improve the signal quality. Since IR, UV and visible light cannot penetrate opaque objects like walls, this effect causes a further decrease in interferences, and additionally raises interesting security aspects.

A common application for IoT is beacon-based indoor positioning. While GPS offers a solid-state solution for outdoor positioning, hence delivering applications such as localization, navigation and tracking, it is impractical for indoor environments as a line-of-sight to several satellites is required. With beacon-based positioning, several beacons are placed

inside a room or building. These beacons send signals via Bluetooth to mobile devices which can estimate their position according to the received signals. Since some mobile devices such as *Google Tango* [1] are already equipped with a ToF camera, the possibility arises to replace the RF beacon based indoor positioning system with the proposed optical camera communication system based on infrared light.

Another wider field of application that arises with this kind of optical camera communication is augmented reality. In recent years, the use of a mobile device that has become more and more requested is one that obtains and illustrates information about its environment. One example of this is a customer walking through a supermarket with his/her smart phone being held by hand. The display shows the real environment via camera app while the integrated ToF camera communicates optically with different products in the shelves tagged with an Optical Beacon. Meanwhile, the mobile phone checks if these articles are on the shopping list. If yes, these items pop up virtually on the display and the location where they are found marked on the shelf. Hence, the customer is not only reminded of the desired article, its exact position is also marked on the display so that the customer is not required to search for it.

Another application example for an optical communication system based on augmented reality is in the field of smart homes. If all smart objects controlled via a smart device are equipped with an Optical Beacon, a user only has to point with his/her smart device including a ToF sensor to the object that should be controlled. As soon as the smart device has established an optical communication to this object, the control panel for this object can be displayed at the smart device. Now, the user can change settings for this object while the ToF sensor of the smart device communicates these changes to the smart object via optical channel.

In this thesis, a camera based communication system is proposed which can be used for applications like indoor positioning or augmented reality as supposed above. A Time of Flight (ToF) camera forms one communication partner and the counterpart is the Optical Beacon, a simple device that is able to communicate optically and process the exchanged data. Infrared light will serve as communication channel. The hardware and software for the Optical Beacon are implemented from scratch. It has to be capable of receiving the infrared pulsed light of the ToF camera, demodulate, decode it and process the received data. In this communication direction, Differential Pulse Position Modulation is used. In order to send data back to the ToF camera, the Optical Beacon has to generate an infrared light signal which can be received by the ToF camera. Therefore, information has to be encoded and modulated with Phase Shift Keying. On the other side of the optical communication channel, the software of the ToF camera has to be extended to make it capable of receiving and sending data. The principle of the complete communication system is illustrated in Figure 1.1. Finally, the system is evaluated and the data rate and bit error ratio are determined.

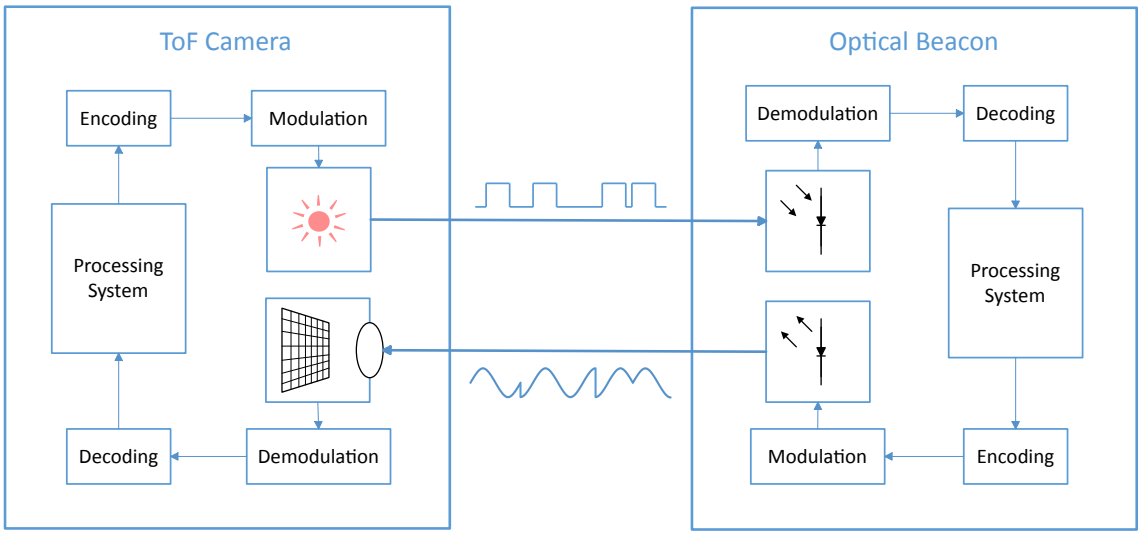

Figure 1.1: A camera based communication system with Time-of-Flight technology. The other communication partner is an Optical Beacon, a simple device which is capable of communicating with a ToF camera. It should be small and cheap in order to use it for various IoT applications.

1.2 Objectives

The focus of this thesis is the development of a communication system between a ToF camera and a simple device, called an *Optical Beacon*, which is able to exchange data optically with ToF cameras. This should build the foundation for various IoT based applications such as indoor positioning or augmented reality. The main goals for this work are:

- Development of the hardware for the Optical Beacon. It has to be capable of receiving the emitted signals of the ToF camera and sending back a phase modulated signal which is detectable for the Tof camera.
- Software implementation of the processing and controlling units of the Optical Beacon in order to allow a sending and receiving functionality.
- Software extension of the ToF camera to provide the ability of receiving data from and sending data to the Optical Beacon.
- Synchronization between ToF camera and Optical Beacon to allow bidirectional communication.
- Evaluation of the proposed communication system to prove its feasibility.

At the end of this project, an Optical Beacon should be developed that is able to communicate with a ToF camera and exchange information.

1.3 Outline

This thesis is structured as follows. First, Chapter 2 gives a general overview of current camera based communication systems. State-of-the-art solutions are presented along with open problems. Chapter 3 shows the design specifications of the system. This includes the hardware design for the Optical Beacon in conjunction with the corresponding software concept in order to allow demodulation and decoding functionality for the receiving part and encoding and modulation functionality for the sending part. On the side of the ToF camera, the necessary software extension is introduced so that it is capable of receiving and sending data. In Chapter 4, the development process as well as implementation details of the hardware and software development are addressed. The results and a performance analysis are presented in Chapter 5. Finally, a conclusion and future outlook are covered in Chapter 6.

Chapter 2

Related Work

In the beginning of this Chapter, Time-of-Flight technology is introduced. Then, since this thesis explores the foundation of an optical communication system comprised of ToF cameras and Optical Beacons, a study of related work in the fields of optical wireless communication and camera-based communication is provided. Advanced implementations are presented as well as issues associated with these state-of-the-art solutions. Furthermore, this Chapter provides insight on optical communication based indoor positioning, which is expected to be among the strongest applications of optical communication.

2.1 Time-of-Flight Principle

In this section, Time-of-Flight technology is introduced. ToF cameras are able to capture 3D images which means that each pixel contains depth information. The technology for getting depth values is based on measuring the time light takes to travel to the scene and back. An illumination unit exposes the scene. It emits pulsed light which is reflected by the scene and travels back to the camera. The time which passes between emission and arrival at the sensor is measured and knowing the propagation speed of light, a distance can be derived.

The state-of-the-art approach is based on continuous modulation. With continuous modulation, pulsed light with modulation frequency $\mathcal{F}_{mod}$ is emitted and the phase shift between the outgoing and incoming signals is measured. This working principle is described by the authors of [2] and illustrated in Figure 2.1.

Photonic Mixer Device

Each pixel of the ToF camera is equipped with a Photonic Mixer Device (PMD) [3]. A PMD consists of an illumination unit and a CMOS sensor which translates photons to electron-hole pairs in the substrate.

The illumination unit exposes the scene. When the reflected light reaches the sensor, the PMD acts as a switch and transfers the produced charges either into storage A or B.

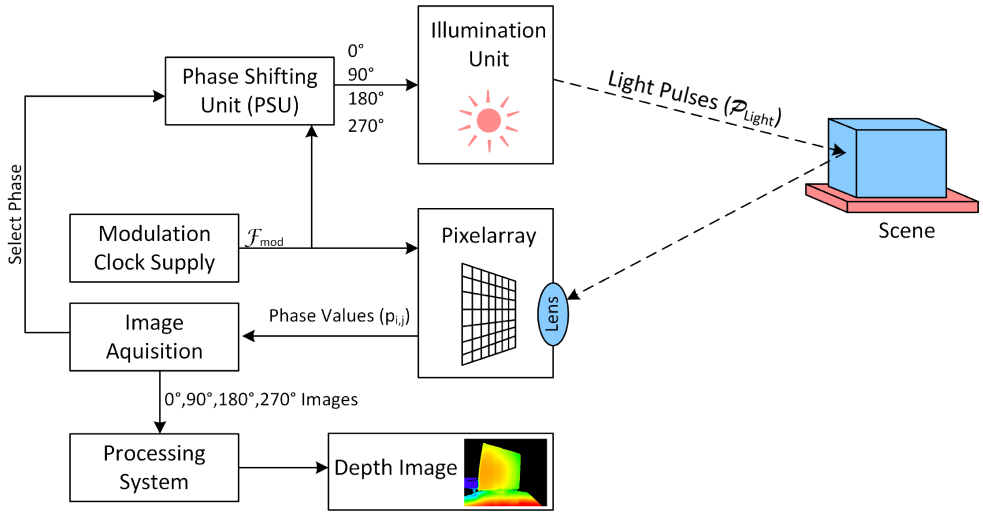

Figure 2.1: Working principle of a Time-of-Flight camera [2].

The decision depends on the logic level of the modulation signal $\mathcal{F}_{mod}$. After a certain period of time, the two storages are read out. The difference between their charges describes the correlation Q between emitted and received signal. For continuous modulation, typically four phase shifted signals (0°, 90°, 180°, 270°) are emitted. With their correlations Q_1, Q_2, Q_3 and Q_4, the phase difference $\Delta\varphi$ can be calculated [4]:

$$\Delta\varphi = arctan\left(\frac{Q_1 - Q_3}{Q_2 - Q_4}\right) \tag{2.1}$$

With $\Delta\varphi$, the speed of light c ($\approx 3 \cdot 10^8 \frac{m}{s}$) and the modulation signal $\mathcal{F}_{mod}$, the distance d to the reflecting object can be determined [4]:

$$d = \frac{c \cdot \Delta\varphi}{4\pi \cdot \mathcal{F}_{mod}} \tag{2.2}$$

2.2 Optical Wireless Communication

The beginning of optical wireless communication (OWC) dates back to ancient Greeks, Romans and Persians who used fire and smoke as visual signals for transmitting information over great distances. For example in 1084 B.C. Agamemnon, lord of Mycenae, installed a line of beacons over a distance of 500 km to spread the news about the fall of Troy [5]. During the French Revolution at the end of 18^{th} century Claude Chappe developed the semaphore line. Swivelling arms were fixed on high masts. Letters could be communicated depending on the position of the arms to each other. One century later, Alexander Graham Bell invented together with Sumner Tainter the Photophone, a device which is capable of transmitting voice using modulated light beams. A bendable mirror is used as transmitter which worked by speaking into its backside. The rays of light reflected by the mirror are captured by the receiver, consisting of a parabolic reflector with

a selenium cell in its focal point. With this setup Bell and Tainter were able to transmit voice over 213 m in 1880 [6].

The interest in the field of free space communication has increased enormously in recent years. Optical communication provides significant advantages over RF-based communication ranging from a high and reusable bandwidth to certain security aspects. In this section, current solutions for Optical Wireless Communication (OWC) are presented.

2.2.1 Electromagnetic Spectrum for OWC

Optical wireless systems for communication constitute an alternative to RF-based technology. Electromagnetic frequencies are used as communication channel ranging from infrared, through visible to ultraviolet light. The entire electromagnetic spectrum is illustrated in Figure 2.2. Compared to RF, the optical medium brings several advantages such as an unregulated large bandwidth, license-free operation and low-cost front-ends. As this thesis shows, with OWC interesting considerations regarding security and safety emerge.

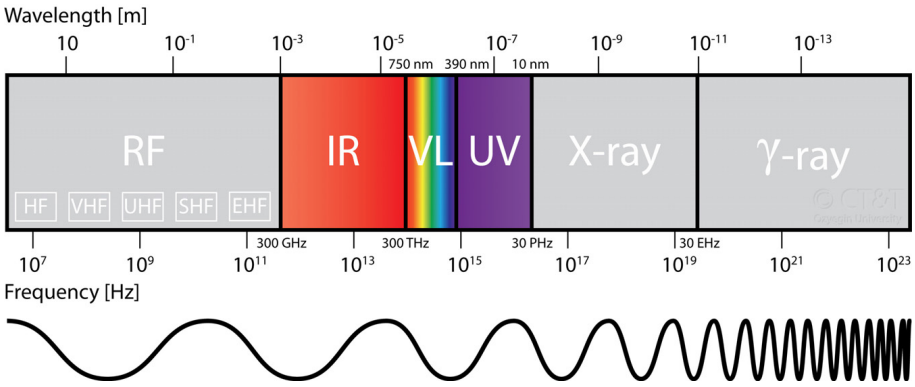

Figure 2.2: The electromagnetic spectrum from RF to γ-rays [7].

OWC in the Infrared Spectrum

In general, IR light operates with wavelengths ranging from 700 to 1000 nm. A suitable spectrum for the usage as communication medium ranges from 780 to 950 nm [8–11]. In this scope, LEDs, laser diodes and low-capacity photo diodes are available at low cost and show a favourable peak responsivity. A drawback of this band is that radiation below 1400 nm can pass through the human cornea and may cause damage to the eye. Therefore, the allowed transmission power for operations in the spectrum of 780 to 950 nm is limited by safety standards (IEC 60825-1 and IEC 62471) [12].

Kahn and Barry [10] provide a broad overview of the field of infrared communication. The authors present the advantages and drawbacks of the infrared medium over RF, present current solutions and cover common issues.

OWC in the Visible Light Spectrum

Visible Light Communication (VLC) is a field of research with increasing interest since it offers an alternative to RF-based WiFi. It provides advantages regarding energy and cost efficiency. Furthermore, since LEDs are increasingly used for illumination, there is no need for additional installation. LEDs which are serving as lighting can additionally be utilized for data transfer.

An application area of VLC is Light Fidelity (LiFi). This term was first introduced by Professor Harald Haas in 2011 [13] and describes the optical alternative to RF-based WiFi. Information is modulated into illumination by varying light intensity at a frequency high enough to be imperceptible to the human eye.

OWC in the Ultraviolet Spectrum

The UV spectrum as communication channel has become a highly investigated research topic [14]. Ultraviolet LEDs, UV filters and UV detectors are developed primarily for the spectrum of 200 to 280 nm, the so called deep UV band. This range is solar blind, meaning that solar radiation can be neglected as it is absorbed by ozone in the upper atmosphere. For receiving solar blind UV light, there exist photo multiplier tubes (PMTs) and avalanche photo diodes (APDs). At the moment, PMTs are heavy and fragile while APDs are expensive. Along with IR light, UV needs to be limited in transmission power to fulfill eye and skin safety requirements. These limitations are determined by the International Commission on Non- Ionizing Radiation Protection (ICNIRP) and the International Electrotechnical Commission (IEC) [14, 15].

2.2.2 Advantages of OWC

As mentioned before, OWC technology provides a couple of advantages over RF-based systems. The most important benefits are depicted in this section.

License Freedom and Large Bandwidth

One of the main advantages of OWC is the fact that there is no need for licensing for the optical channel. At the same time, a huge bandwidth is available over the entire spectrum of IR, UV and visible light. Regarding line-of-sight communications, the fact is added that the bandwidth becomes reusable. For example, if the communication is limited to a single room, the bandwidth can be reused in all other rooms of the building.

Radio-Frequency-Interference

Due to the fact that IR, UV and visible light are placed in another frequency range than RF, the advantage is obtained that the radiation emitted by OWC does not interfere with RF. Hence OWC will neither disturb nor be disturbed by electronic devices.

Security

Since electromagnetic waves in the spectrum between UV and IR cannot penetrate walls, an ambiguous property is obtained. It can be seen as an disadvantage in fields of non-line-of-sight communication that the signal is captured inside a room or building. Regarding line-of-sight transmission, this behavior serves as benefit. The local isolation offers immunity against eaves-dropping [10].

2.2.3 Common Modulation Techniques for OWC

This section depicts typical modulation techniques used for OWC, which can be categorized into single-carrier and multiple-subcarrier modulation.

Single-carrier Modulation

Single-carrier modulation means, that only one carrier is used for data transmission. In the fields of OWC, the carrier is an visible, infrared or ultraviolet light signal.

- **On-off Keying**
  On-off Keying (OOK) is the simplest form of amplitude modulation. Two states are distinguished depending on whether the signal is present (high) or absent (low) during a specified period of time. OOK is vulnerable to noise since amplitude modulation is known to be failure-prone [8].

- **Pulse Position Modulation**
  Pulse Position Modulation (PPM) is a modulation technique for time-discrete signals. A fixed period of time, referred to as cycle duration, is divided into 2^M time slots. A pulse is then shifted by a specific time inside this period. This principle is illustrated in Figure 2.3a.

  As Hou et al. [8] point out, PPM accomplishes a higher signal bandwidth and power efficiency compared to OOK. A major challenge for PPM is time synchronization between transmitter and receiver. Further problems occur with the presence of multi path interferences. If echoes are received, determining the correct pulse position becomes further complicated.

- **Differential Pulse Position Modulation**
  Differential Pulse Position Modulation (DPPM) is similar to PPM. But instead of shifting the constant pulse to different positions, the pause duration is varied. This is illustrated in Figure 2.3b. An advantage compared to PPM is that no synchronization is required. Moreover, Shiu et al. [16] show that DPPM achieves better performance regarding power- and bandwidth efficiency than PPM.

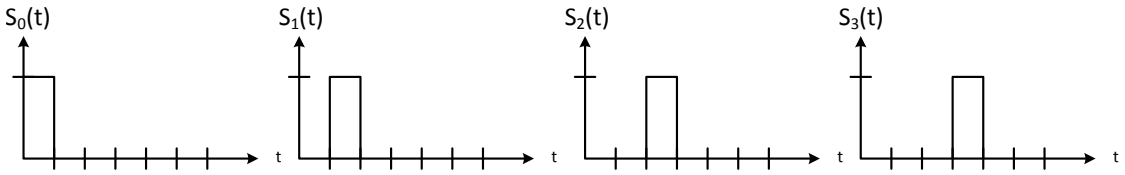

(a) 4-PPM. The pulse is shifted by one of four possible delays.

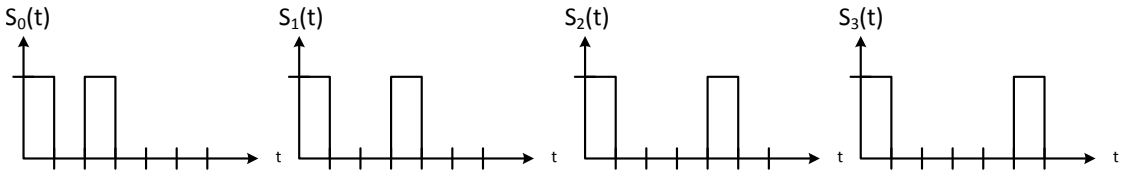

(b) 4-DPPM. Here the pause length between two pulses is varied, not the pulse position.

Figure 2.3: PPM and DPPM.

Multiple-subcarrier Modulation

In Multiple-subcarrier Modulation (MSM) systems, multiple bit streams are first modulated onto subcarriers at different frequencies. These signals are then added up and modulated onto the optical carrier, using phase, intensity or most commonly frequency modulation. According to Carruthers et al. [17], MSM allows communication at higher data rates and bandwidth efficiency than single-carrier modulation systems, whereas low power efficiency is a considerable drawback.

2.3 Optical Camera Communication

In the last years, the technological equipment of smart devices has improved enormously. Recent smart phones include a variety of sensors such as iris scanners, fingerprint sensors, barometers, etc. Beside different interfaces, sound and camera modules are among the ever-improving features of smart phones. This lead to a tremendous research effort on optical communication with smart phone cameras. In Optical Camera Communication (OCC), the image sensor can operate as receiver, while a display, embedded flashlight, WiFi or IR LED can be applied as transmitter. A big advantage of using smart phones for optical communication is that there is no need for extra hardware since the existing one can be completely reused.

An application example is to use cell phones for indoor navigation. A downlink could be established via VLC by a light source like a LED lamp that is already used for lighting. Information for indoor navigation is then sent by the visible light communication link, received by the camera and displayed to the user. The device's display can be additionally used to send back information for feedback like orientation via its display. This example is illustrated in Figure 2.4. In the following section, state-of-the-art solutions for OCC as well as associated problems are outlined.

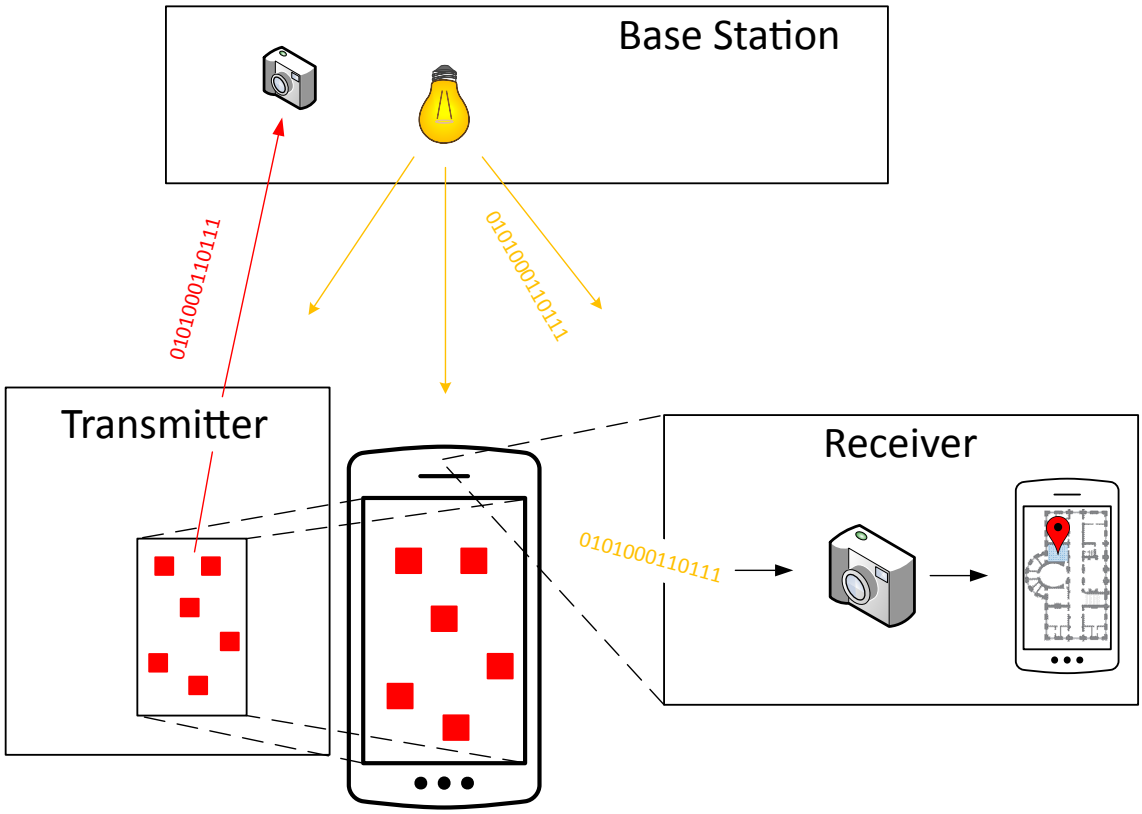

Figure 2.4: Example of OCC with a smart phone serving as receiver and transmitter for indoor navigation. The device's camera receives the modulated light beams of the LED lamp. After demodulation, the information can be presented on the display. Additionally, the display operates as a transmitter and emits modulated information back to the base station.

2.3.1 Receiver

Compared to OWC, where normally a non-imaging device like an APD or PIN photo diode operates as receiver, in OCC cameras are used for fetching modulated optical signals.

Optical Communication Image Sensor

The authors of [18] propose a vehicle-to-vehicle communication system which consists of a LED transmitter and a camera receiver. The camera receiver applies a special CMOS image sensor, the Optical Communication Image Sensor (OCI). This kind of sensor consists of an image pixel array IPx and a newly invented communication pixel array CPx. The image pixel array provides a gray scale image and a 1-bit image which is captured with an extremely short exposition time. Thus, an image is obtained which presents bright parts

as logical 1 and everything else as logical 0. With the combination of the gray scale image and the 1-bit image, the position of the light sources in the scene can be determined. When this positions are known, the communication pixels at these coordinates are activated and are used for optical communication. This system allows a high speed communication as well as a LED tracking of the transmitter. A data rate of 10 Mb/s is achieved.

RGB Camera

A camera consists of an image sensor, an image lens and a circuit to read out the exposed pixels. Light falls through the lens and is projected on the image sensor. Multiple photo diodes placed on the image sensor translate the incident light into a voltage that is proportional to the number of absorbed photons. Each pixel is connected to a circuit that converts the voltage generated by the pixel into a binary signal. Cameras are classified into two categories depending on the way they read out the pixel data, these are rolling shutter and global shutter cameras.

In the past, global Shutter cameras normally used a charge coupled device (CCD) as image sensor. For some time, also CMOS sensors are available with global shutter. Such sensors expose all pixels simultaneously per frame. This approach has the advantage that despite motion blur artifacts virtually do not occur. The ToF camera which is used for this thesis has a global shutter sensor.

Rolling shutter cameras expose their pixels sequentially in contrast to global shutter, either row-by-row or column-by-column. Each row or column is exposed per time unit. With this method motion artefacts occur when fast moving objects are photographed. Rolling Shutter cameras typically use CMOS image sensors. Their circuitry-wise realization is less complex than that of Global Shutter what implies lower costs. So far, Rolling Shutter cameras are primarily used in smart phones due to their smaller size and lower costs.

Cahyadi et al. [19] propose an OCC application with a dual camera working as receiver and a LCD display as transmitter. With this method they achieved a data rate of 11.52 bps within a distance of up to 2 m. A digital single-lens reflex camera was used in combination with a dual LED by Luo et al. [20]. Here a transmission rate of 500 bps was accomplished with a distance of maximally 1.5 m. This data rate might be high enough for localization-based information, but the distance shows potential for improvement.

Infrared Cameras

Bui and Kiravittaya [21] came up with the idea to use a surveillance camera as receiver while an IR LED operates as transmitter. Information is modulated onto the light intensity of the IR LED. This scenario is designed to offer a low-rate communication. With a frame rate of 90 fps a data rate of 45 bps was achieved. This kind of communication link was considered to build the uplink part of a communication system. Whereas a downlink is designed to transfer high data rates, an uplink is intended to transfer only short messages like an acknowledge or a download request. Hence it is sufficient to transmit data at lower rates. A potential setup can be seen in Figure 2.5.

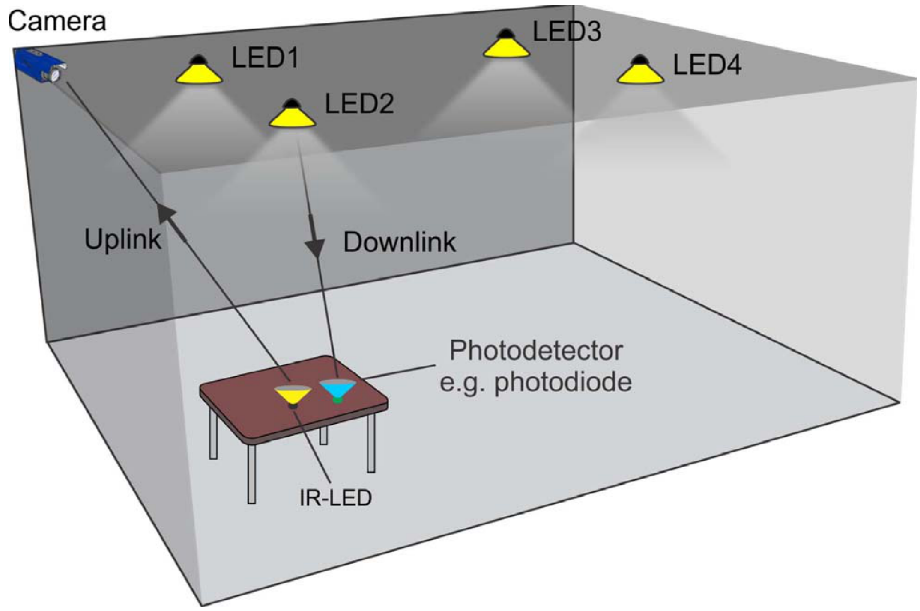

Figure 2.5: IR-based OCC system with surveillance camera as receiver and IR LED as transmitter [21].

Yuan et al. [22] presented another method for OCC with an IR-based camera. Unlike intensity-based modulation with an IR LED, this approach is based on the phase shift of reflected light using a Time-of-Flight camera. This approach is described in detail in Section 2.4.1.

2.3.2 Transmitter

In OCC, different light sources may serve as transmitter. This can be LEDs, laser diodes or displays. Danakis et al. [23] use a LED with OOK as modulation technique, whereas a 30 fps web cam is used as receiver. Nguyen et al. [24] propose a system where a LCD display is used as transmitter. Here multi colors encoding based on OOK is implemented. In 2014, another approach for display to camera communication is demonstrated by Fath et al. [25]. Instead of OOK, visual patterns are used for information coding.

2.3.3 Modulation Techniques

Since image sensors may deliver more information than single photo sensors as they are usually used for OWC, new considerations about modulation schemes arise. This section shows the most important modulation techniques for OCC.

OOK

When OOK is used in the fields of visible light communication, it has to be considered that the flickering of light should not be perceptible to the human eye. Therefore, a frequency

of at least 100 Hz is required. According to the theorem of Nyquist-Shannon, the sampling frequency of the camera has to be twice the frequency of the light source, thus at least 200 Hz have to be used. Hence, high speed cameras have to be used to fulfill these frequency requirement.

Undersampled Frequency Shift OOK

Undersampled Frequency Shift OOK (UFSOOK) is a variation of OOK in order to operate with non-highspeed cameras. When commercial cameras with a frame rate of about 30 fps are used, the frequency of the light source has to be half as high, that means 15 fps. With this frequency, the flickering of the light becomes perceptible to the human eye. In order to prevent this, the low base-band signal has to be shifted to a higher frequency. This technique was proposed by Roberts in 2013 [26].

Exploitation of Rolling Shutter Effect

As described in Section 2.3.1, CMOS cameras expose the scene row-by-row or column-by-column. This effect can be utilized to obtain a data rate that is higher than the camera's frame rate. Therefore, the light source operates at the frequency at which the columns/rows are exposed. The light source should either be on and produce a bright line in the image or off to result in a dark one, as it can be seen in Figure 2.6a. In this manner, an image of light and dark lines rises where each line represents a logical zero or one. Such a recorded image can be seen in Figure 2.6b. This technique was first proposed by Danakis et al. [23]. In a CMOS sensor, a row or column can be exposed for the next

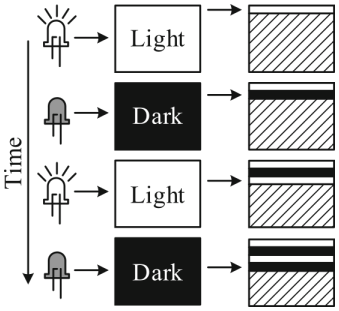

(a) The light source is on or off for the time interval in which a row or column is exposed.

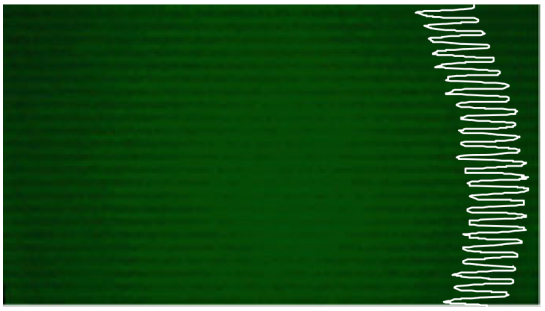

(b) A recorded image with a resolution of 1920 x 1080 pixels illuminated by a green LED; the white waveform shows the sum of pixel values per line.

Figure 2.6: Sample image of the exploitation of the roller shutter effect [27].

frame as soon as the read out of the row or column of the current frame has finished. Thus, the image acquisition of the next frame has not to wait until the acquisition of the current frame has ended. As a result, OCC systems with CMOS sensor-based cameras achieve higher data rates than its CCD counterparts. Thus, a sampling rate in the kHz range can be achieved as depicted by Cailean and Dimian [28]. Hence, even cameras with low frame rates will have no problems with perceptible flickering.

A drawback of this modulation technique is that the distance between LED and camera has to be close enough, so that the major part of a column or row is illuminated by the light source to classify it as bright or dark. Nguyen et al. [29] showed that a camera's frame rate is not fixed as assumed. In their experiment the frame rate varied between 20 and 35 fps instead of the specified 30 fps. This effect results in a mismatched synchronization between receiver and transmitter and leads to errors.

LCD-based Modulation

So far, modulation techniques for OCC based on switching a LED on and off were described. In contrast to these, there exist LCD- and digital signage based modulation schemes. These are denoted as low data rate methods because most commercial screens have a refresh rate of about 60 Hz. The most common known example for this visual modulation are QR codes. The LCD display serving as transmitter displays a QR code while the receiver consisting of a camera records this image. Then, an image processing algorithm can demodulate the signal to extract information.

An advantage of screen-to-camera modulation is that this method can benefit from the usage of Visual MIMO (Multiple-Input Multiple-Output). It is similar to RF MIMO, where multiple antennas for transmitting and receiving are used to improve the signal quality and hence increase the data rate. With respect to Visual MIMO, a pixel array respectively the screen serves as multiple output while the pixels of the image recorded by the camera act as multiple input. This scheme can be seen in Figure 2.7. This brings advantages on the one hand to achieve higher transmission distances and on the other hand, the data rate can be increased. Another benefit comes with the usage of different colors for modulation. In this manner, the data rate can be further increased. A drawback is that the camera operating as receiver must not move in order to avoid motion blur. Additionally, the distance between sender and receiver is limited with respect to the resolution. Single pixels need to be distinguishable. For example Yuan et al. [30] proposed a Visual MIMO system where the information is invisibly embedded in images.

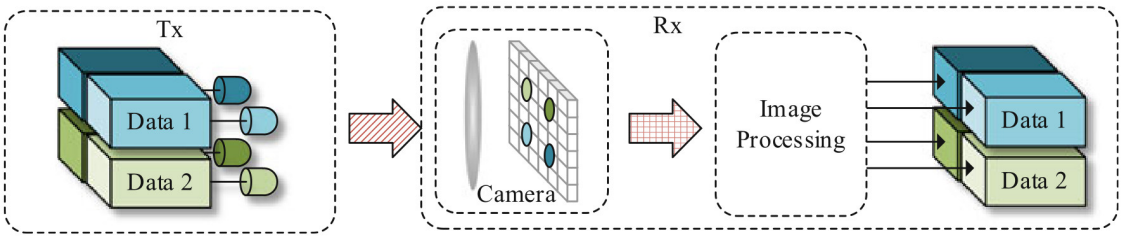

Figure 2.7: Visual MIMO in OCC system [27].

2.3.4 Applications

Vehicle-to-Vehicle Communication

One possible application for OCC is Vehicle-to-Vehicle (V2V) communication. This is becoming possible since an increasing number of vehicles is equipped with LED lamps as well as with front and rear cameras. This circumstance offers the opportunity to reuse this already installed hardware for a communication system between cars and other traffic participants. In this manner, safety messages, warnings and other traffic relevant information can be exchanged. This scheme can be seen in Figure 2.8. As outlined by Ghassemlooy et al. [27], V2V communication brings several advantages over RF-based technologies:

- The costs and complexity are low.
- The directional line-of-sight propagation of light beams allows positioning with high precision. Hence, the error can be significantly reduced compared to RF-based positioning.
- A high traffic density, as it occurs during the rush hour, causes a high number of RF signals and therewith associated interferences will lead to high packet loss and hence high delays. Since OCC is based on visual contact, communication only takes place between neighboring vehicles and thus results in lower interferences and a better signal quality.

Takai et al. [31] show the basics for a V2V communication based on LED transmitters and a high speed camera. They were able to achieve a data rate of 10 Mb/s. The authors of [28] outlined the current challenges (by 2017) regarding V2V communication with VLC. The main issues which have to be solved are to increase the robustness to noise, increase the data rate and also the communication range.

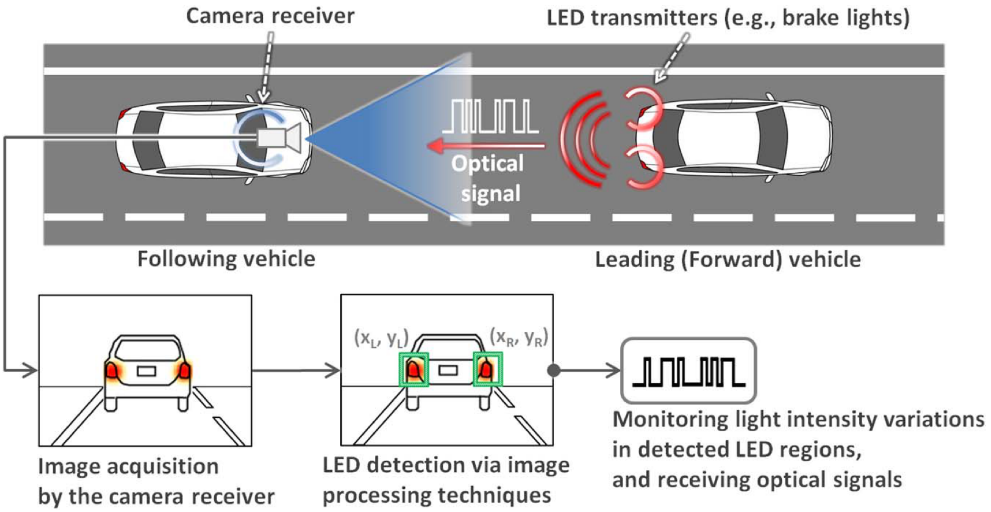

Figure 2.8: Vehicle-to-Vehicle communication with OCC [31].

Indoor Positioning

A promising application area for OCC is indoor positioning. LED lamps seem to suit best for serving as transmitting unit. They are the emerging choice for illumination since LEDs are energy efficient, highly reliable and have a long life-time. Additionally, they can be used to transmit information for localization that is modulated via light, more precisely via the frequency at which the LED switches between on and off. Now, a user may move through a building with a smart phone in his or her hands and the camera demodulates the information from the recorded images and offers a navigation on the display to the user. This topic will be discussed more precisely in Section 2.5.

2.3.5 Problems

Although OWC and OCC are highly investigated fields of research, there are still open issues that need further studies for improvement. The most important problems are outlined in the following section.

In the fields of Visible Light Communication it has to be considered that the switching between ON and OFF state of the light source will result in flickering at low frequencies. The switching frequency has to be higher than 100 Hz to become imperceptible to the human eye.

With respect to line-of-sight applications, there has to be always a visual contact between transmitter and receiver. With the usage of cameras as receivers, for example a smart phone's camera, it is presumably that the user who holds the device in his or her hands will move during the communication process. The movement may lead to motion artifacts and thus to transmission errors. When the link is lost there is the need for a recovering mechanisms.

Since OCC is basically an asynchronous communication system, there is the need for synchronization between transmitter and receiver for some modulation techniques. This can be a challenging task depending on the modulation technique and the used hardware.

The data rate is limited by the device's frame rate when cameras are used as receiving unit. In order to exceed this limitation, provided modulation techniques have to be used as UFSOOK or exploitation of the rolling shutter effect.

2.4 Communication Systems based on Time-of-Flight

2.4.1 First Phase Messaging System with Time-of-Flight Camera

In 2014, Yuan et al. [22] presented a method for OCC with a ToF camera. Unlike intensity-based modulation with an IR LED, this approach is based on the phase shift of reflected light. In this system, the IR LED serving as transmitter does not modulate information by varying the intensity but by manipulating the phase of the emitted light signals.

One of the main difficulties for a communication system based on a ToF camera is that the modulation frequency of the ToF sensor and the frequency of the sender which shifts the phases have to be exactly the same. If an extra oscillator is used for generating the modulation frequency on sender-side, the frequencies will differ due to constructional inequality between the oscillators of the sender and of the ToF sensor. The approach of Yuan et al. uses no extra oscillator. Instead, the light which is emitted by the ToF camera for exposition is captured by the sender with a photo detector, is amplified and then used as modulation signal. Thus, the frequency at sender-side is the same since it is a copy of the modulation frequency of the ToF camera.

The authors use four different phases which are used for light modulation. Hence, one LED can transmit two bits. In order to increase the data rate, they use nine LEDs instead of one LED. One of them is used to indicate that transmission is active while the other eight LEDs transmit data by selecting one of the four different phases. With this system, a data rate of 960 bps at 60 fps was achieved. This is called *Phase Messaging Array* by Yuan et al.

This communication method provides several advantages. First, compared to intensity-based modulation, reflections and ambient illumination do not degrade the signal. As Yuan et al. [22] point out, a benefit over RGB cameras is that ToF cameras are realized with global shutter technology. Hence, motion artifacts as they arise from the rolling shutter effect are negligible.

A drawback of this approach is that a high resolution is used in order to distinguish the nine different LEDs and this drops the data rate. Moreover, since Yuan et al. work with depth images, four raw images have to be captured in order to obtain one depth image. This is another factor which decreases the data rate. The system proposed in this thesis works with the smallest possible resolution. Hence, a data rate of 7000 bps is expected although only one LED is used. Furthermore, instead of working with depth images, this approach modulates data directly in raw images and hence the data rate is four times higher compared to working with depth images. Another limitation for the system of Yuan et al. results from the distance between sender and ToF camera. While the ToF camera could increase its exposition time in order to operate at high distances, the photo detector of the sender has to still be able to detect the continuous light emitted by the ToF camera. Otherwise, the sender can not recover the signal of the ToF camera and as a result has no modulation frequency to switch the LEDs on and off. For this thesis, an extra oscillator is used for the generation of the modulation frequency. An approach was found to combat the problem which arises from varying frequencies between ToF camera and sender which is explained in [22]. Thus, a communication link for mid-range distances can be established. Finally, Yuan et al. developed a unidirectional communication system. The sender can communicate to the ToF camera but not vice versa. This thesis implements a novel modulation technique on the one hand, and allows additionally a bidirectional communication system where the ToF camera can transmit data back to the sender.

2.4.2 OptiSec3D - Secure Communication

Plank et al. propose a communication system based on Time-of-Flight technology in order to realize a secure communication channel [32]. The work of these authors is the basis for this thesis. The communication system of this thesis should serve as an extension of the work by Plank et al.

The main idea of this system is to use additional information, such as distance, location information, etc., in order to establish a secure channel. This additional information can be obtained by the ToF camera with sensing its communication partner. In 2015, they published a survey paper [33], where the vulnerability of wireless RF-based communication systems is discussed. The OptiSec3D approach is further analyzed in this survey [32], regarding how the risk of relay attacks can be reduced with this ToF communication system. In [34], Plank et al. propose an algorithm, how the synchronization problem between sender and ToF camera can be tackled. This problem results from different modulation frequencies between sender and ToF camera, as it was first described by Yean et al. [22].

2.4.3 ToF Indoor Positioning with Reflective Markers

In 2017, Plank et al. [2] proposed a novel approach for an indoor positioning and pose estimation system based on Time-of-Flight imaging. This is a marker-based system, where the ToF camera measures distances and the incident angles of markers in its field-of-view and hence determines their 3D positions. In the next step, the detected markers can be matched with the pointcloud of a reference model and thus provide the orientation and position of the ToF camera. In order to simplify the identification of the visible markers, it is proposed to replace the passive markers by active beacons which communicate their ID over the optical channel to the ToF camera. The importance and impact of location-awareness for mobile devices is emphasized by the same authors [35]. Another paper of these authors [36] shows the applicability for ToF based communication in critical environments in the fields of autonomous driving.

2.5 Indoor Positioning based on Optical Communication

Regarding positioning, the Global Positioning System (GPS) is the leading technology in this field. More and more smart devices are equipped with GPS, starting from cell phones, watches, cameras, glasses to dog collars. However, since GPS needs line-of-sight to several satellites, it is almost impracticable for indoor environments. Thus, new ideas are required to achieve a realization of indoor navigation. There are different approaches to accomplish this task based on WiFi, Bluetooth and VLC.

For Indoor Positioning based on VLC, satellites are replaced by beacons (light sources like LEDs) which are placed inside a building and communicate with a mobile device to locate it. Therefore, the position of all beacons has to be known in advance. Then, the beacon transmits information such as an ID via light to the device. If the device gets IDs from several beacons in its field-of-view and is able to find its relative position to these,

the global position can be estimated. An overview about such indoor positioning systems based on VLC is presented by the authors of [11], [27] and [37].

2.5.1 Beacon Localization Algorithms

For VLC beacon based indoor positioning, it is necessary that the device determines its relative position to the beacons it sees. In combination with the beacons positions, this leads to the position of the device within a meaningful coordinate system. In this section, the most important algorithms to find out the distance and/or angle between beacon and device are presented.

Proximity

This is the simplest algorithm for coarse positioning. Hereby, the beacon transmits an unique ID to the device. In view of the fact that the communication is based on light, the device knows that it is located inside the radiation area of the beacon's light source. This is illustrated in Figure 2.9. Then, the device sends the ID via WiFi or ZigBee to a base station that knows the positions of all its beacons [37]. Hence, a rough position can be estimated. According to the size of the beacon's radiation the estimated position can be an undesirable large region. The authors of [38] make use of a 6-axis-sensor to measure azimuth and tilt angle and hence minimize the estimated area.

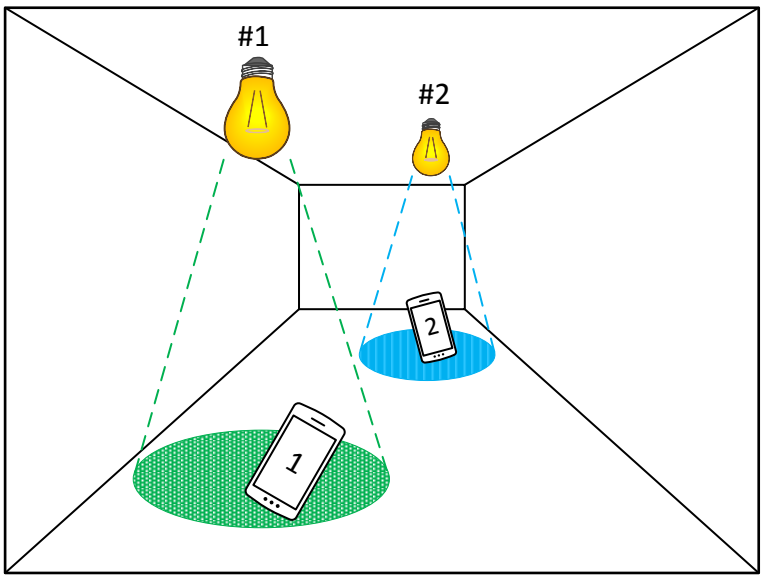

Figure 2.9: Indoor positioning based on proximity approach.

Fingerprinting

Fingerprinting measures location-dependent data inside a room, such as light intensity or signal strength, and then exploits the occuring irregularities. A plurality of factors is responsible for the invariance of the measurements. A major influence are the distance and orientation of the light source. Reflections, light scattering, constructional differences of equal LEDs and other effects additionally affect the measured values. To make use of this disparity, all the different features (fingerprints) inside a room have to be measured and saved first. Then, when the position for the mobile device should be determined, the current data is measured and compared to the features saved in the database. In this manner, the position can be estimated. For matching the measured data and the previously saved features, probability, k-nearest-neighbor or correlation are used.

Liu et al. [39] use a combination of light intensity, a special signal pattern and a unique ID for each beacon for fingerprinting. The signal is modulated in an OOK approach at a high frequency. For receiving they use the rolling shutter effect of a smart phone camera. Their results show that the system has a high accuracy if the brightness or the luminance is greater than a certain threshold.

Trilateration

In order to estimate a position using trilateration, the distances between the device and at least three beacons have to be known. Hereafter, the most common distance-based algorithms are presented:

- **Time of Arrival (TOA)**

  The distance between the mobile device and at least three beacons has to be known for 3D positioning. Therefore, light signals are emitted by the beacons and the time of arrivals are measured by the device. Then, these measured values are multiplied by the speed of light to derive the distances. Now, the position can be estimated using trilateration. Therefore, spheres are spanned around the beacons whose light was received with radius of the distances that were measured. The intersection of these circles corresponds to the estimated position. A simplified 2D example is visualized in Figure 2.10a. d_1, d_2 and d_3 are three measured distances and b_1, b_2 and b_3 are the corresponding beacons. The red cross points to the estimated position. To assign the arrivals of the signals to the corresponding beacons, OFDM can be used. A drawback of this solution is that a highly accurate synchronization between device and beacons is required.

- **Time Difference of Arrival (TDOA)** Time Difference of Arrival is similar to TOA, but instead of measuring the times of arrival, the time differences of the arriving light signals are measured. Then, by multiplying the measured time differences by the speed of light, the differences of distances can be obtained. With respect to two beacons and all points that have a constant difference of distances to the pair of beacons, a hyperbola can be designed. If the device receives signals from at least three different beacons, two hyperbolas can be drawn and their intersection

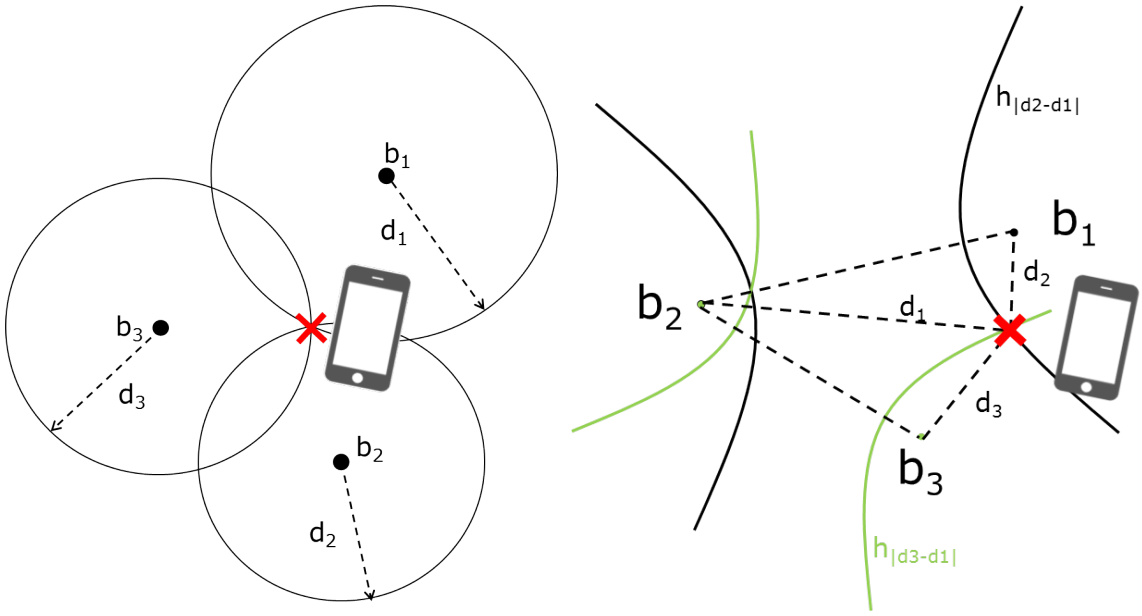

(a) TOA (b) TDOA

Figure 2.10: Time of Arrival and Time Difference of Arrival measurements for distance estimation.

can be assumed as estimated 2D position. Figure 2.10b illustrates this scheme. b_1, b_2 and b_3 are again three beacons, $h_{|d3-d1|}$ and $h_{|d2-d1|}$ are the hyperbolas that are constructed from the two differences of distances (derived from the measured time differences) $|d3 - d1|$ and $|d2 - d1|$.

To extract the measured time differences of an arriving signal, either time division multiplexing or frequency division multiplexing algorithms are used.

The authors of [40] use frequency division multiplexing with a sinusoidal signal. At the receiving side, band passes are used to separate the signals. Then, the phase differences between the signals are calculated and used for TDOA algorithm. They were able to achieve a location accuracy that is less than 1 cm in the space of 5m x 5m x 3m.

- **Received Signal Strength**

  Received Signal Strength (RSS) exploits the effect of attenuation of emitted light strength. This methods aims to translate the difference between emitted and received signal strength into a corresponding distance. The final position can be estimated with trilateration similar to TOA.

  As outlined in [37], the propagation of light is affected by reflections, obstruction, multi-path effects and other factors. Hence, the main challenge using RSS is to find a reliable path loss model for an accurate distance estimation.

  The authors of [41] propose a 3D indoor positioning system based on RSS distance estimation. Nguyen and Jang [41] show that the accuracy could be improved when the number of LED stations was increased.

Vision Analysis and Trilateration

Most approaches to obtain distances or angles with vision analysis are based on trilateration. Hereby, images recorded by a camera are analyzed with computer vision algorithms. There exist several different approaches.

One possible method is to make a sequence of images of the indoor environment beforehand and save it. Then, when positioning is required, the actually captured image is compared to the saved ones. Another idea is to use an algorithm that is capable of object (feature) detection and match the identified object with a database that knows its position. To simplify feature detection dedicated markers can be used. This makes the system more robust against changes of illumination. Moreover, with the usage of markers, unique IDs and also scaling can be realized.

2.5.2 Multiplexing

Most positioning algorithms, like the ones that are based on trilateration, need to receive the signals of several beacons to accomplish a position estimation. Moreover, the receiving unit has to be able to distinguish between these signals. Therefore, multiplexing techniques have to be applied to these systems. The most important approaches are presented in the following section.

Time Division Multiplexing

The probably simplest solution is Time Division Multiplexing (TDM). Hereby, signals are sent at a certain period of time. Therefore, all beacons as well as the receiver have to be synchronized. In some positioning systems, this might be an unwanted requirement. Another drawback arises with the increasing time consumption when more beacons are used. Furthermore, flickering has to be taken into account with TDM. Assuming that every beacon gets a time slot per cycling duration for emitting a signal, the time between these emissions increases with a rising number of beacons. However, this time needs to be small enough to ensure that the light source's blinking remains imperceptible to the human eye.

Frequency Division Multiplexing

Frequency Division Multiplexing (FDM) is similar to TDM, but instead of distinguishing various signals based on time, information is modulated onto carriers of different frequencies. Additionally, this method works asynchronously and in comparison to TDM, no synchronization is required. A specialized form of FDM is Orthogonal Frequency Division Multiplexing, a widespread technique that is widely used in the fields of Optical Wireless Communication.

The authors of [42] carry out a performance comparison between TDM and FDM for an indoor positioning system based on VLC. Their results show that the synchronization error resulting from TDM has a non-negligible impact on the localization error. Hence, using FDM for multiplexing in the same system provides a higher accuracy than TDM.

Wavelength Division Multiplexing

Wavelength Division Multiplexing (WDM), or also called Color Division Multiplexing, is a technique where different wavelengths are used for modulation. A camera's image sensor is able to separate a light signal into different colors according to their wavelength. The most common color filter is the Bayer Filter. Hereby, the image sensor is covered by an array that consists of 50% green, 25% blue and 25% red filters. The reason for the higher coverage of green is that the human eye is far more sensitive to green in comparison to the other colors. A Bayer Filter can be seen in Figure 2.11. Due to the wide optical bandwidths of blue, red and green, there are areas where their wavelengths overlap and hence inter-channel interferences occur. Another drawback is that such a structure shows a high complexity and is expensive [9].

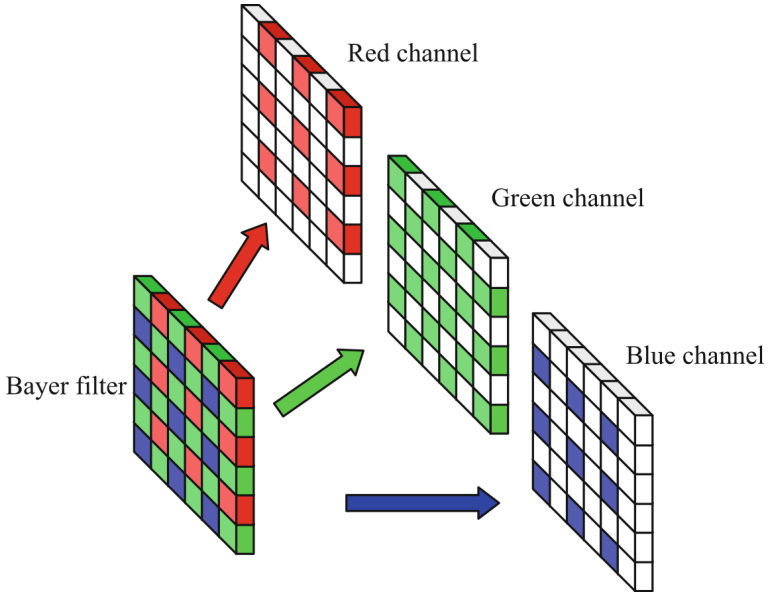

Figure 2.11: Bayer Filter [27].

2.5.3 Philips Indoor Positioning

Philips Systems [43] has developed an indoor positioning system based on VLC for retailers. This system consists of Philips LED fixtures which transmit a unique code beside their main purpose of lighting the room. The transmitted code can be detected by smart phone cameras which can further calculate the position based on the received codes. Philips ensures an accuracy of 30 cm.

2.5.4 ToF Sensor based Positioning

Time-of-Flight cameras have seen a rapid development in the last two decades, and are becoming increasingly used in mobile devices. As described in Section 2.5, there are two non-negotiable requirements to achieve beacon-based 3D indoor-positioning. First, the positioning device needs a contact to at least three beacons and their IDs. Second, in order to determine its relative position to these beacons it has to calculate the distances or the angles to the beacons.

This thesis aims to lay the foundation of the communication layer of a novel indoor positioning system. It introduces a transceiver unit for optical beacons, capable of receiving and transmitting data from ToF sensors. In this future positioning system, ToF systems can use these beacons to determine their position and orientation at unprecedented frame rates. The ToF camera can communicate via infrared light to all Optical Beacons which are in its field-of-view and thus get their IDs or localization information. In order to calculate the distances to the Optical Beacons, the ToF camera employs a new communication protocol with embedded depth image capture, which enables to track the distances of the beacons while maintaining a communication link.

The usage of a ToF camera over any other indoor positioning system based on optical communication provides several advantages. First, a depth image, which is captured by the ToF sensor, does not only provide the distances to the light sources (beacons), additionally the angles between the beacons can be calculated. Thus, triangulation and trilateration algorithms can be combined in order to increase the precision of the position estimation. Since the communication between beacon and ToF camera is based on depth measurements of the camera, data collection for trilateration/triangulation and data exchange to obtain the ID of the beacon can be done in the same step. Thus, only one system can fulfill two tasks whereas normal cameras would need additional hardware to obtain distance or angle data. The system provided in this thesis is capable of of taking depth images at up to 100 Hz while also being able to sample modulated light sources at 7000 Hz. These high sampling rates allow fast position updating, while also providing a reasonable fast optical communication link. Another benefit results from the bidirectionality of the communication system. In contrast to most VLC based positioning systems, an uplink can be installed which allows the ToF camera to communicate to the beacon. If the ToF camera is aware of its position and detects a new beacon which has not been configured yet, the camera could estimate the position of this beacon and in the next step transmit the position over the uplink. Thus, the camera can not only estimate its own position with the help of the other beacons, it can reversely make beacons aware of their position.

Chapter 3

Design

This Chapter gives an overview of the requirements regarding software and hardware specifications for this project. This includes first a description of the different software platforms used for this thesis. Further, the applied modulation and coding schemes are presented along with problems and possible solutions. Another important subject is the synchronization between ToF camera and Optical Beacon.

3.1 Requirements

This project aims to implement an optical communication system between a ToF camera and an Optical Beacon. Therefore, a stable communication channel should be developed for bi-directional data exchange. The design goals are specified as follows:

- **Hardware Implementation of the Optical Beacon**

  The hardware for a physical device should be developed which is able to communicate with a ToF camera. The platform consists of a microcontroller system, controlling a receiving unit which captures infrared light emitted by the ToF camera and a sending unit capable of emitting infrared light which is detectable by the ToF camera.

- **Software Implementation of the Optical Beacon**

  A software should be implemented for the Optical Beacon which enables communication to the ToF camera. The software should be able to decode incoming and encode outgoing messages. Further, it has to control the hardware and handle decoded instructions from the ToF camera.

- **Software Extension of the ToF Camera**

  The existing software of the ToF camera has to be extended to allow communication with an Optical Beacon. Hence, the camera should be able to detect signals which are emitted by the Optical Beacon and decode these messages. Additionally, the ToF camera should be able to decode messages and manipulate its illumination unit to send messages to the Optical Beacon.

- **Synchronization**

  Since the ToF camera and the Optical Beacon have separated clock supply units and do not run on the same frequencies, synchronization is required.

- **Robustness**

  The communication channel should be sufficiently robust to reach a distance of a few meters and cope with varying lighting conditions.

3.2 Existing Platform

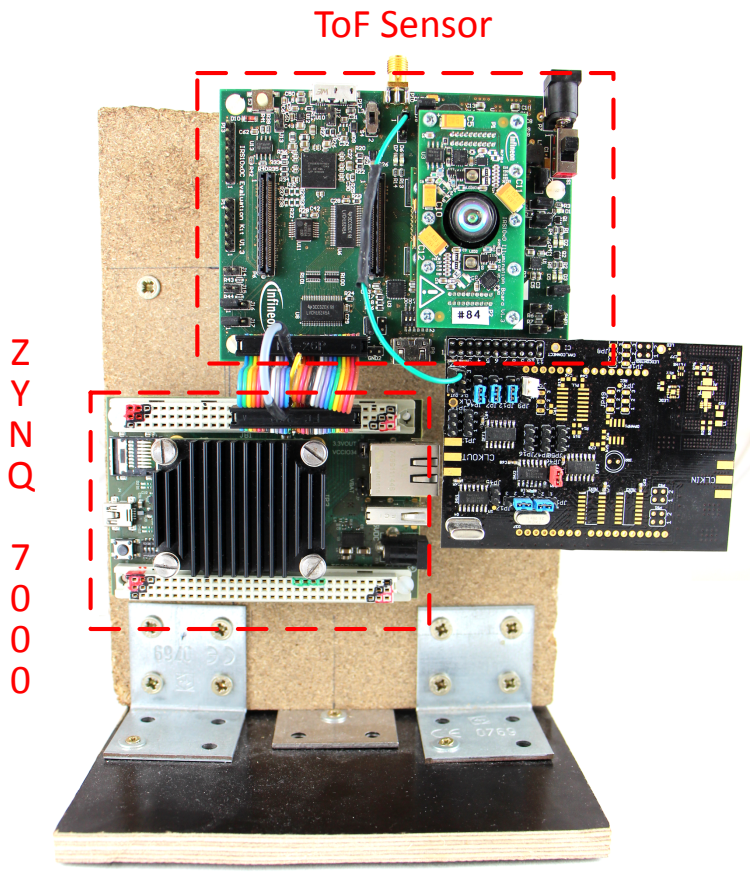

Figure 3.1: Existing ToF Platform used for this project.

This section describes the existing platform building the foundation of this thesis. An Infineon REAL3^{TM} sensor based on Time-of-Flight technology from PMD Technologies is used as ToF platform. The sensor is connected to a Xilinx Zynq 7000 platform, a System-on-Chip (SoC) providing the hardware programmability of a Field Programmable Gate Array (FPGA) and the software programmability of an ARM-based processor. A parallel interface transfers captured data from the ToF sensor to the Zync, while an I^2C interface

allows the configuration of the ToF camera. The software implementation resulting from the work of Plank et al. [34] forms the starting point of this project.

The hardware and software components for the receiving unit of the Optical Beacon are both implemented from scratch as well as the software for the sending unit. The Printed Circuit Board (PCB) developed in the master thesis of Armin Schoenlieb [44] operates as hardware for the sending unit. Figure 3.1 shows the hardware setup of the ToF platform.

3.3 Optical Beacon Platform

This section describes the hardware and software components which are used to develop the Optical Beacon.

3.3.1 Overall System Architecture

A system should be developed which is able to receive modulated signals emitted by the ToF camera and decode these signals. Additionally, this system may generate modulated infrared signals which can be received and decoded by the ToF camera. Therefore, the system is designed as following.

A photo diode with infrared filter receives the modulated pulsed light from the ToF camera and transforms the incoming photons into a current via the photo electric effect. This electric signal is amplified and digitalized by a hardware module and then passed to a microcontroller which demodulates and decodes the signal and extracts the included information. Since the ToF camera is able to measure the phase shift of pulsed infrared light, such a phase shifted signal has to be generated by the Optical Beacon. Therefore, a circuit is used which can shift a clock signal by 0°, 90°, 180° and 270°. This phase shifted signal switches an infrared LED on and off and thus modulates information into the light pulses.

3.3.2 Hardware for the Receiving Unit

A photo diode is used to receive signals from the ToF camera. A high-pass and a low-pass filter ensure that only frequencies of a desired range pass. Since the current generated by the photoelectric effect is only in the μA range, an amplifier is used to amplify the resulting voltage dropping at a parallel resistor. This amplified signal is passed to a comparator which decides if the signal resembles a logical high or low. The output of the comparator is then fed to an input pin of the microcontroller. The reference voltage for the comparator is controlled by the microcontroller. Finally, the microcontroller demodulates and decodes the signal and performs further processing. A block diagram of the circuit is illustrated in Figure 3.2.

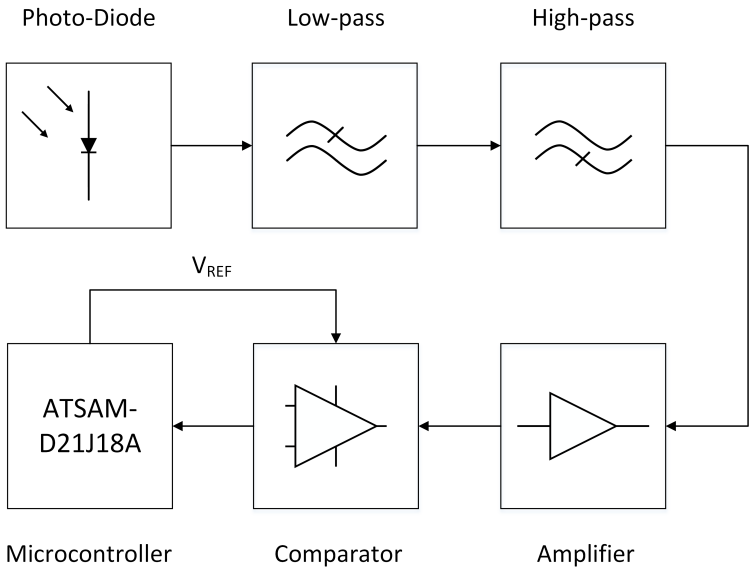

Figure 3.2: Block diagram of the receiver circuit of the Optical Beacon. The pulsed light emitted by the ToF camera is received by a photo diode, filtered, amplified, digitized and finally passed to a microcontroller for further processing.

Filter System

The signal which is received by the photo diode is low-pass filtered in the beginning to attenuate high-frequency interferences. Along with the low-pass filter, a high-pass filter is installed. The main purpose of the high-pass is to filter DC components of the signal like sun light.

Comparator

The comparator serves as 1-bit Analog-to-Digital Converter (ADC) and generates a digital signal. If the continuous signal of the photo diode is higher than the reference voltage V_{ref}, then the output of the comparator is high, and if it is beneath V_{ref}, the output is low. Hence the comparator detects light pulses emitted by the ToF camera. The output of the comparator is connected to a digital input pin of the microcontroller. The reference voltage V_{ref} is controlled by the microcontroller via a Proportional-Integral-Derivative (PID) controller.

Amplifier

The analogous signal generated by the photo diode is digitized by the comparator. Hence, a signal with steep edges is preferred for a clear detection. The original waveform of the diode is mainly produced by its internal capacity and hence resembles the loading and discharging curve of a capacitor. Using a high amplification steepens the rising and

falling edges of the curve and generates a rough square-wave signal. Another benefit of amplification is that the signal is no longer in the range of mV, but rather is extended to a range between 0 V and 3.3 V. This allows a better classification of the signal to high or low.

Adjustable Gain

A non-inverting amplification circuit is used. The gain of the amplifier is adjusted by the resistance ratio between the two resistors R_1 and R_2 in the feedback loop. The gain A is calculated by Formula 3.1. In order to change the gain at runtime, the resistor R_1 is replaced by a digital potentiometer which can be controlled by the microcontroller. This is illustrated in Figure 3.3.

$$A = 1 + \frac{R_2}{R_1} \tag{3.1}$$

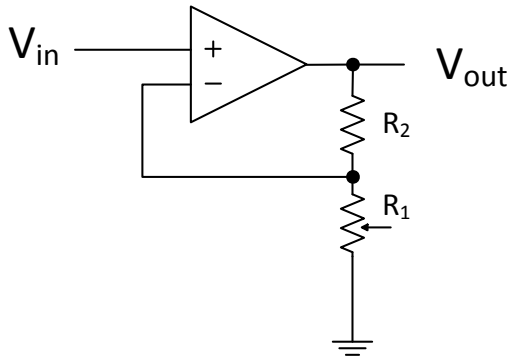

Figure 3.3: One of the two resistors for the non inverting amplifier is replaced by a digital potentiometer. Hence, the gain can be changed at runtime.

ATSAMD21J18A Microcontroller

For this project the decision was made to use the ATSAMD21J18A microcontroller from Atmel. This chip is equipped with all necessary components like Digital-to-Analog Converter (DAC), different interfaces, Real Time Counter (RTC), etc. The microcontroller comes with an evaluation board which provides easy access to the features of the ATSAMD21J18A. The ATSAMD21J18A and its components are described more precisely in Section 3.3.4.

In the setup of this project, two microcontrollers are used. The first one controls receiver hardware components like the reference voltage V_{ref} of the comparator and the gain of the amplifier. The second one is responsible for data processing, thus for demodulating and decoding the received signal, encoding and modulating the new signal and controlling the sending unit.

3.3.3 Hardware for the Sending Unit

The sending unit has the task to generate phase shifted light pulses which can be received and decoded by the ToF camera. Therefore, a circuit is used which was implemented in the master thesis of Armin Schoenlieb [44].

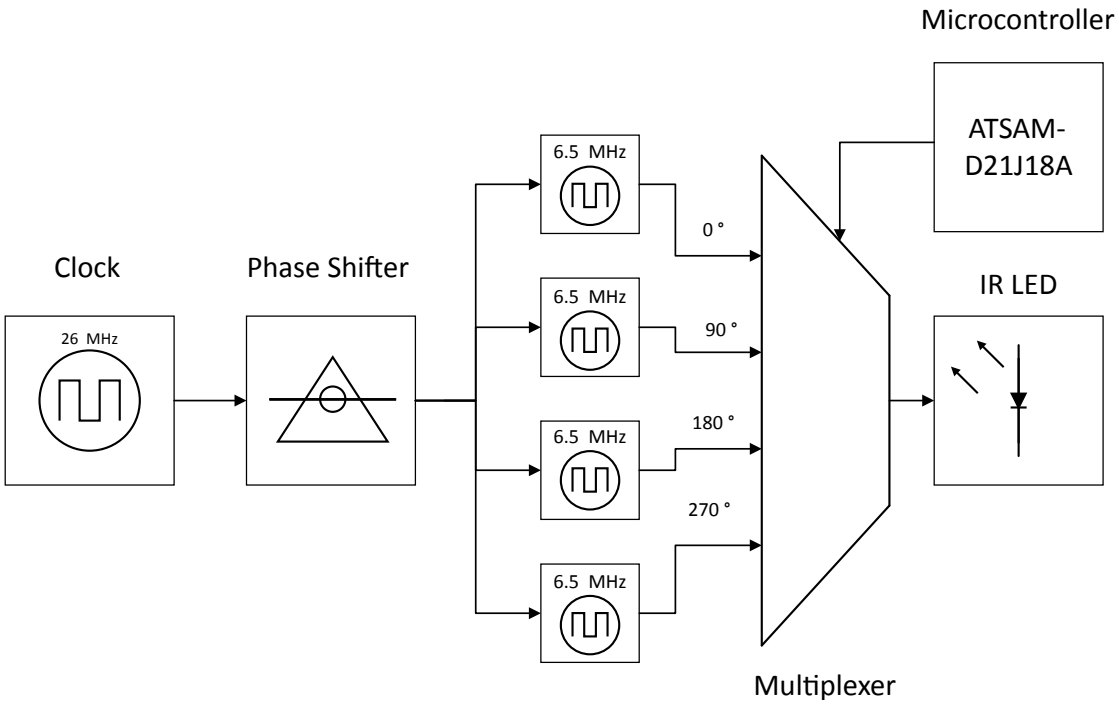

Figure 3.4: Block diagram of the sending hardware.

An IR LED is switched between ON and OFF. The switching frequency and the duty cycle are controlled by the clock signal of the circuit. A phase-shifter generates four different signals, shifted by 0°, 90°, 180° or 270°. This procedure generates phase shifted light pulses which can be detected by the ToF camera. Since the phase-shifter is able to generate four different signals, four distinguishable states can be modulated. The four phase shifted clock signals are fed to a multiplexer. The desired phase can be chosen from the multiplexer with a control signal which is produced by the microcontroller. Finally, the selected phase shifted clock signal switches the IR LED on and off. A block diagram of the sending unit is illustrated in Figure 3.4.

Phase-Shifter

The phase-shifter consists of 2 d-flipflops which allow quadrature phase shift. The four output signals of the flipflops have a phase of 90° difference. These four signals are fed into the multiplexer. Depending on the control signal of the multiplexer, one of these four signals is forwarded to the output. Table 3.1 illustrates the truth table of the output values Q_1 and $\overline{Q_1}$ of the first d-flipflop and Q_2 and $\overline{Q_2}$ of the second d-flipflop. Q_1 shows the

signal with 0° phase shift, $\overline{Q_1}$ with 180°, Q_2 with 90° and $\overline{Q_2}$ with 270° phase shift. The

Q_1	1	1	0	0	1	1	0	0	1	1
$\overline{Q_1}$	0	0	1	1	0	0	1	1	0	0
Q_2	0	1	1	0	0	1	1	0	0	1
$\overline{Q_2}$	1	0	0	1	1	0	0	1	1	0

Table 3.1: 2 d-flipflops are used to achieve a quadrature phase shift. Q_1, $\overline{Q_1}$, Q_2 and $\overline{Q_2}$ show the output values of the phase-shifter.

control signal for the multiplexer is produced by three GPIO pins of the microcontroller. With these three pins, binary values are generated indicating which signals should be passed through.

3.3.4 ATSAM Microcontroller

The centerpiece of the Optical Beacon is the ATSAMD21J18A microcontroller from Atmel. This is a low-power, high-efficiency 48 MHz microcontroller with an Cortex-M0 architecture. This section outlines the most important components which are used for this project.

SAM D21 Xplained Pro Evaluation Board

The evaluation board can be powered from an external 5 V power supply, from the embedded debugger USB or from the target USB. It provides an embedded debugger and also a virtual COM-port for an UART communication, both via USB. Further, there is an external 32 kHz crystal oscillator, a 8 Mb serial flash, a LED, two hardware buttons and three extension headers. With the extension headers, there come interfaces such as UART, SPI, I^2C, different GPIO pins, an ADC and DAC, ground pins and voltage pins for 5 V and 3.3 V.

Interfaces

The ATSAMD21J18A offers SPI, UART and I^2C interfaces which are placed on the extension headers. Each header offers all three interfaces. The SPI interface is used to adjust the resistance of the digital potentiometer. UART serves as communication channel between the two microcontrollers.

Real Time Counter

The RTC is used to generate interrupts at periodic intervals. It uses the interal 32 kHz RC-oscillator and has a prescaler to divide the frequency of the periodic intervals into the desired end-frequency between 1 Hz and 32 kHz.

Time Counter

The TC allows to get the current time or more precisely the current number of CPU ticks. If this number is divided by the frequency of the CPU, a time value in seconds is obtained. So, the TC is used to determine the duration while the signal is high and while it is low to get pulse and pause durations.

DAC

The DAC provides the output voltage which is used as reference voltage V_{ref} for the comparator.

External Interrupt Handler

The External Interrupt Handler is used to detect interrupts which are triggered either by the logic level or change of the logic level of certain pins and call their corresponding interrupt routines. This is used to detect falling and rising edges of the output of the comparator. Hence, pulses and pauses of the ToF signal can be detected.

Demodulation Unit

The demodulation unit is responsible to demodulate the signal which is obtained by the comparator. Since DPPM is used as modulation method for the sending data from the ToF camera to the Optical Beacon, the duration while the signal is high (t_{pulse}) and while it is low (t_{pause}) has to be determined. For calculating a pause duration, the time between a falling and the following rising edge has to measured. For a pulse time, the measurement has to be made between a rising and a falling edge. This is illustrated in Figure 3.5.

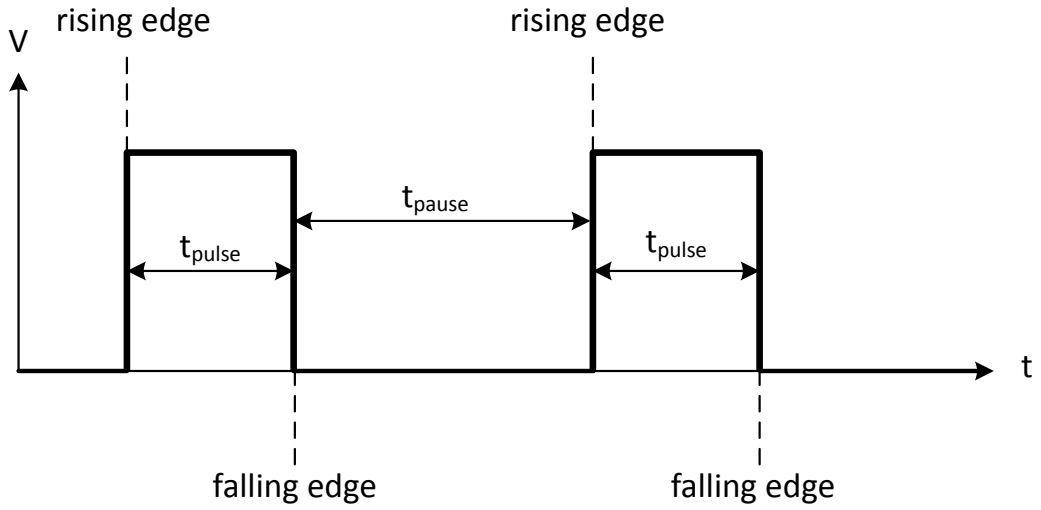

Figure 3.5: The time t_{pulse} refers to the time between rising and falling edge. t_{pause} is the time between falling and rising edge.

Modulation Unit

While DPPM is used for sending data from the ToF camera to the Optical Beacon, a modulation technique based on phase shifting can be used for the other communication direction (from the Optical Beacon to the ToF camera). Since the phase-shifter, described in Section 3.3.3, is able to generate four phase shifted signals, Quadature Phase Shift Keying (QPSK) is used in this system. This can be potentially improved in future work. With phase shift keying (PSK), information is modulated into the phase of a signal. QPSK is a special form where four different phases are used. Each phase resembles a point on the constellation diagram as is illustrated in Figure 3.6. The four phase shifted signals are generated by the phase-shifter and fed to a multiplexer. With three GPIO pins of the microcontroller, the signal with the desired phase shift can be passed through the multiplexer. The implementation of QPSK for this work is described more precisely in Section 3.6.

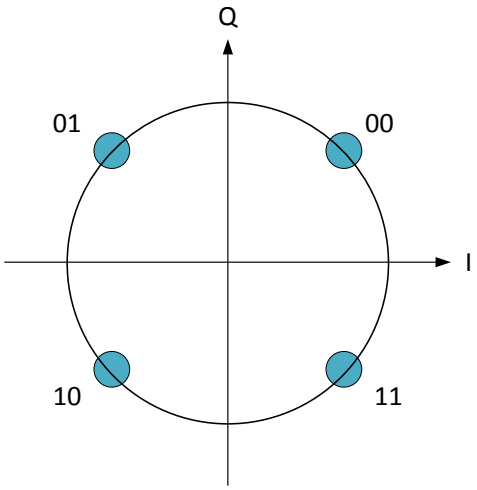

Figure 3.6: An illustration of QPSK.

3.4 The ToF Platform

Beside the Optical Beacon, the ToF camera is the second partner of the communication system. It has to be capable of receiving and decoding information as well as encoding and sending data. In this section, the most important components of the ToF camera are illustrated and how they are used to form a receiving and a sending unit.

3.4.1 Receiving Unit

When the ToF camera acts as receiver, it has to be in imaging mode and capture images of the IR LED of the Optical Beacon. Since a captured raw image contains information about the phase between outgoing and incoming signal for each pixel, it is possible to use highly efficient but yet nearly unexplored modulation method of quadrature phase shift keying

of pulsed light (PLQPSK). A measured phase value is a value between 0 and 4095. In this thesis, a phase value measured by the ToF camera is referred to as $phase_{tof}$. The Optical Beacon sends pulsed light with 0°, 90°, 180° or 270° phase shift. Values which denote a phase with respect to PLQPSK, thus a value between 0° and 360°, is called $phase_{plqpsk}$. In order to reconstruct the $phase_{plqpsk}$ of a communication partner's modulated light source, the ToF camera captures an image and calculates the average over the phase_{tof} values of all pixels, containing modulated light. Then, this averaged phase_{tof} value has to be transformed to a phase_{plqpsk} on the constellation diagram and matched to one of the four phases used for PLQPSK. It can then be decoded in a further step.

Exposure Time

Since the ToF camera has to capture an active modulated light source (the IR LED of the Optical Beacon), a short exposure time is sufficient. Additionally, a short exposure time results in a small capturing time which brings the advantage that the number of pictures which can be captured per second can be maximized. This increases the achievable data rate. Hence, the exposure time is chosen as small as possible so that the IR LED can still be detected.

Resolution

The ToF camera is able to take pictures with a resolution of 352 x 288 pixels. With this resolution, the time it takes to read out 352 x 288 pixels determines how many images can be captured per second and thus the data rate. However, a smaller resolution is considered in order to increase the possible data rate. The approach for this work is to first sample with the full resolution of 352 x 288 pixels to find the light source of the Optical Beacon. In the next step, the camera is reconfigured to the smallest possible resolution of 32 x 16 pixels. The region of interest for these pixels is set to the location where the light source was found beforehand.

Modulation Frequency

The modulation frequency $\mathcal{F}_{mod}$ affects the phase measurement as described in Section 2.1. The ToF camera assumes that the light pulses which arrive at the sensor after reflection have exactly the same frequency as $\mathcal{F}_{mod}$. In case of a normal depth measurement, the light pulses which are emitted by the ToF camera are modulated with $\mathcal{F}_{mod}$ and thus the frequency of the reflected signal is the same.

In this project, the light pulses which arrive at the ToF sensor are not the reflected pulses sent out by the ToF camera but rather the the light pulses which are generated and emitted by the Optical Beacon. Since the Optical Beacon uses its own oscillator for the modulation of the light pulses, the modulation frequency of the Optical Beacon and the one of the ToF camera will not be exactly the same due to the constructional inequality of their components. This problem is solved in this project with a new ToF synchronization approach, which is explained in detail in Section 3.5.1.

3.4.2 Sending Unit

The illumination unit of the ToF camera is used as sender. The exposure time (pulse duration) as well as the time between two exposures (pause duration) can be adjusted. With these two variable parameters, DPPM can be implemented. The pulse duration is kept constant while information is modulated by varying the pause duration. In sending mode, the camera operates at a frequency of 26 MHz.

Pause Times

Because DPPM is used for modulation, information has to be modulated with different pause durations. Varying the pause times and keeping pulse times short gives additional energy savings. The pause time can be set via integer value x_{pause}. The real time t_{pause} results from:

$$t_{pause} = \frac{x_{pause} \cdot 1024}{133MHz} \tag{3.2}$$

133 MHz refer to the frequency of the system clock of the ToF camera. The smallest resolution between to different pause times is $x_{pause} = 1$ resulting in approximately $8\mu s$ according to Formula 3.2.

Pulse Times

Similar to pause times, pulse times can also be set via an integer value x_{pulse}. Here, the resulting pulse time t_{pulse} is calculated with:

$$t_{pulse} = \frac{x_{pulse} \cdot 8}{26MHz} \tag{3.3}$$

26 Mhz refer to the frequency of the modulation clock of the ToF camera. When very low pulse times are used, it has to be considered if the response time of the comparator in the Optical Beacon is short enough to detect such short pulses. For this project, a pulse time of about $5\mu s$ seems to be a good compromise between using a short pulse time to achieve a high data rate, and being long enough for robust detection with the Optical Beacon's receiving unit.

3.5 System Requirements for Communication

In this section, particular requirements are covered which are indispensable to allow a communication in both directions between a ToF camera and an Optical Beacon.

3.5.1 Modulation Frequency Synchronization

As outlined in Section 3.4.1, a frequency difference between P_{light} of the Optical Beacon and $\mathcal{F}_{mod}$ of the ToF camera is likely to occur. According to the tolerances of the oscillators

of the ToF camera and the Optical Beacon, a frequency difference of up to 1560 Hz may occur. This frequency offset leads to a phase$_{tof}$ error which is illustrated in Figure 3.7. The modulation frequency $\mathcal{F}_{mod}$ of the ToF camera determines if either bucket A or B is

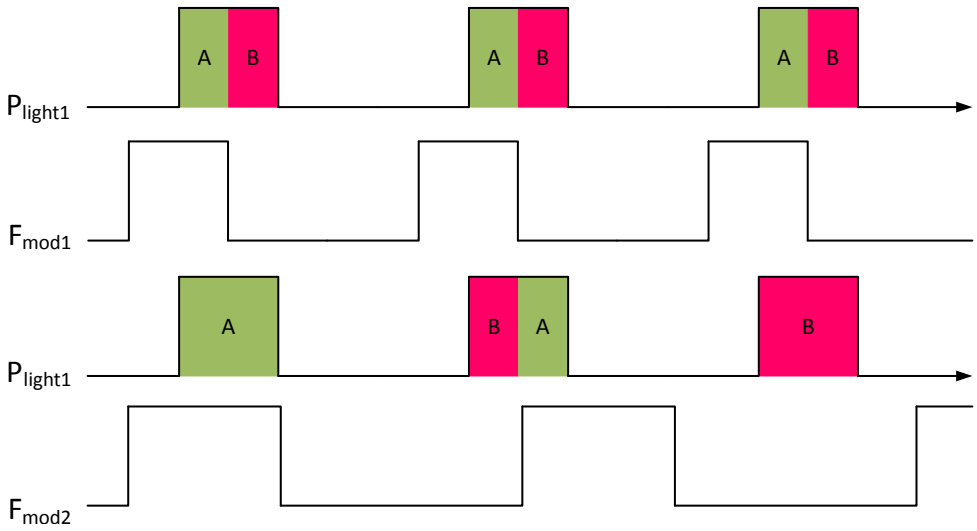

Figure 3.7: The phase$_{tof}$ value of each pixel is calculated by the difference between the storages A an B. If the modulation frequency $\mathcal{F}_{mod}$ and the frequency of the pulsed light P$_{light}$ differ, the voltages of A and B will also be different.

charged as explained in Chapter 2.1. While $\mathcal{F}_{mod}$ is high, bucket A is filled and while $\mathcal{F}_{mod}$ is low, bucket B is filled. Then, the difference between the voltages of the buckets A and B determines the phase shift between outgoing and incoming signal. P$_{light1}$ is a pulsed light signal emitted from the Optical Beacon which arrives at the ToF sensor. $\mathcal{F}_{mod1}$ is a modulation clock which has exactly the same frequency as P$_{light1}$. Because both frequencies are equal, the relation between the buckets A and B is constant over time. $\mathcal{F}_{mod2}$ shows a modulation frequency which is slightly lower than the one of the emitted light P$_{light1}$. The drift of the pulses of $\mathcal{F}_{mod2}$ with respect to P$_{light1}$ leads to different charges of A and B. If we assume that the Optical Beacon emits light with a constant phase$_{plqpsk}$ and $\mathcal{F}_{mod}$ equals P_{light}, the camera should always sample the same phase$_{tof}$ value. Thus, each of the four phases which are emitted by the Optical Beacon (0°, 90°, 180°, 270°) should refer to a certain measured phase$_{tof}$ value as it is illustrated in Figure 3.8a. As shown in Figure 3.8b, the four phase$_{tof}$ waves will cross each other, if there is a frequency difference. At the moment, it is impossible to match a measured phase$_{tof}$ value to the correct phase$_{plqpsk}$ unambiguously when two phases cross. As a result, a correct demodulation is not possible. An approach to tackle this problem is to decrease the frequency difference between $\mathcal{F}_{mod}$ and P_{light} as far as possible as it was proposed by Plank et al. [34]. This can be done by calculating the frequency $\mathcal{F}_{error}$ of the drifting phases$_{tof}$ and adjust the frequency of the ToF camera by this value.

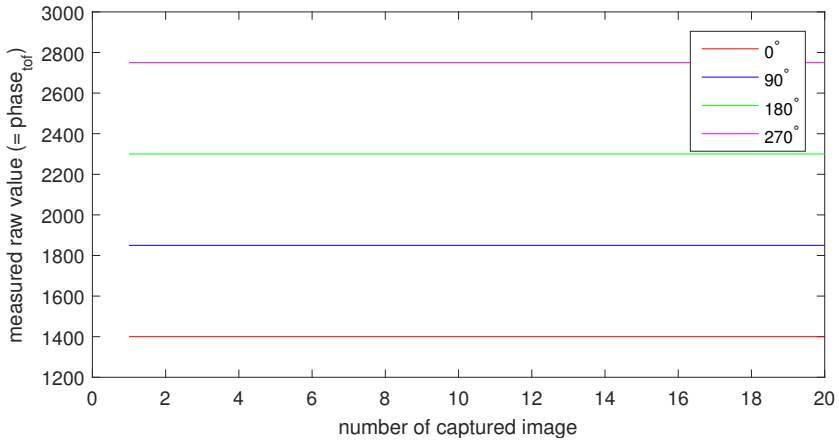

(a) If $\mathcal{F}_{mod} = P_{light}$, each phase_{plqpsk} (0°, 90°, 180°, 270°) refers to a certain measured value phase_{tof}.

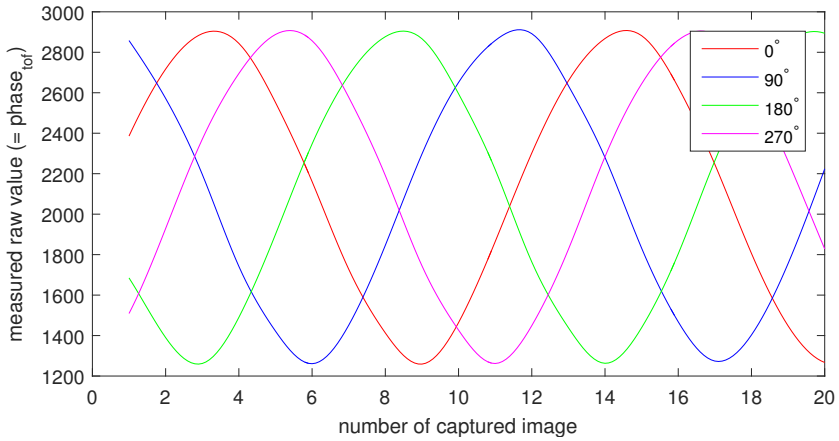

(b) Illustration of the impact of a difference between modulation frequency $\mathcal{F}_{mod}$ (at the ToF camera) and the pulsed light frequency P_{light} (IR LED of the Optical Beacon). Due to the phase drift, which is caused by the frequency difference, the phase values change periodically in a sinusoidal fashion.

Figure 3.8: Illustration of the impact of a frequency difference between ToF camera and Optical Beacon.

3.5.2 Determination of the Quadrants for PLQPSK

Another factor which influences the measured phase_{tof} and demodulated phase_{plqpsk} of a modulated light source is the distance between Optical Beacon and ToF camera. Thus, it is unknown which phase_{plqpsk} will be demodulated at the ToF camera while it is known which phase_{plqpsk} was emitted by the Optical Beacon. Therefore, the quadrants for classification are not fixed and predefined, instead they will be determined at runtime depending on the first measured phase_{tof} and resulting phase_{plqpsk} value. This method is similar to differential pulse position keying, where the difference between two phases is considered rather than the phase itself.

It is assumed that the first phase_{plqpsk} emitted by the Optical Beacon is 0°. Thus, the first measured value phase_{tof} at the ToF camera and its transformation to the constellation diagram phase_{plqpsk} will define the first quadrant. With respect to this initial measurement, the other quadrants are defined. With this solution, it is ensured that the phase_{plqpsk} value which is emitted by the Optical Beacon and the demodulated phase_{plqpsk} at the ToF camera refer to the same quadrant. However, with this approach the information of the first measured phase_{tof} is lost.

3.6 Modulation

In this project, two different modulation techniques are used. For the communication direction from the ToF camera to the Optical Beacon, DPPM is used. For the other communication direction, from the Optical Beacon to the ToF camera, a different approach can be used since a ToF camera has the unique possibility to demodulate phase-shifted signals on the pixels, providing a reliable and efficient modulation scheme. Hence, the most obvious modulation technique is phase shift keying. Phase shift keying is depicted in the following section.

Due to the fact that the phase-shifter of the Optical Beacon is capable of shifting four different phases, PLQPSK is used as phase shift keying technique. A phase_{tof} value is a value between 0 and 4095, which represents a value for autocorrelation between outgoing and incoming signal, rather than an angle in degree or radians. Thus, the measured phase_{tof} values have to be transformed to the constellation diagram in order to be able to use PLQPSK. With PSK, a phase is represented as a complex value. Hence, two carriers are used in this work. A sine and a cosine carrier are modulated which represent the imaginary part i and the real part q of this complex value. So, the Optical Beacon has to generate a sine and a cosine representation of the clock signal P_{light}. Since cosine is the same function as a sine just shifted by 90°, the desired P_{light} represents the sine function and the same P_{light} shifted by 90° represents the cosine. This means, the Optical Beacon has to send two different phases_{plqpsk} to transmit one point of the constellation diagram. Consequently, the ToF camera has to capture two images in order to transform these two measured phase_{tof} values to a point in the constellation diagram. Table 3.2 illustrates how two phases_{plqpsk} are used to each represent one point/phase P_{plqpsk} in the constellation diagram. The ToF camera assumes that the measured phase_{tof} value of the first captured

P_{PLQPSK}	P_{light1} (sine)	P_{light2} (cosine)
0°	0°	90°
90°	90°	180°
180°	180°	270°
270°	270°	0°

Table 3.2: P_{PLQPSK} is the point in the constellation diagram which is transmitted. Therefore, two carriers P_{light1} and P_{light2} are used to form the sine and cosine representation of this point.

image corresponds to the sine (p_{φ_i}) and the second one to the cosine (p_{φ_q}) representation of the complex value which was sent by the Optical Beacon. The imaginary part (p_{φ_i}) is plotted on the x-axis and the real part (p_{φ_q}) on the y-axis.

Since p_{φ_i} and p_{φ_q} are values between 0 and 4095 which also means both values have a non-negative sign, the obtained points will all be placed in the first quadrant. Hence, for a correct transformation from p_{φ_i} and p_{φ_q} to the constellation diagram, they have to be translated to the points $P_{\varphi_{iconst}}$ and $P_{\varphi_{qconst}}$ which are placed around the origin in order to occupy all four quadrants of the constellation diagram. This is illustrated in Figure 3.9. The translation is achieved by the calculation presented in Formula 3.4. In order to

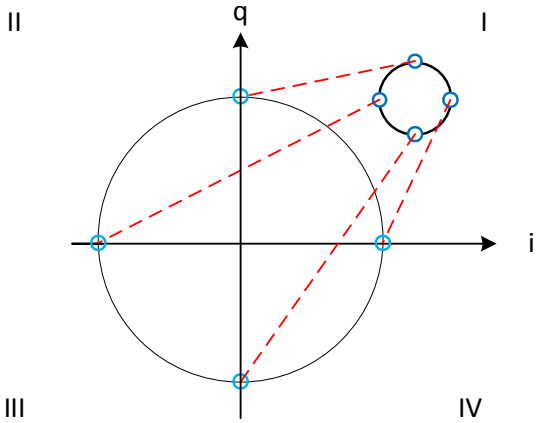

Figure 3.9: Translation of the points to achieve a placement around the origin in all quadrants.

determine the minimum and maximum occurring values for p_{φ_i} and p_{φ_q}, a set of several phase$_{tof}$ values is required (P_{φ_i} and P_{φ_q}), for which it is known that these values include representative values for phase$_{plqpsk}$ values of 0°, 90°, 180° and 270°.

$$\begin{aligned} P_{\varphi_{iconst}} &= p_{\varphi_i} - \frac{(max(P_{\varphi_i}) + min(P_{\varphi_i}))}{2} \\ P_{\varphi_{qconst}} &= p_{\varphi_q} - \frac{(max(P_{\varphi_q}) + min(P_{\varphi_q}))}{2} \end{aligned} \tag{3.4}$$

The angle of the point $[P_{\varphi_{iconst}}, P_{\varphi_{qconst}}]$ with respect to the x-axis can be calculated with the arctan2 function:

$$\varphi = arctan2\left(\frac{P_{\varphi_{iconst}}}{P_{\varphi_{qconst}}}\right) \tag{3.5}$$

3.7 Coding

This section introduces coding techniques for DPPM and PLQPSK in order to maximize the channel capacity. The following notation elements which describe the coding schemes will be now defined and used consistently. *Symbols* are distinguishable states like different

phases in the case of PLQPSK and different pause times for DPPM. In the field of information theory, *information* is a sequence of symbols from an alphabet in a strict order. In this thesis, *information* is referred to as *codeword*. N determines the number of symbols which make up a codeword and M represents the number of total codewords. q is the number of distinguishable symbols, hence the size of the alphabet. In a quaternary coding for example, it would be {0, 1, 2, 3}. The number of symbols per second is called baud rate. The number of codewords depends on the number of symbols q and the number of symbols used per codeword M:

$$M = q^N \tag{3.6}$$

Channel capacity C denotes the maximal rate at which information can be transmitted over a communication channel and is expressed in units of information per unit time. In this thesis, C is expressed in codewords per second *cps*.

3.7.1 DPPM

When DPPM is used as modulation scheme, symbols differ from each other by different lengths of the pause time t_{pause} between two pulses. Since the length of a pause can be chosen freely at the ToF camera, any number of different pause times and hence different symbols can be selected. Equation 3.6 shows that an increasing number of codewords M yields in an increasing number of symbols per codeword when q is kept constant. Because the symbols are formed by different pause times, an increasing number of codewords results in an increasing number of pause times. Since the duration of a codeword t_{cw} is the sum of each time it takes to transmit a single symbol (see Formula 3.7), an increasing number of codewords will increase t_{cw} and thus decrease the channel capacity (see Formula 3.8).

$$t_{cw} = \sum_{i=0}^{N-1} t_{pause_i} \tag{3.7}$$

$$C = \frac{1}{t_{cw}} \tag{3.8}$$

Thus, the question arises if it is useful to use a binary coding scheme ($q = 2$) or take advantage of the arbitrary selectable number of different symbols (pauses) and use a q-ary coding technique (q = n). Therefore, in the following section binary (q = 2) and quaternary (q = 4) coding are compared.

Binary vs Quaternary Coding for DPPM

The minimum t_{pause} which can be set for the ToF camera is about 126 μs. The minimum step size at the ToF camera is 1. According to Equation 3.2, a step size of $x_{pause} = 1$ results in $\sim$8 μs. Thus, the smallest difference between two different pause times is 8 μs. If binary coding is used, the two smallest possible pause times to form two different symbols are 126 μs and 134 μs.

For comparison of binary and quaternary coding, an example is given to show the impact of the selected coding scheme on the channel capacity. For this example, the number of total codewords M is 16. According to Forumla 3.6, N is calculated by:

$$N = \lceil log_q(M) \rceil \tag{3.9}$$

With $q = 2$ and $M = 16$, Formula 3.9 results in $N = 4$. Table 3.3 illustrates the set of codewords formed by binary symbols {0,1}. In Table 3.4, the logic levels are replaced by

codeword	symbol 1	symbol 2	symbol 3	symbol 4
1	0	0	0	0
2	0	0	0	1
⋮	⋮	⋮	⋮	⋮
15	1	1	1	0
16	1	1	1	1

Table 3.3: Set of codewords with binary coding. $q = 2$, $M = 16$, $N = 4$; the symbols are {0,1}.

their corresponding pause duration t_{pause}. According to Table 3.4, the average codeword duration t_{cw} is 520 μs; this results in an average channel capacity of 1923 codewords per second. In Table 3.5, a quaternary coding scheme ($q = 4$) is illustrated. The number of

codeword	t_{pause_1} $[\mu s]$	t_{pause_2} $[\mu s]$	t_{pause_3} $[\mu s]$	t_{pause_4} $[\mu s]$	t_{cw} $[\mu s]$	channel capacity $[cps]$
1	126	126	126	126	504	1984
2	126	126	126	134	512	1953
⋮	⋮	⋮	⋮	⋮	⋮	⋮
15	134	134	134	126	528	1893
16	134	134	134	134	536	1865
average	130	130	130	130	520	1923

Table 3.4: The logic levels of Table 3.3 are replaced by their corresponding pause times.

codewords M is still 16. According to Formula 3.9, the number of symbols per codeword $N = 2$. The average codeword duration t_{cw} is 276 μs and the channel capacity is 3623 codewords per second. Compared to the results of the binary coding scheme in Table 3.4, the channel capacity is 1.8 times higher with quaternary coding than binary coding.

Q-ary Coding for DPPM

Section 3.7.1 has demonstrated that binary coding does not necessarily achieve the best channel capacity for DPPM. In the given example with $M = 16$, a quaternary coding

codeword	symbol 1	symbol 2	t_{pause_1} $[\mu s]$	t_{pause_2} $[\mu s]$	t_{cw} $[\mu s]$	channel capacity $[cps]$
1	0	0	126	126	252	3968
2	0	1	126	134	260	3846
⋮	⋮	⋮	⋮	⋮	⋮	⋮
15	3	2	150	142	284	3521
16	3	3	150	150	300	3333
average	-	-	138	138	276	3623

Table 3.5: Set of codewords with quaternary coding. $q = 4$, $M = 16$, $N = 2$; the symbols are {0,1,2,3}.

resulted in a higher channel capacity. If now a q-ary coding is chosen for the same example of $M = 16$ with $q = 16$, there are 16 different symbols $\{0, 1, 2, ..., 14, 15\}$ and only one symbol per codeword ($N = 1$) is required. As Table 3.6 illustrates, a channel capacity of 5376 codewords per second is achieved. Hence, a q-ary coding with $q = 16$ results in a 1.4 times better performance than quaternary coding and is 2.8 times better than binary coding. Thus, the question arises if a q-ary coding with $q = M$ will always result in the highest possible channel capacity as in this example. This question is answered in the following section.

codeword	symbol 1	t_{pause_1} $[\mu s]$	t_{cw} $[\mu s]$	channel capacity $[cps]$
1	0	126	126	7936
2	1	134	134	7462
3	2	142	142	7042
⋮	⋮	⋮	⋮	⋮
15	14	238	238	4201
16	15	246	246	4065
average	-	186	186	5376

Table 3.6: Set of codewords with q-ary coding. $q = 16$, $M = 16$, $N = 1$; the symbols are {0,1,2...,15}.

Optimum q for Q-ary Coding for DPPM

Let X_{chars} be a vector which contains all symbols in decimal representation. For example, $q = 4$ results in $X_{chars} = \{0, 1, 2, 3\}$. X_{perms} is a vector which contains all possible permutations of N symbols taken from the vector X_{chars}. With $q = 4$ and $N = 2$ for example, X_{perms} is a 4^2x2 matrix with the corresponding permutations {0,0; 0,1; 1,0; ...; 2,3; 3,2; 3,3} . X_{digit_sum} is a vector which contains the digit sums for each row in X_{perms} and $X_{digit\_sum\_sorted}$ is a vector which contains the elements of X_{digit_sum} sorted in ascending order. Now, in

assumption that each codeword is transmitted with the same probability, the average channel capacity can be calculated with:

$$C = \left(\frac{1}{M} \sum_{k=0}^{M-1} \left(N \cdot 126\mu s + X_{digit\_sum\_sorted}[k] \cdot 8\mu s \right) \right)^{-1} \tag{3.10}$$

If q is varied for different values in the range of $2 <= q <= M$, a graph arises which shows the achieved channel capacities for different combinations of q and N with a constant M. If now the parameter M is varied additionally (see Formula 3.11), several graphs can be plotted as demonstrated in Figure 3.10.

$$C_i = \left(\frac{1}{M} \sum_{k=0}^{M-1} \left(N \cdot 126\mu s + X_{digit\_sum\_sorted}[k] \cdot 8\mu s \right) \right)^{-1} \Big|_{2<=i<=M} \Big|_{4<=M<=n} \tag{3.11}$$

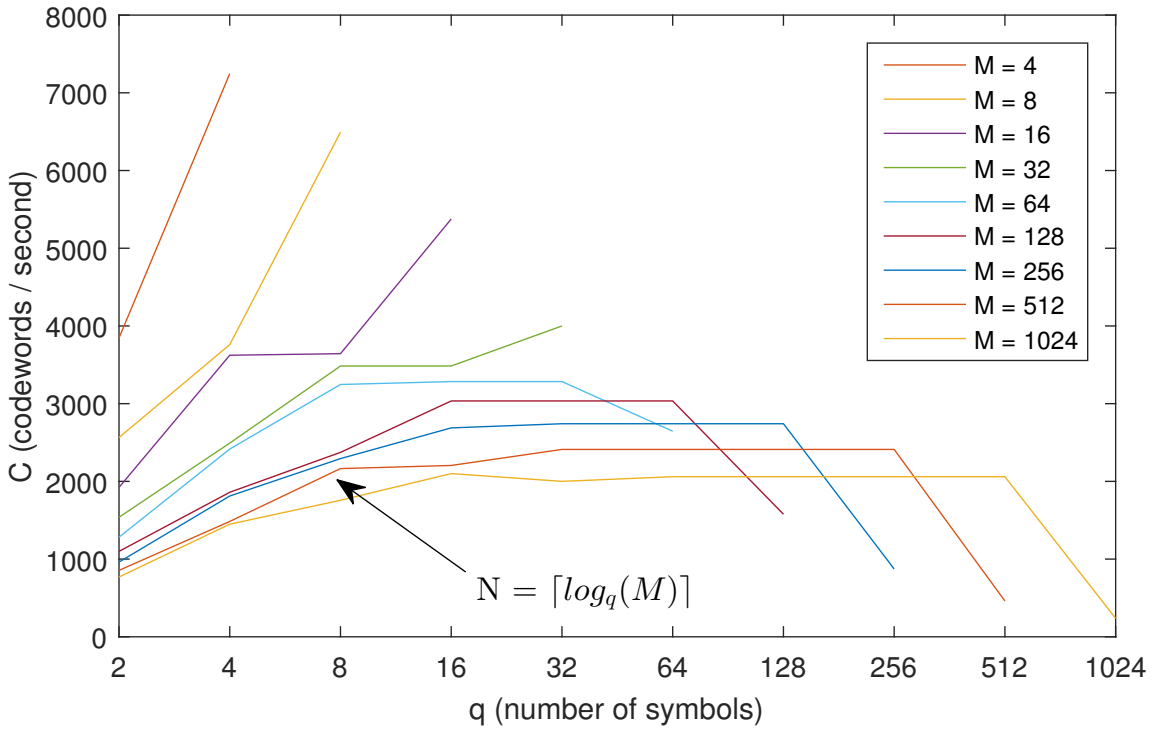

Figure 3.10: Relation between q, N, M and channel capacity C. For $M <= 32$, the maximum channel capacity is achieved with $q = M$. For $M > 32$, the highest channel capacity is obtained with $N > 1$ and $q = \sqrt[N]{M}$.

It can be seen that the highest channel capacity with $q = M$ can only be achieved with $q = M <= 32$. For a $M > 32$, q has to be greater than one to maximize the channel capacity.

3.7.2 PLQPSK

While q is an arbitrary selectable parameter for DPPM, for PLQPSK it is fixed. Since the Optical Beacon is capable of producing four different phases, $q = 4$. Thus, the used symbols are $\{0°, 90°, 180°, 270°\}$.

The camera is capable of capturing approximately 7000 pictures per second with the lowest pixel resolution. Since one symbol is transmitted with two phases (symbol in sine and cosine representation), it should be able to receive about 3500 symbols per second.

3.8 Synchronization

The Optical Beacon has to emit light with a constant phase_{plqpsk} for at least the integration time in which the pixels capture the incoming light. This is illustrated in Figure 3.11. *phase 1* is emitted exactly during the integration time of the ToF camera and thus it will be detected correctly. If the phase_{plqpsk} is changed during the capturing phase (*phase 3* and *phase 4*) or emitted for a shorter period of time (*phase 2*), it is indeterminate which phase_{plqpsk} will be demodulated by the camera. Hence, synchronization is required. The

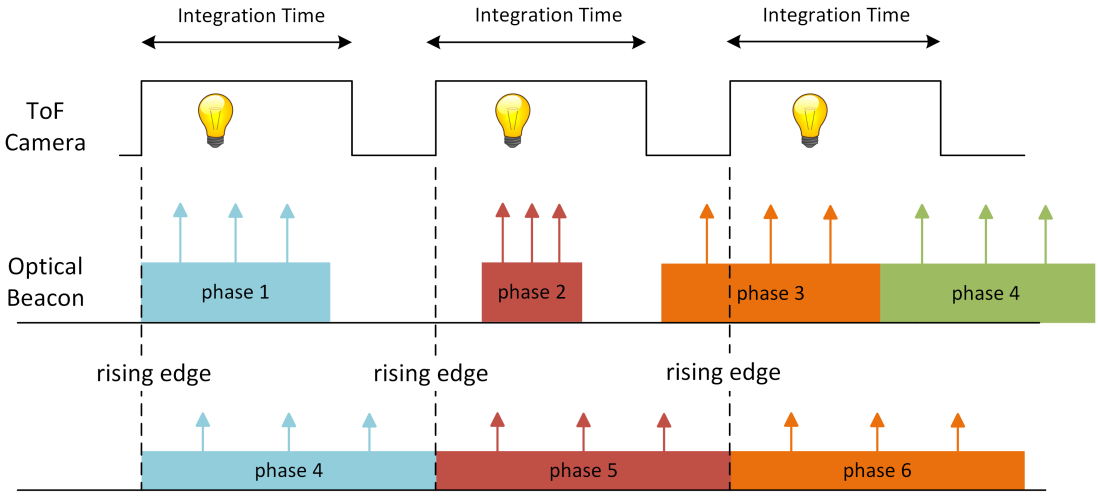

Figure 3.11: A phase_{plqpsk} has to be emitted during the integration time of the ToF camera and may not change in this period of time. Otherwise, the demodulated phase_{plqpsk} is indeterminate. Thus, synchronization is required.

Optical Beacon has to be aware of the moment when the camera starts to capture an image. This can be achieved by detecting the rising edge of the illumination pulse. Thus, as soon as the Optical Beacon detects a rising edge it starts to emit a certain phase_{plqpsk} until the next illumination pulse is detected. This is illustrated by *phase 4* to *phase 6* in Figure 3.11.

3.9 Considerations for basic Communication Protocol

Since two different modulation techniques are used depending on the communication direction, two different protocol considerations are made.

3.9.1 Protocol for PLQPSK

For the communication link applying PLQPSK, a start pattern is required. This start pattern fulfills two purposes. First, it indicates the start of a data stream. Second, as mentioned in Section 3.6, the measured phase_{tof} values $\text{P}_{\varphi i}$ and $\text{P}_{\varphi q}$ have to be translated so that a distribution in all four quadrants in the constellation diagram is reached. In order to calculate the correct translation factor, the center of the unit circle has to be calculated on which the translated points are placed. Therefore, points in all areas of the circle are required. If for example only two points from the same quadrant are known, the correct center can not be estimated. Hence, the start pattern transmits 0°, 90°, 180° and 270° for at least once. So, points in all four quadrants are given and thus the center and further the translation factor can be calculated.

3.9.2 Protocol for DPPM

When the camera is configured, a frame with 32 pulses and 32 pauses can be defined and hence modulated. Then, when the camera starts to run, this frame is emitted repetitive. If another frame with new codewords is desired for transmission, the camera has to be stopped, reconfigured with a new frame and started again. This process takes about 7 ms and thus a frame can not be transmitted immediately after the previous one.

Chapter 4

Implementation

This Chapter describes the working process of this project. It gives a detailed overview of the hardware development process, from the choice of the used components to an explanation of the functional principle of the developed circuits. Furthermore, the software development process is outlined. This includes a description of the used software tools and environments and the applied algorithms. Finally, the implementation of the different modulation techniques and the corresponding coding schemes are discussed.

4.1 Development

In this section, the workflow of the development process is described as well the used software tools.

4.1.1 Development Workflow

Figure 4.1 provides an overview of the workflow of the development process. The most important components are described in more detail.

Hardware Development (Optical Beacon)

The first step is to develop a hardware component that is able to receive and demodulate infrared light pulses of the ToF camera. Therefore, the correct hardware components need to be chosen and the circuit has to be built. After verification, the circuit needs to be connected to the Atsam microcontroller.

For the hardware component which controls the sending unit, the existing circuit of the Thesis [44] is used. It contains a phase-shifter whose output controls the switching mechanism of the IR LED. This circuit is also connected to the Atsam microcontroller.

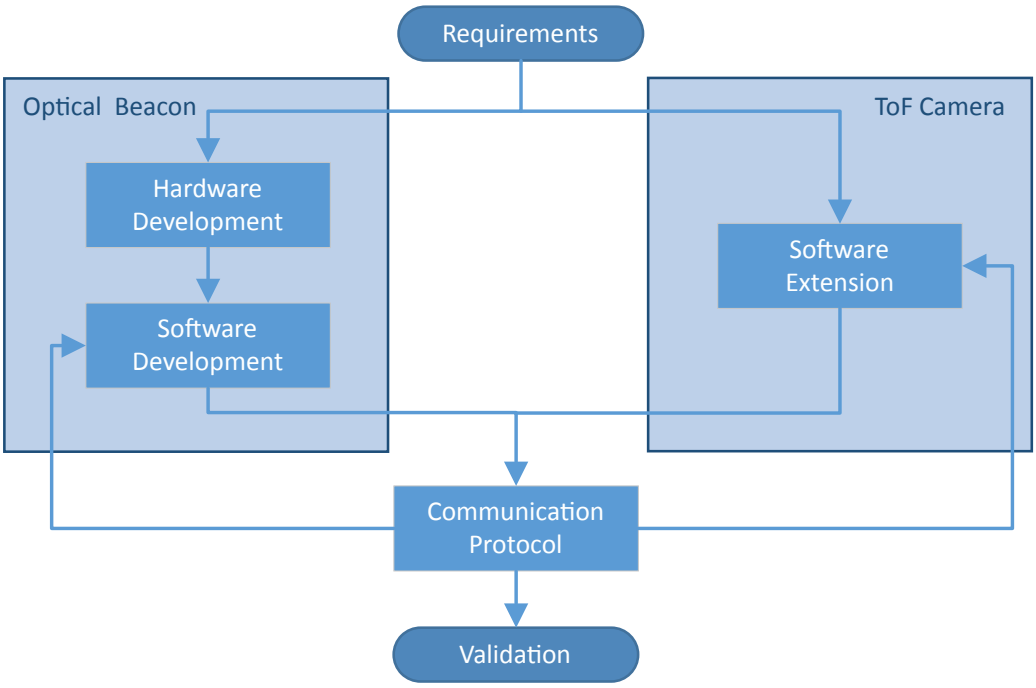

Figure 4.1: Workflow of the development process.

Software Development (Optical Beacon)

The control unit of the Optical Beacon is the Atsam microcontroller. On the one side, it controls several hardware components of the sending and the receiving circuit which provides a proper modulation and demodulation of the outgoing and incoming signals. On the other side, the Atsam decodes and encodes messages and handles received instructions. Additionally, the Atsam is able to synchronize with the ToF camera, which is a requirement to allow communication from the Optical Beacon to the ToF camera, as explained in Section 3.7.2.

Software Extension (ToF Camera)

The existing code of the ToF camera has to be extended to give the ToF sensor transmitting and receiving capabilities. For the sending unit, DPPM modulation has to be implemented, while PLQPSK modulation is implemented for the receiving unit. Furthermore, a coding scheme for encoding and decoding is developed.

Communication Protocol and Validation

A simple protocol is developed to fulfill the requirements described in Section 3.9. The system should be evaluated with different lighting conditions and different distances between ToF camera and Optical Beacon. Hence, the reliability and robustness of the system should be determined. Therefore, the necessary testing software has to be implemented.

4.1.2 Environment and Tools

In order to develop a system which consists of different hardware modules, several software tools and developing environments are used. These are Xilinx SDK, Atmel Studio and Matlab.

Atmel Studio

Atmel Studio [45] is a free development environment based on Visual Studio to program Atmel microcontrollers. It consists of project management, an editor, a debugger and tools to write on the microcontroller. As programming language, Assembler, C and C++ are supported. Furthermore, it includes the Atmel Software Framework (ASF). ASF simplifies the programming since it offers an abstraction to the hardware layer. Each hardware component that is used has to be manually imported via the ASF Wizard.

For this project, Atmel Studio is used for the programming and debugging of the two ATSAMD21J18A microcontrollers. With this tool, the modulation and demodulation unit, the encoding and decoding unit and the data processing are implemented. Furthermore, the hardware controller (gain controller, controller for a correct reference voltage V_{ref}, control of GPIO pins) are developed with Atmel Studio.

Matlab

Matlab, a short form for *matrix laboratory*, is a powerful desktop environment for numerical computing and visualization [46]. Matlab is a proprietary programming language developed by MathWorks. It offers several functions for data analysis and simulation, like different plotting functions, matrix manipulations and many other mathematical operations. Beyond that, it provides a wide range of toolboxes, for example for neural networks, control systems, signal processing, audio systems, computer vision, etc.

For this thesis, Matlab is used to interface with the ToF camera over an UART interface to allow debugging. Data that is captured by the ToF camera is analyzed and visualized with Matlab. It is also possible to transmit and visualize complete images and hence generate a live stream of the camera.

Xilinx SDK

Xilinx SDK is an integrated Design Environment based on Eclipse for programming Xilinx microprocessors. It is a complete IDE that comes with an editor, compilers, build tools, flash memory management and JTAG debug integration [47].

Xilinx SDK is used to develop signal processing and communciation software for an ARM Cortex A53 processor, which is embedded in the Xilinx Zynq 7000 platform. This work builds on an existing system, which uses an I2C bus and parallel data connection to control the ToF sensor with real-time system capabilites. The existing system was developed within the master thesis of Armin Schoenlieb [44], Christoph Ehrenhoefer [48]

and the work of Plank et al. [34]. The programing language is C++. With this tool chain, the sending and receiving unit of the ToF camera is implemented.

4.2 Overall System Architecture

Figure 4.2 illustrates the general structure of the communication system. The ToF camera

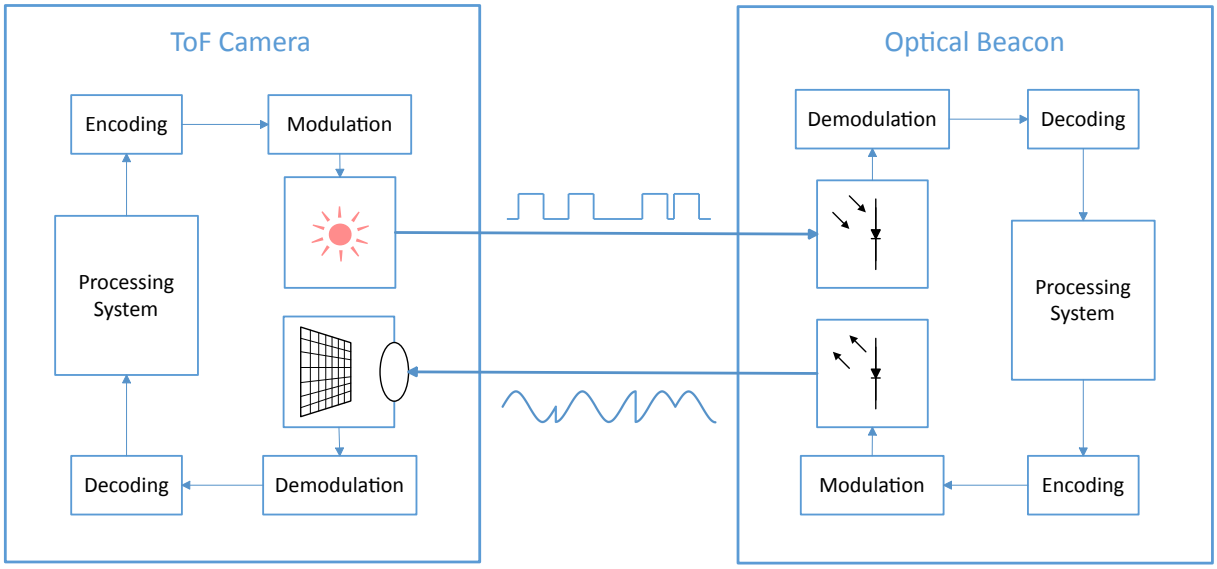

Figure 4.2: System architecture illustrated for the ToF camera and for the Optical Beacon. For communication from the ToF camera to the Optical Beacon, DPPM is used. For the other direction, PLQPSK is deployed.

consists of a processing system which processes data and controls the sending and receiving unit. In order to send data to the Optical Beacon, the ToF camera encodes the message in the first step and then modulates the information on the emitted light pulses of the illumination unit with DPPM. For the receiving procedure, the captured light emitted by the Optical Beacon is first demodulated (via PLQPSK) and then decoded to extract the message. The Optical Beacon consists of optical sending and receiving units and a processing system. In this case, the sending unit is an infrared LED and the receiving unit is a simple photo diode. In the next two sections, all components of the ToF camera and the Optical Beacon and their implementation are explained in detail.

4.3 Hardware Development of the Optical Beacon Platform

This section deals with the hardware implementation of the Optical Beacon platform. This includes the choice of the selected hardware components, their cooperation in a circuit and the functional principle. Figure 4.3 shows the setup of the Optical Beacon.

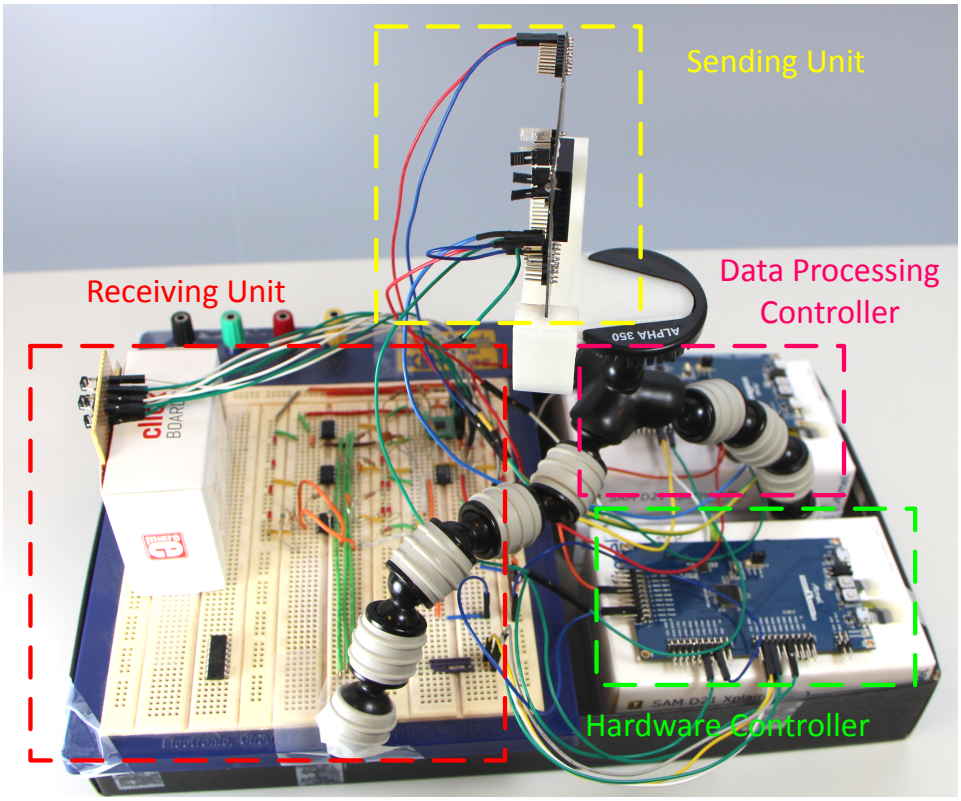

Figure 4.3: Hardware setup of the Optical Beacon.

4.3.1 Hardware Components for the Optical Receiving Unit

As explained in Section 3.3.2, the Optical Beacon consists of a photo diode, a low-pass and a high-pass filter, an amplifier, a comparator and a microcontroller. These components and their implementation are explained in this section.

Photo diode

In this project, a Silicon PIN photo diode with daylight filter (*BPW 34 FA*) is used in order to receive the signals of the ToF camera. Its optical filter is optimized for wavelengths between 730 nm and 1100 nm and reaches its maximal sensitivity at a wavelength of 880 nm. Since the infrared light of the ToF camera has a wavelength of 850 nm, the filter is placed in a perfect range to let the light of the ToF camera pass and filter ambient light. The maximal switching time is 20 ns and hence allows a switching frequency of 50 MHz. The photo diode provides a large field-of-view with a half angle of $\pm 60°$. In order to reach a higher field-of-view, four photo diodes are used in parallel to capture the ToF signal instead of one photo diode.

Digital Potentiometer

As explained in Section 3.3.2, one of the two resistors which form the relation for the amplification is replaced by a digital potentiometer. A *MCP4161* is used which provides a resistance in the range of 0 to 50 kΩ. The resistance is set by the microcontroller via SPI.

Comparator

The decision for the choice of an appropriate comparator focuses on the speed of the comparator. The comparator has to detect the light pulses which are emitted by the ToF camera. These light pulses will have a minimal duration of 5 μs. Within this duration, the comparator has to detect the rising edge and pull its output to high. Then, the digital input pin of the microcontroller, connected to the output of the comparator, needs to detect that the signal has switched from low to high. Finally, the interrupt which results from the logic high at this digital input pin has to be processed by the interrupt handler of the microcontroller and call the corresponding callback. Hence, the response time of the comparator has to be fast enough that the microcontroller has enough time to detect the rising edge and fire the corresponding callback before the pulse is over. In order to fulfill the requirement of a fast response time, the comparator *LT1011* is chosen. It has a response time of typical 150 ns and maximal 250 ns.

Cascading Active High-pass Filters

In order to amplify the signal generated by the photo diodes, an *ADA4891* is used. This is a low cost, high speed rail-to-rail amplifier. A side effect of high amplification is that not only the desired signal, but also disturbances are amplified. If disturbances occur in a frequency range that can pass between the high-pass and low-pass filter and are amplified with high gain, these disturbances can be barely distinguished from a DPPM signal. Hence, a structure of cascading active high-pass filters is implemented. It can be seen in Figure 4.4. The gain and cut-off frequency of the first active high-pass filter are chosen in such a way that the diode signal is amplified enough to allow a reliable sampling for the comparator while disturbances are filtered. It is an additional benefit for sampling that the edges of the pulses become steep. If the signal strength of the signal decreases, as it is illustrated by the blue line in Figure 4.5a, the pulse becomes too low for sampling. If the gain was now further increased to amplify the signal even more, also disturbances would be amplified. Instead, the output of the first active high-pass is fed to a second one. This is illustrated by the green line in Figure 4.5a. Gain and cut-off frequency of the second active high-pass filter are again chosen in order to only amplify the diode signal and filter disturbances. Finally, the output of the second active high-pass filter is connected to the input of a third one (yellow line in Figure 4.5a). Table 4.1a to Table 4.1c show the chosen parameters for the amplifiers and high-pass filters and the resulting gains and cut-off frequencies. Each cut-off frequency f_c is calculated with Formula 4.1:

$$f_c = \frac{1}{2\pi RC} \tag{4.1}$$

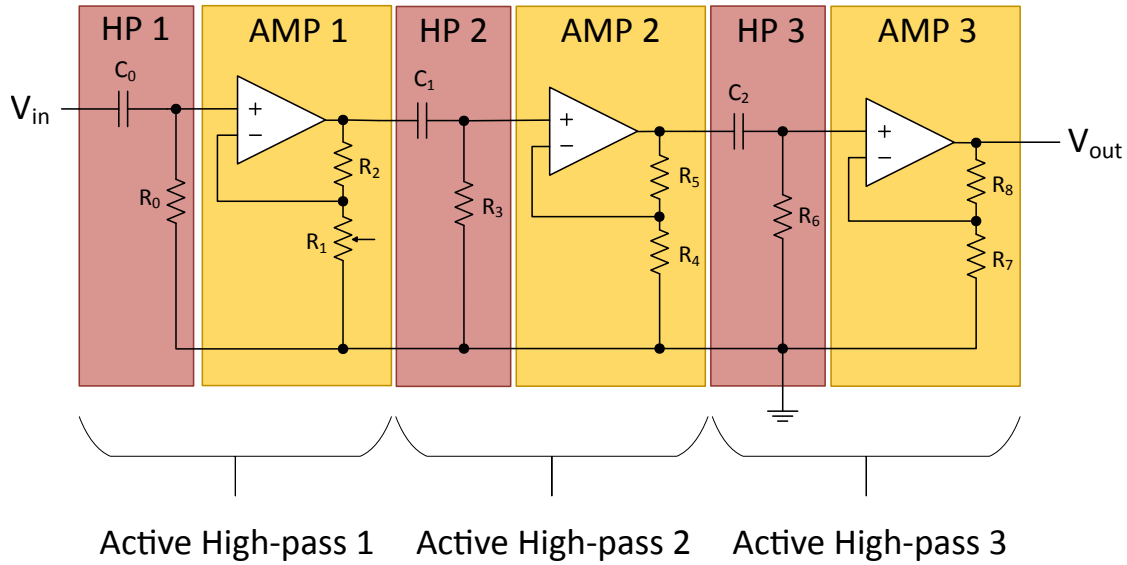

Figure 4.4: Structure of cascading active high-pass filters. The diode signal is amplified while disturbances are filtered.

The first capacity C_0 comes from the internal capacities of the four diodes. Each photo diode has an internal capacity of 72 pF which results in a total capacity of 288 pF since parallel capacities are added together (Formula 4.2).

$$C_{total} = C_1 + C_2 + ... + C_n \tag{4.2}$$

Figure 4.5a demonstrates the signal of the diodes with low signal strength as it occurs at

Amplifier 1			High-pass 1		
R_1	R_2	A	C_0	R_0	f_c
$k\Omega$	$k\Omega$	-	pF	$k\Omega$	kHz
0-50	110	3,2 - 100	288	8.2	67

(a) Active high-pass filter 1

Amplifier 2			High-pass 2		
R_4	R_5	A	C_1	R_3	f_c
$k\Omega$	$k\Omega$	-	pF	$k\Omega$	kHz
51	110	3,1	680	15	15

(b) Active high-pass filter 2

Amplifier 3			High-pass 3		
R_7	R_8	A	C_2	R_6	f_c
$k\Omega$	$k\Omega$	-	pF	$k\Omega$	kHz
46	560	13	680	46	5

(c) Active high-pass filter 3

Table 4.1: Component values for the cascading active high-pass filters.

a higher distance or if an obstacle is in the line of sight. The result is that less photons arrive at the photo diodes and hence less current is produced. Less current results in less voltage at the parallel resistance next to the photo diodes. The blue line refers to the

output of the first active high-pass, the green to the second and the yellow line to the output of the third active high-pass. Figure 4.5b demonstrates the three outputs with a good signal strength of the input signal.

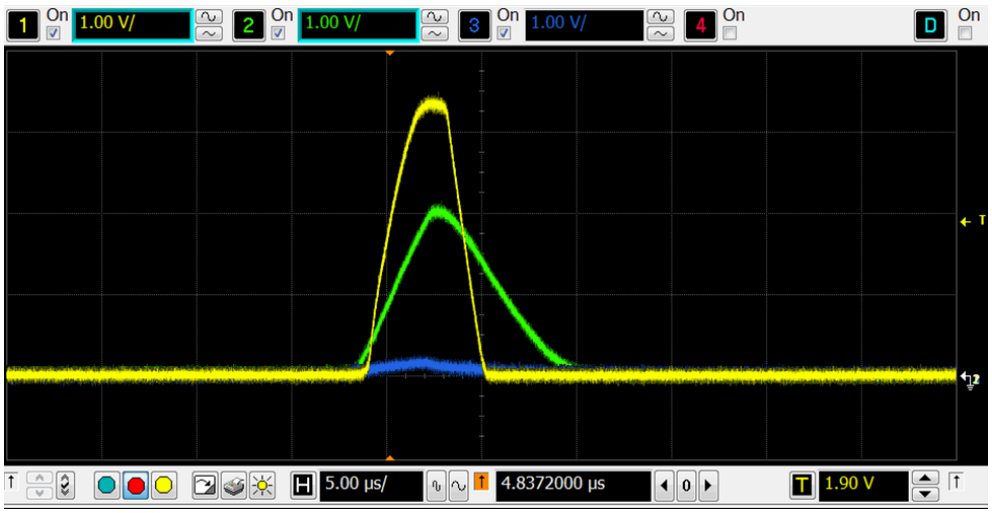

(a) Amplification outputs of a signal with low signal strength.

(b) Amplification outputs of a signal with good signal strength.

Figure 4.5: Demonstration of the three output signals of active high-pass filter 1 (blue line), 2 (green line) and 3 (yellow line).

High-Pass Filter - Cut-Off Frequency

Considering the optical channel between ToF camera and Optical Beacon, two different kinds of light disturbances can be distinguished. The first occurs when the amount of ambient light increases. Here, the distance between ambient light and the peak of the light pulse of the ToF camera, thus the SNR, decreases. This is demonstrated in Figure

4.6b. In order to provoke this effect intentionally, a halogen light is used and placed near the the optical channel. The problem with an increased ambient light manifests in too many photons reaching the photo diode. The second light disturbance occurs when the incoming ambient light rapidly decreases. This effect can be achieved by disturbing the optical channel; for this project, an obstacle is placed in the line of sight and thus weakens the light signal which is emitted by the ToF camera.

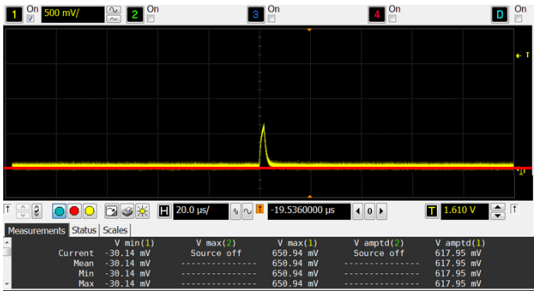

(a) No light disturbance. The high-pass filter suppresses the ambient light and thereby removes the DC component of the signal.

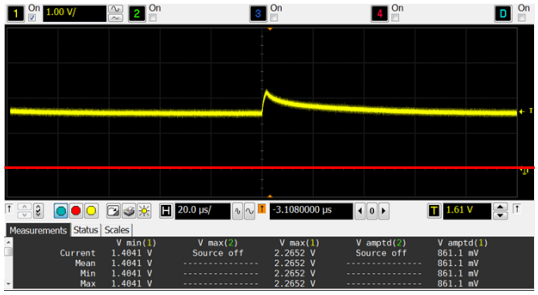

(b) Disturbance produced by an increased ambient light. The ambient light cannot be filtered completely and leaves a DC component.

Figure 4.6: A light pulse measured at the photo diode. The red line marks 0 V to illustrate the DC component on the right side. On the left side, the DC component is completely filtered by the high-pass.

In order to counteract disturbances produced by increasing light strength, the cut-off frequency f_c of the high-pass filter may be chosen high enough to filter the DC component and maximize the SNR. In the case that an obstacle weakens the signal while the cut-off frequency is of a high value, the amplitude of the pulse shrinks and the edges flatten. In this case, the flat edges of the signal will not be able to pass the high-pass filter. To combat the problem of a weak signal when an obstacle blocks the line of sight, the cut-off frequency may be of a low value. In this case, more frequencies may pass the filter and hence the flat edges of the weak signal can pass. However, if now the ambient light increases, the DC component will increase since it cannot be filtered completely anymore and the distance between peak and DC component will decrease. A large portion of ambient light will result in a DC component that reaches the same voltage level as the light pulse and thus the light pulse cannot be distinguished from the ambient light anymore. An additional problem with this solution is that now also disturbances with high frequencies may pass the filter. In fact, a high cut-off frequency results in robust detection if the ambient light increases, but weak signals will not be able to pass the filter. In the other case, a low cut-off frequency allows the detection of even weak signals, but an increased ambient light cannot be handled and disturbances can pass the filter. The resulting detection quality depending on different signal shapes and cut-off frequencies is summarized in Table 4.2. As Table 4.2 illustrates, a middle cut-off frequency seems to be the best choice.

	Pulse Detection Quality with		
	low f_c	middle f_c	high f_c
weak signal	good	middle	bad
normal signal	middle	good	middle
signal with high DC component	bad	middle	good

Table 4.2: Overview of the detection quality depending on the cut-off frequency and signal shape (normal, weak signal or signal with high DC component).

Setup of the Microcontrollers

This thesis aims to show the feasibility of the proposed communication system. The result is a demonstrator and not a final system. When processing received data and controlling the hardware components, the microcontroller has to fulfill certain speed requirements explained in detail in Section 4.4.2. Thus, for simplicity, two microcontrollers are used instead of a single one, which divides the work in order to be fast enough.

Figure 4.7 illustrates the interconnection of the two micro controllers to the other hardware components. The first microcontroller, which is referred to as *Hardware Controller*, is responsible for the control of the different hardware components of the receiving unit. The second microcontroller, *Data Processing Controller*, has to perform modulation and demodulation, encoding and decoding, and it also needs to process the data which is received or transmitted. The connections are explained in the following list:

(a) V_{ref} is the threshold used by the comparator. If the input voltage is higher than the threshold, then the output of the comparator is high. Vice versa, if the input voltage is lower than the threshold, then the output is low. Thus, the comparator digitizes the diode signal.

V_{ref} is produced by the DAC of the first microcontroller. It is a single wire that outputs the voltage defined by the microcontroller.

(b) The signal *resistance* is used for the adjustable gain which is explained in Section 3.3.2. The connection uses SPI to transmit the resistance. Thus, *resistance* consists of the following wires: *SCLK*, *MOSI*, *MISO*, $\overline{SS}$.

(c) *diode_digitized* is the output of the comparator and is connected to a GPIO pin of each microcontroller. It corresponds to the digitized form of the diode signal. *diode_digitized* is a single wire which is either low or high. The first microcontroller (*Hardware Controller*) uses *diode_digitized* to control V_{ref}. The second microcontroller (*Data Processing Controller*) demodulates and decodes *diode_digitized* and processes the extracted data.

(d) *data* is a UART connection between the two microcontrollers to exchange information. It consists of two lines, R_x and T_x.

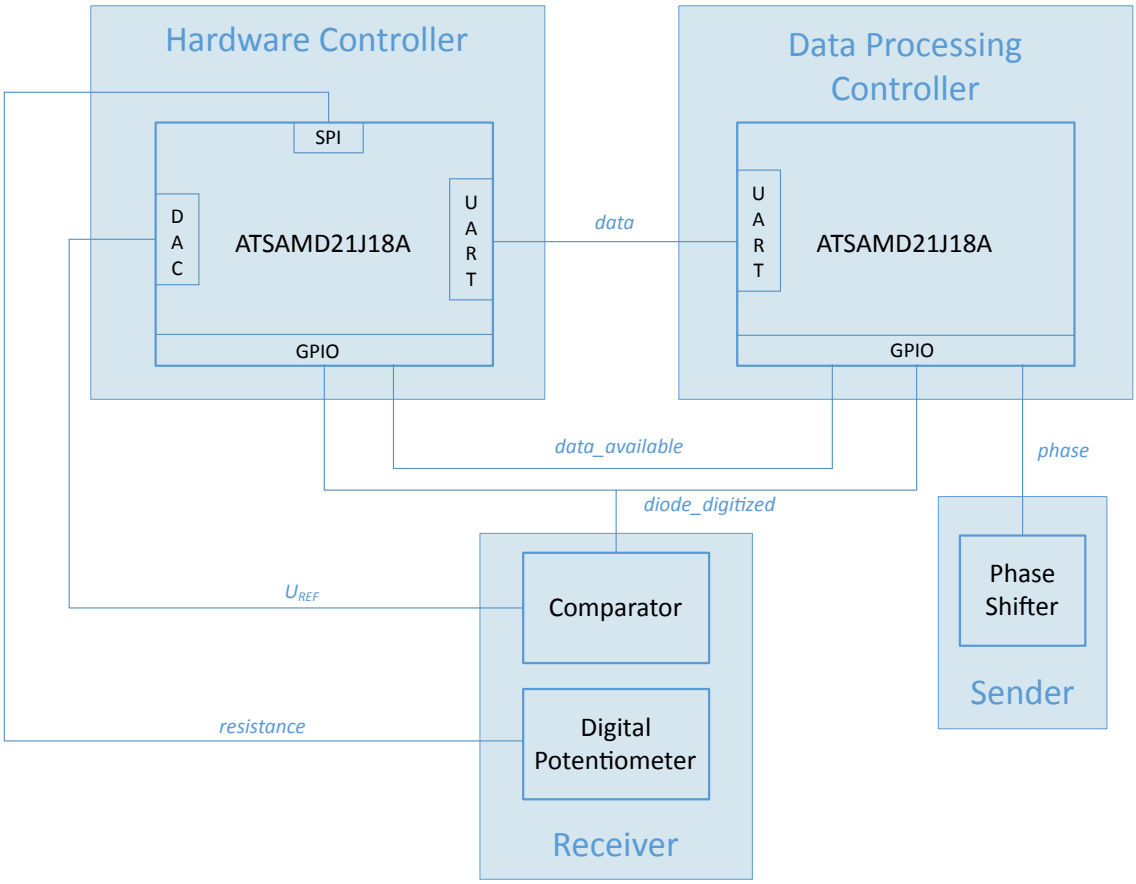

Figure 4.7: Interconnection of the hardware components of the Optical Beacon.

(e) *data_available* is a signal which indicates if data is available on the UART connection. It connects each a GPIO pin of the two microcontrollers. A read operation with UART is blocking and thus keeps the microcontroller that wants to read from working until data is available on the data line. Thus, *data_available* is used. The microcontroller begins to read only if the signal is set to high.

(f) *phase* is used to tell the phase-shifter which phase_{plqpsk} shift should be outputted. Three GPIO pins are required to control the output of the multiplexer inside the phase-shifter.

4.3.2 Hardware Components for Sending Unit

The centerpiece of the sending unit was developed in the context of Armin Schoenlieb's master thesis [44]. This section describes the hardware components that are selected and placed on the board.

IR LED

The IR LED *SFH 4715S* is placed on the board as light source for the sending part of the Optical Beacon. The *SFH 4715S* provides high efficiency and has a centroid wavelength of 850 nm. Since the ToF camera expects a wavelength of 850 nM, it is placed in an ideal range. A heat sink is placed on the backside of the LED to dissipate heat.

Oscillator

As clock source a *HC-49/U* crystal oscillator is chosen. It has a tolerance of of 30 ppm at 25°C which results in 780 Hz. Since the ToF camera and the Optical Beacon both use this crystal oscillator, the total frequency difference between them can reach 1560 Hz in the worst case.

4.4 Software Development for the Optical Beacon Platform

This section deals with implementation details about the software regarding the Optical Beacon. The microcontroller is described which is responsible for the control of the different hardware components (*Hardware Controller*) as well as the other microcontroller that processes the received signals and handles the extracted information (*Data Processing Controller*).

4.4.1 Hardware Controller

This section describes the software implementation for the microcontroller that is responsible for controlling the hardware components. This includes a PID controller for regulating the threshold of the comparator, a gain controller that changes the amplification of the received signal dynamically and a UART communication to the Data Processing Controller.

PID Controller for Thresholding

Since DPPM is used as modulation technique for the communication link from the ToF camera to the Optical Beacon, information is modulated into the pause durations between pulses. For the following considerations, the pulse and pause duration is constant. If the signal strength of the received signal increases or decreases, the waveform of the received pulses changes. This may happen when the distance between sender and receiver changes for example. The change of the signal's waveform causes a change of the measured pulse duration if the reference voltage of the comparator is kept constant. This effect is illustrated in Figure 4.8. The red line represents a received pulse of lower signal strength and the blue line a pulse with higher signal strength. From the point of view of the ToF camera, both pulses and pauses have the same duration. If the blue and red pulses are now compared with respect to the reference voltage U_{ref1}, the measured pulse durations t_{pulseA} and t_{pulseB} are not the same. Unfortunately the pause durations are influenced by

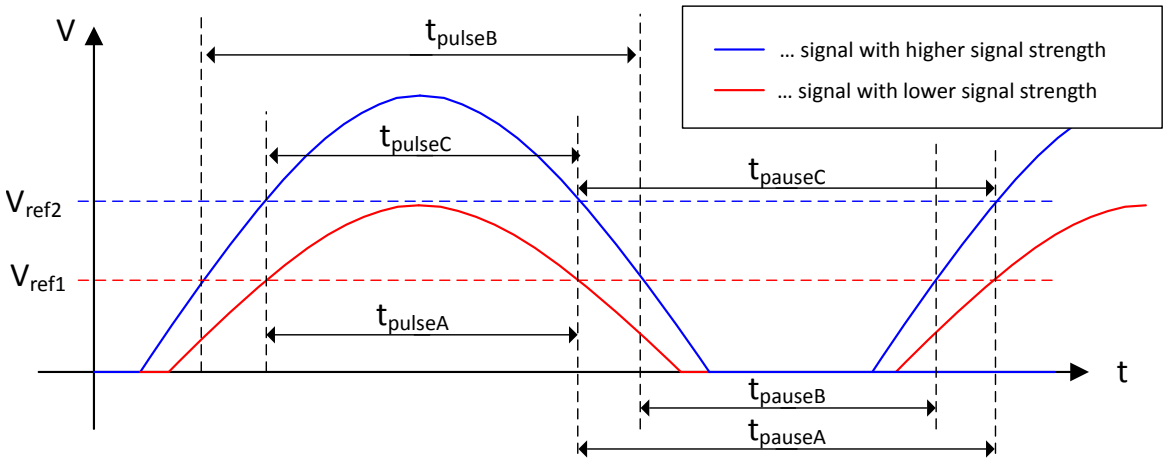

Figure 4.8: Illustration of the impact of varying signal strengths on the measured pulse duration t_{pulse}. The blue line shows a light pulse with high and the red line a pulse with a low signal strength. In order to measure the same pulse lengths for pulses of different intensity, the reference voltage V_{ref} has to be increased/decreased.

this effect as well, as can be seen with t_{pauseA} and t_{pauseB}. Under such circumstances, the signal can not be demodulated and decoded unambiguously with respect to DPPM.

A solution for this problem is to vary the reference voltage. In Figure 4.8, if the reference voltage is increased to the level of U_{ref2}, the measured pulse t_{pulseC} has the same duration as t_{pulseA}. Thus, a controlling mechanisms is implemented that regulates the reference voltage at runtime to keep the ratio between pulses and pauses constant and hence allows unambiguous demodulation and decoding. Therefore, the microcontroller for hardware controlling operates as PID controller to fulfill this requirement. It measures the pulse duration of incoming pulses and tries to keep them constant. If the duration is too high or low, the output is changed to counteract this drift. The mathematical principle of a PID controller is depicted in Formula 4.3.

$$v(t) = \underbrace{K_p e(t)}_{P} + \underbrace{K_i \int_0^t e(\tau)d\tau}_{I} + \underbrace{K_d \frac{de(t)}{dt}}_{D} \tag{4.3}$$

v(t) is the calculated output, hence the new reference voltage. $K_p e(t)$ describes the proportional part of the PID controller. The error e(t) is the difference between the current duration and desired duration and is multiplied by the proportional coefficient K_p. While e(t) accounts for present error values, the integral part $K_i \int_0^t e(\tau)d\tau$ sums up the errors over time and drives the error to zero. K_i is the integral coefficient. Finally, the derivative part $K_d \frac{de(t)}{dt}$ adjusts the speed of the system response and is controlled by the derivative coefficient K_d.

A configuration phase is employed before starting the communication, since the microcontroller has to determine a setpoint for the pulse duration which acts as setpoint for the PID controller. It is assumed that the signal has a good signal strength in the configura-

tion phase and thus the peak of the pulse spreads over the complete voltage range of 3.3 V. In this case, the reference voltage is set to half of the voltage range because now it has a considerable scope to rise and fall if the signal strength changes. Now, the microcontroller measures 50 pulses and calculates the average of these durations. This average value acts as the desired setpoint for the PID controller.

Adjustment of Reference Voltage V_{ref}

The reference voltage V_{ref} is set via DAC. Therefore, the DAC pin of the microcontroller is connected to the threshold pin of the comparator. The DAC is a 10 bit converter. Hence, a desired voltage value V_{dac} has to be transformed to its 10 bit representation N_{dac} with Formula 4.4 and can then be set by the microcontroller.

$$N_{dac} = \frac{2^{10}}{3.3V} \cdot V_{dac} = \frac{1024}{3.3V} \cdot V_{dac} \tag{4.4}$$

UART Communication

As mentioned in Section 4.4.1, the hardware controller determines a setpoint $t_{setpoint}$ for the pulse duration that is controlled by the PID controller. This pulse duration must be known by the Data Processing Controller in order to demodulate and decode incoming signals. Hence, $t_{setpoint}$ is transmitted via UART.

The receive R_x and transmit T_x pins of the microcontrollers are connected inversely. Additionally, each a GPIO pin of the microcontrollers is connected and serves as a line that notifies if data is available (*data_available*). When the hardware controller has determined $t_{setpoint}$, it writes this data via UART and pulls *data_available* to high. When the microcontroller for Data Processing detects that *data_available* was pulled to high, an interrupt is fired. In the routine, which belongs to this interrupt, the UART read function starts and thus the data ($t_{setpoint}$) is received.

Gain Controller for Amplification

As already mentioned in Section 4.4.1, a change of the signal strength results in a change in the waveform of the received signal. It may occur that the waveform changes so much that no reference voltage can be found by the PID controller to achieve the desired pulse duration. For example, when the signal strength decreases and the voltage peak of the pulse shrinks, the resulting pulse duration may be too low even if V_{ref} is set to the broadest part of the pulse. This is illustrated in Figure 4.9. Here, the blue curve represents a pulse detected by the photo diodes with good signal strength. Its pulse length with respect to the reference voltage V_{ref} is the setpoint $t_{setpoint}$. The red solid wave shows a pulse of lower signal strength. Now, even if V_{ref} is set to the lowest voltage level, the resulting pulse duration will be too low since the complete pulse is smaller than the desired duration $t_{setpoint}$.

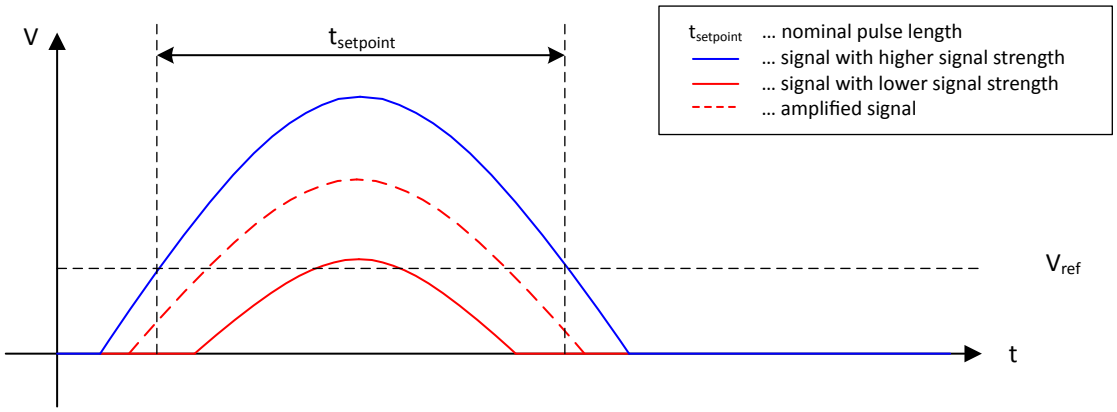

Figure 4.9: The blue curve represents the waveform of a detected pulse with good signal strength while the red solid curve is a pulse with lower signal strength. For the weaker signal, there is no voltage level for the reference voltage V_{ref} to achieve the nominal pulse duration $t_{testpoint}$. Hence, the signal with low signal strength is amplified to achieve the desired pulse length. This amplified signal is illustrated by the red dashed curve.

In order to tackle this problem, the waveform of the signal is controlled in such a manner that it is possible at any time to set a reference voltage resulting in the desired pulse length. This is achieved by varying the gain at runtime. In the example of Figure 4.9, the gain is increased and thus the peak of the signal with low signal strength is blown up. The gain is increased until a V_{ref} can be set where the desired pulse length is reached. This is illustrated by the dashed red curve in Figure 4.9. This gain adjustment is controlled by the microcontroller and set to the digital potentiometer via SPI. If the signal peak shrinks and V_{ref} deceeds a certain threshold, then the gain of the amplifier is increased. Conversely, if V_{ref} exceeds a certain voltage level, the gain is decreased.

4.4.2 Data Processing Controller

The data processing controller is responsible for demodulating and decoding incoming signals emitted by the ToF camera. Furthermore, it controls the sending unit. This section describes the necessary software implementation for this microcontroller.

Demodulation Unit

Since DPPM is used for the communication direction from the ToF camera to the Optical Beacon, information which has been modulated into the pauses of the signal has to be extracted. Thus, the microcontroller has to determine the durations of the pauses between pulses.

In order to determine the duration of a pause, the time between a falling and rising edge has to be measured as described in Section 3.3.4. Therefore, the output of the comparator is connected to a GPIO pin of the microcontroller. Two interrupts are installed for this

GPIO, one for a falling and one for a rising edge. In the routine for a falling edge, the current time in clock ticks is read out via TC and stored in the variable $t_{falling}$. In the routine for a rising edge, the time is read out again and stored in t_{rising}. The difference of the two stored time values represents the duration of a pause in clock ticks. In order to achieve a time in seconds t_{pause}, the result of the subtraction has to be divided by the CPU clock:

$$t_{pause} = \frac{t_{falling} - t_{rising}}{48MHz} \tag{4.5}$$

It has to be considered that code which is executed in an interrupt routine has to be fast enough to be handled before the next interrupt occurs. An average pulse duration is about 5 μs, hence the execution of the routine for the rising edge needs to be finished before the routine for the next falling edge is called. Otherwise, since the microcontroller does not support multi-processing, the routine for the falling edge is only executed after the routine of the previous rising edge has finished. This means, that the routine for the falling edge is called too late and hence the measurement of the following pause duration will not be correct.

In Section 3.7, it was explained that it is useful for a q-ary system to use more than one symbol per codeword for a $M > 32$. For this project, a number of 64 codewords is desired. As Figure 3.10 shows, with $M = 64$, the highest channel capacity can be achieved with q is 8, 16 or 32. Hence, $q = 8$ will be used and thus $N = log_q(M) = log_8(64) = 2$. In the first step, a set of valid pause times (= symbols) has to be determined. This is done with Formula 4.6 and happens in the configuration phase.

$$pause_i = \frac{1}{133MHz} \cdot 1024 \cdot (x_{pause} + i) \cdot \Big|_{0 <= i < q=8} \tag{4.6}$$

x_{pause} refers to the parameter for the pause time which is set at the ToF camera as it is described in Section 3.4.2. Further, a set of codewords CW has to be generated based on different permutations of these symbols. If now a pause time $pause$ is measured, it has to be classified to the corresponding $pause_i$ and thus matched to the appropriate symbol. Therefore, it is tested if $pause$ fits into any valid range of a $pause_i$. A valid range is defined by:

$$pause_i - t_{threshold} <= pause <= pause_i + t_{threshold} \tag{4.7}$$

$t_{threshold}$ is determined by Formula 4.8. It is the half of a pause duration. This algorithm which matches a measured pause time to a symbol is illustrated in Figure 4.10.

$$t_{threshold} = \frac{x_{pause}}{2} \cdot \frac{1}{133MHz} \cdot 1024 = \frac{1}{2} \cdot \frac{1}{133MHz} \cdot 1024 \tag{4.8}$$

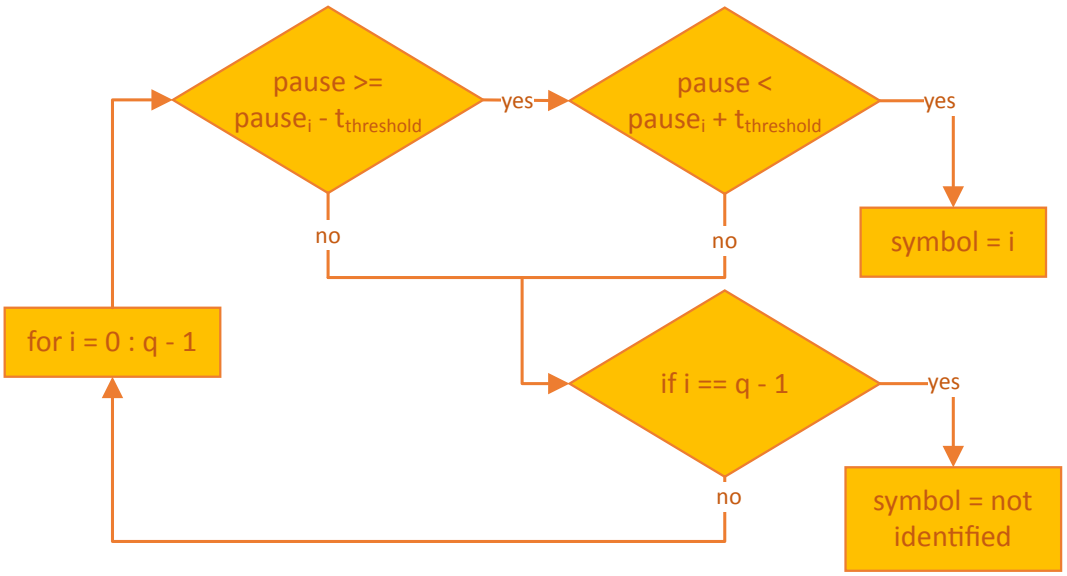

Figure 4.10: Illustration of the algorithm to demodulate a symbol. If the measured pause duration *pause* can be assigned into a valid range of a symbol $pause_i$, then this $pause_i$ is the demodulated symbol. If no match can be found, *pause* could not be demodulated.

Decoding Unit

While the demodulation unit determines the durations of pauses and pulses and matches the pauses to symbols, the decoding unit has to interpret these symbols and decode the included information. Since $q = 8$ and $N = 2$, two symbols form a codeword. In order to simplify the identification, if a received and demodulated symbol refers to the first or second symbol in a codeword, two different pulse times are used, $pulse_1$ and $pulse_2$. Now, if the pulse time before a symbol refers to the duration $pulse_1$, the symbol is the first symbol of a codeword. If a pulse with duration $pulse_2$ is detected before a symbol, the symbol refers to the second symbol of the codeword. This allows further error detection capabilities. If two pulses $pulse_2$ arrive consecutively, hence two second symbols of a codeword are received subsequently, there was an error. The same applies when two consecutive $pulse_1$ are received.

$pulse_1$ and $pulse_2$ are calculated with Formula 4.9. *pulse_length* refers to the pulse length which was measured by the microcontroller for hardware controlling and transmitted by UART as described in Section 4.4.1.

$$pulse_i = pulse\_length + i \cdot \frac{1}{26MHz} \cdot 8 \Big|_{0 <= i <= 1} \tag{4.9}$$

The procedure to match a measured pulse time *pulse* to a corresponding $pulse_i$ is the same as for decoding pause times, but with the only difference that $t_{threshold}$ is the half of

a pulse time:

$$t_{pulse\_threshold} = \frac{x_{pulse}}{2} \cdot \frac{1}{26MHz} \cdot 8 = \frac{1}{2} \cdot \frac{1}{26MHz} \cdot 8 \tag{4.10}$$

The whole process from decoding the first pulse, first pause, second pulse and second pause is illustrated in Figure 4.11. A codeword is valid, if the combination of the first

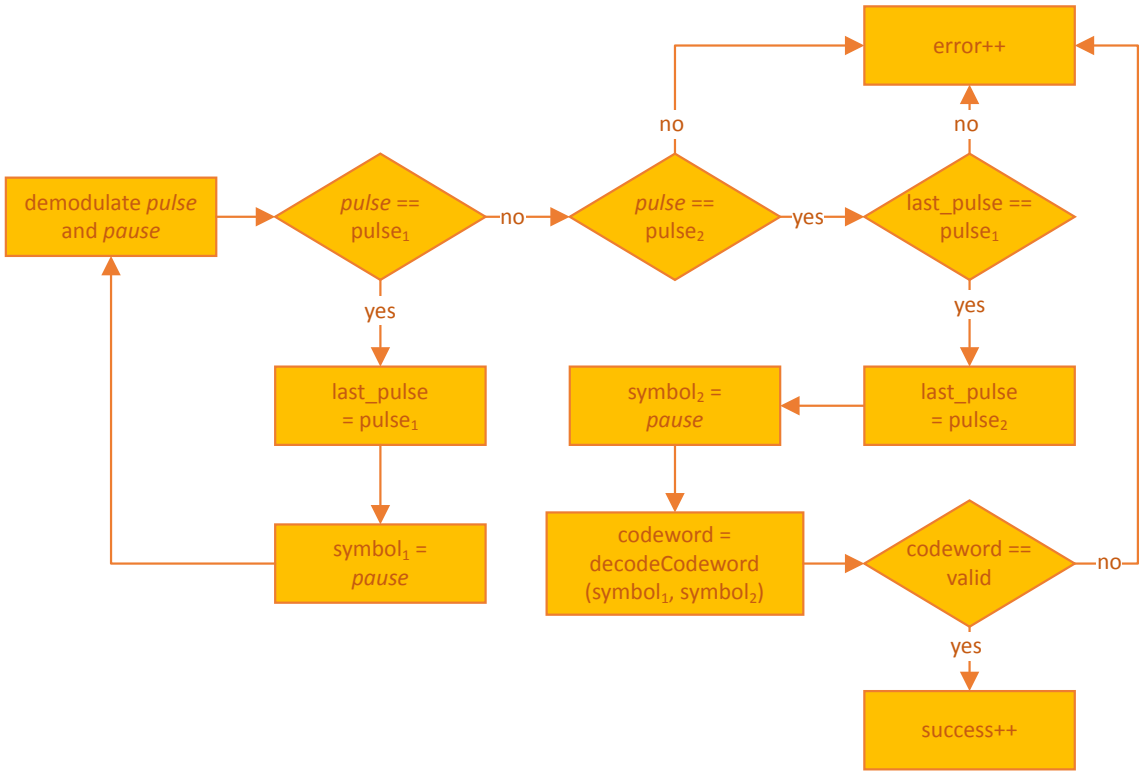

Figure 4.11: Illustration of the algorithm to decode a codeword. If a measured pulse refers to $pulse_1$, the following decoded pause forms the first symbol of the codeword. A decoded pause following on a pulse which matches to $pulse_2$ forms the second symbol. If the combination of $symbol_1$ and $symbol_2$ refers to a valid permutation inside the vector of possible codewords CW, the codeword can be decoded.

demodulated pause (symbol 1) and the second demodulated pause (symbol 2) is a valid permutation in CW.

Encoding Unit

As defined in the previous section, a number of 64 different codewords $M = 64$ is desired. Hence, the number of symbols per codeword $N = log_q(M) = log_4(64) = 3$. Since PLQPSK needs two carriers to modulate one symbol as it was explained in Section 3.6, six $phases_{plqpsk}$ have to be transmitted for a codeword made up of three symbols.

In order to encode a desired codeword, the corresponding permutation of the three symbols has to be found in *CW* by looking it up in a table. Then, each symbol of the codeword has to be sent twice. First, in its sine representation by transmitting the phase_{plqpsk} which belongs to this symbol and next by transmitting this phase shifted by 90° for the cosine representation.

Modulation Unit

The modulation unit has the task to modulate information into the light beam which is emitted by the IR LED of the sending unit. PLQPSK is used for the communication from the Optical Beacon to the ToF camera. As outlined in Section 3.7.2, $q = 4$ and the symbols are $\{0°, 90°, 180°, 270°\}$.

In order to select a certain phase_{plqpsk} of the phase-shifter, the desired output of the multiplexer has to be selected. This is achieved through three GPIO pins of the microcontroller, which are connected to the selection pins of the multiplexer. The multiplexer expects three lines because eight outputs are possible. Due to the fact that only four outputs are used for this project, two lines are actually necessary to select the corresponding phase_{plqpsk}. The third line is used to enable and disable the IR LED. If the most significant bit is set to high, an output > 4 is switched through. The four clock signals in different phases_{plqpsk} are only outputs $<= 4$, thus the outputs > 4 result in a constant low output and hence disable the IR LED. Vice versa, a low signal for the most significant bit indicates that an output $<= 4$ is selected and hence a valid clock signal is switched through which controls the IR LED and turns it on and off.

In order to transmit the six phases_{plqpsk} correctly which are required for one codeword, synchronization is required as it was explained in Section 3.8. The Optical Beacon starts to emit the first phase_{plqpsk} when the interrupt for a rising edge occurs since this indicates that the camera has just started to capture an image. When the next interrupt occurs, the next phase_{plqpsk} is selected from the phase-shifter and emitted.

4.5 Software Extension for the ToF System

This section describes the software implementation that allows the ToF camera to communicate with an Optical Beacon. This includes the necessary parts to enable modulation and demodulation as well as encoding and decoding.

4.5.1 System Overview

The communication unit of the ToF camera is implemented as state machine. The callback *onNewFrame* is executed every time a new image is captured. The ToF system implementation provides pointers to the raw data of the image as function arguments. There are three different states, *INIT*, *SEND* and *RECEIVE*. An overview is illustrated in Figure 4.12.

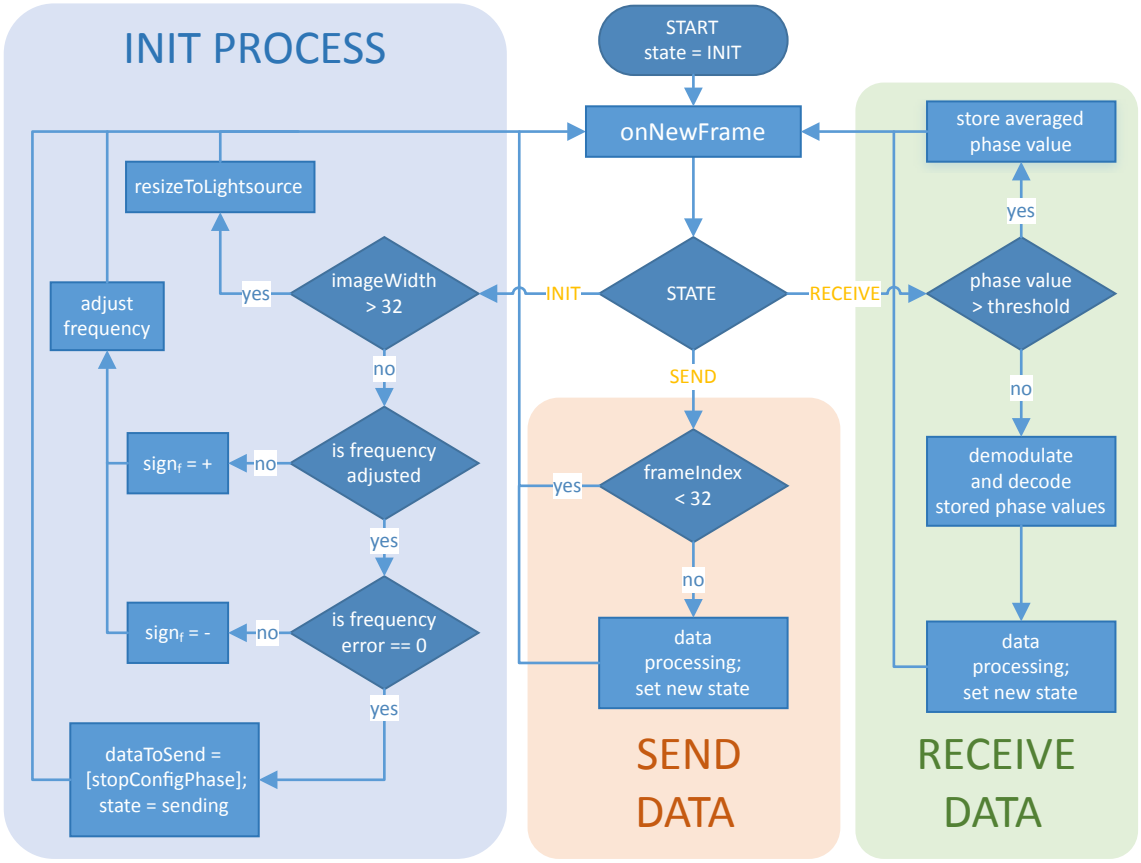

Figure 4.12: Overview of the software extension of the ToF camera to allow communication to an Optical Beacon. It is implemented as state machine which performs an initialization in the first step and is then able to send and receive data.

State INIT

The state *INIT* is selected at the startup and lasts until the configuration process between ToF camera and Optical Beacon has finished. In the start function, the full resolution (352 x 288 pixel) is set in order to detect the light source of the Optical Beacon. Then, it is determined, if a light source and thus an Optical Beacon willing to communicate is located inside the field of view. During this phase, the Optical Beacon has the IR LED turned on and sends with constant phase shift. If a light source is detected, the camera is reconfigured with 32 x 16 pixel resolution with a region of interest to the pixel position where the light source was located. The smaller resolution leads to faster read out. As a result, the faster capturing process allows to capture significantly more images per second and consequently increases the data rate.

The next important step in the initialization process is to synchronize the frequency as explained in Section 3.5.1. The goal is to decrease the frequency difference $\mathcal{F}_{error}$ between ToF camera and Optical Beacon as far as possible. Thus, $\mathcal{F}_{error}$ has to be determined. Since the Optical Beacon emits light with constant phase shift, it is safe to assume that

the captured phase_{tos} values are constant over time. But as outlined in Section 3.5.1, due to the frequency difference, the phases_{tof} oscillate in a sinusoidal fashion over time. Hence, enough phase_{tof} values are recorded so that several periods of this sinusoidal signal are captured. Here, a phase_{tof} value refers to an averaged phase value over the 32x16 pixel image. Then, the zero crossings of the signal are determined where the threshold $phases_{midrange}$ refers to the zero line. $phases_{midrange}$ is the mean of the maximum and minimum occurring phase_{tof} values:

$$phases_{midrange} = \frac{max(phases) + min(phases)}{2} \tag{4.11}$$

Each time when the signal crosses this threshold, a zero crossing is identified and the current time value $ticks_{current}$ is stored. Since $ticks_{current}$ is in CPU ticks, it has to be transformed to seconds:

$$t_{current} = \frac{ticks_{current}}{666666687} \cdot 2 \tag{4.12}$$

The time differences between every second zero crossing refer to a period duration. Finally, the inverse of the average of all measured period durations results in $\mathcal{F}_{error}$. This process is illustrated in Figure 4.13.

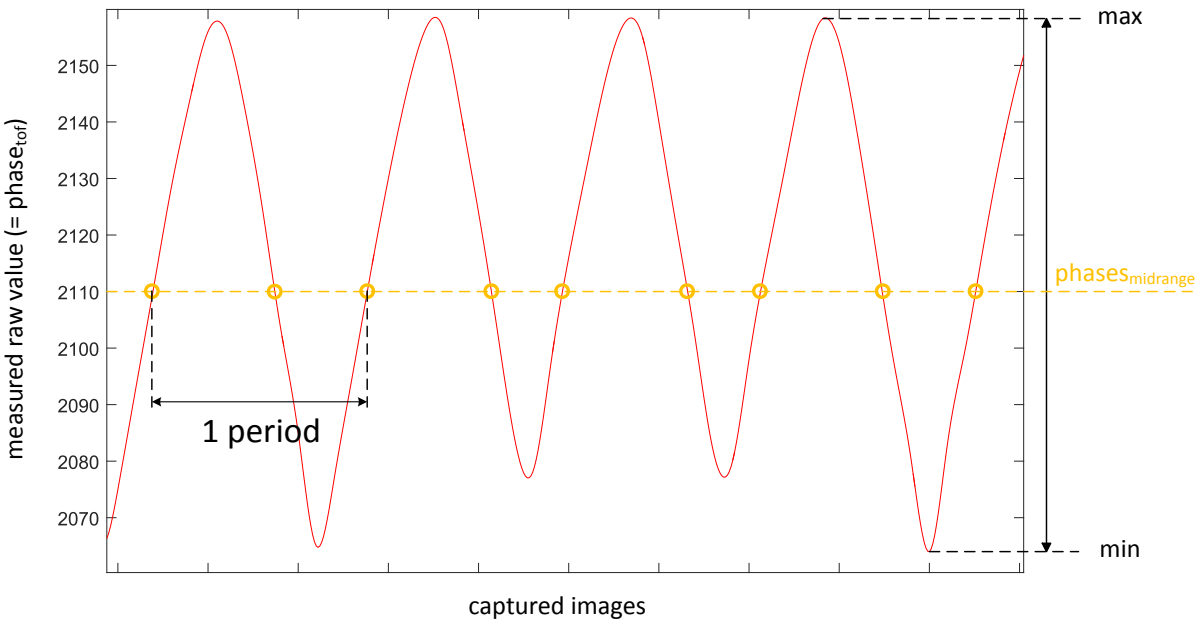

Figure 4.13: Plot of 50 measured and averaged phase_{tof} values which show the frequency difference $\mathcal{F}_{error}$ between ToF camera and the Optical Beacon. Although the Optical Beacon emits the same phase_{plqpsk} constantly, the measured phase_{tof} values at the ToF camera show a sinusoidal waveform.

Now that $\mathcal{F}_{error}$ is determined, it is known that the modulation frequency $\mathcal{F}_{mod}$ of the ToF camera is either too high or too low by $\mathcal{F}_{error}$. In order to find out, it is assumed that $\mathcal{F}_{mod}$ is too low and thus $\mathcal{F}_{mod}$ is increased by $\mathcal{F}_{error}$. With this new frequency, again $\mathcal{F}_{error}$ is determined. If $\mathcal{F}_{error}$ is now zero, the previous assumption was correct and the frequency of the ToF camera is now synchronized. Otherwise, if $\mathcal{F}_{error}$ is now larger than

before, the assumption was wrong. Obviously, $\mathcal{F}_{mod}$ is too high and thus will by decreased by $2 \cdot \mathcal{F}_{error}$.

Now that the camera can sample the modulated light source and the pixel reference frequency is adjusted to the Optical Beacon, the end of the configuration phase is reached. The ToF software changes its state to $SEND$ in order to transmit an instruction to the Optical Beacon to stop the configuration mode and turn off the IR LED.

State SEND

In the state *SEND*, the provided data is encoded, modulated and transmitted to the Optical Beacon. As mentioned in Section 3.9.2, a communication frame with a fixed size of 32 pulses and pauses can be defined. Thus, 32 symbols can be transmitted. As a result, the callback $onNewFrame$ will be executed 32 times. Therefore, in state SEND, 31 calls of $onNewFrame$ have to be ignored. Only at the 32^{nd} execution, the sending procedure has finished since the last pulse of the frame is reached. Now, it is decided how the state machine should continue. The state either remains *SEND*, if more data should be transmitted or changes to *RECEIVE*, if the camera should receive data from the Optical Beacon.

State RECEIVE

In the state *RECEIVE*, the camera captures images first and then demodulates and decodes the received data. Next, the decoded data is processed and it is decided how to continue. The state can either remain *RECEIVE* if more data shall be received or it can change to *SEND* if the camera wants to send data.

If the execution time of $onNewFrame$ is too long, a further call is missed and thus a captured image is lost. Hence, the measured phase_{tof} values are averaged and stored into a buffer in order to keep the execution time short. The received data is processed only after the last image was received. Now, the ToF camera has enough time to demodulate and decode the stored phase_{tof} values.

However, it is required to determine which phase_{tof} was the last of the transmission in order to know when to start with data processing. From the view of the Optical Beacon, after emission of the last phase_{plqpsk} it switches the IR LED off. This means, the ToF camera has to detect if the IR LED is on or off. This can be achieved by comparing the measured phase_{tof} value with a threshold. If it is higher than the threshold, the IR LED is on and thus the Optical Beacon is still transmitting. If the phase_{tof} value is beneath the threshold, the IR LED was turned off and the ToF camera can now start to demodulate and decode the stored phase_{tof} values.

4.5.2 Demodulation Unit

The demodulation unit has the task to classify a measured and averaged phase_{tof}, which is a value between 0 and 4095, to one of four phases_{plqpsk}, thus to a symbol. According to PLQPSK, each quadrant of the constellation diagram refers to one symbol.

Therefore, the phases_{tof} are first translated to achieve a placement of the phase_{tof} values in all four quadrants as described in Section 3.6. Next, two consecutive phases_{tof} are each combined to a point p_φ in the constellation diagram where the first value refers to the sine representation and hence to the imaginary part b and the second value to the cosine representation and thus to the real part a. Then, the angle φ is calculated. Since the C++ *atan2* function returns an angle in the range of [-π, +π], φ is calculated with:

$$\varphi = \frac{180}{\pi} \cdot \begin{cases} atan\left(\frac{b}{a}\right), & \text{if } b > 0 \\ atan\left(\frac{b}{a}\right) + 2\pi, & \text{otherwise} \end{cases} \tag{4.13}$$

$\frac{180}{\pi}$ is the conversion from radians, which is returned by the $atan2$ function, to degrees.

Definition of the Quadrants

In order to allow matching an angle φ to a quadrant, these quadrants have to be defined first. The first point P_1 results from the first two measured phase_{tof} values is determined as midpoint p_{q1} of the first quadrant. Since each quadrant has 90°, the range of the first quadrant Q_1 is defined as:

$$\varphi_{p_{q1}} - 45^\circ <= Q_1 <= \varphi_{p_{q1}} + 45^\circ$$

Now that the first quadrant is defined, the midpoint p_{q2} of the second quadrant is calculated. With respect to PLQPSK, its angle has to have an angle of 90° to p_{q1}. As soon as p_{q2} is known, the range of this quadrant can be defined in the same manner as for p_{q1}. Finally, p_{q3} and p_{q4} can be defined and also their ranges with the same procedure. This is illustrated in the left image of Figure 4.14.

Assignment of φ to a Quadrant

Now that all four quadrants are defined, the angle φ of a demodulated point can be classified to the corresponding quadrant:

$$\varphi_{p_{qi}} - 45^\circ <= \varphi <= \varphi_{p_{qi}} + 45^\circ \Big|_{1 <= i <= 4} \tag{4.14}$$

That i, for which this inequation is true, refers to the corresponding quadrant Q_i.

Impact of Frequency Difference $\mathcal{F}_{error}$

Although the modulation frequency of the ToF camera is adjusted in the configuration phase, the occurring phase drift can only be minimized to a certain degree but not eliminated. Now that the measured phases_{tof} are demodulated, the phase drift results in a

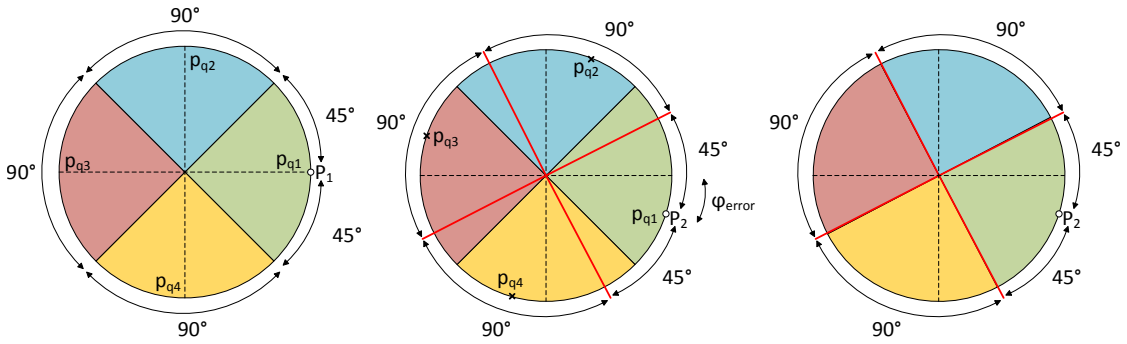

Figure 4.14: The left image illustrates how the four quadrants are defined based on the first demodulated point P_1. The middle image shows how the drifting angle occurring from the frequency difference between Optical Beacon and ToF camera can be controlled. After each demodulated point, all four quadrants are redefined based on the most recently demodulated point. In the right image, the redefined quadrants can be seen.

drifting angle φ. Under the assumption that the Optical Beacon again emits light with constant phase$_{plqpsk}$, the same angle should always be demodulated. Instead, the demodulated point p_φ will drift and thus the angle φ changes by φ_{error} over a certain time period. With respect to the constellation diagram, the demodulated point p_φ considered as phasor will rotate around the origin of the constellation diagram. Thus, a direct demodulation is not possible. The direction of rotation depends on whether the modulation frequency of the ToF camera is lower or higher than the frequency of the Optical Beacon.

In order to allow a correct demodulation, the definition of the quadrants is not fixed, instead rotate in circle based on the current error angle φ_{error}. Therefore, the drift of the angle φ_{error} is calculated first. φ_{error} is the deviation of the currently demodulated φ from the angle which belongs to the midpoint of the corresponding quadrant. Then, all midpoints are translated by φ_{error} in order to compensate the angle drift. This is illustrated in Figure 4.14 in the middle image. Then, in the same manner as described in Section 4.5.2, all four quadrants are redefined after each sample (right image in Figure 4.14). Now, a correct classification is possible as long as φ_{error} is smaller than 45°. Now that the phasor was classified to a symbol, it can be passed to the decoding unit.

4.5.3 Decoding Unit

Three symbols are each required to decode a codeword. Therefore, their combination in the right order is looked up in the table for all permutations CW and thus the correct codeword is obtained.

4.5.4 Encoding Unit

In order to send data from the ToF camera to the Optical Beacon, the desired data has to be encoded first. As outlined in Section 4.4.2, eight different symbols are used while

two symbols form a valid codeword. One symbol refers to one x_{pause} (explained in Section 3.4.2). The symbols are $\{18, 19, 20, 21, 22, 23, 24, 25\}$. The first symbol is 18 because values for $x_{pause} < 18$ cannot be performed by the camera. This means, even if x_{pause} is selected as smaller than 18, the real pause duration will last the same time as $x_{pause} = 18$.

Then, the encoding unit has to find the permutation in CW which corresponds to the desired codeword. When the correct pause duration $pause_1$ and $pause_2$ for this codeword are determined, the pulse times $pulse_1$ before $pause_1$ and $pulse_2$ before $pause_2$ have to be defined. For $pulse_1$, $x_{pulse} = 15$ and for $pulse_2$, $x_{pulse} = 25$ is chosen.

4.5.5 Modulation Unit

Now that data which should be sent to the Optical Beacon is encoded, it has to be modulated into the infrared light pulses of the ToF camera. As mentioned in Section 4.5.1, a frame of 32 different pulses and pauses can be defined. Hence, 16 codewords can be transmitted since two symbols are required per codeword. In the encoding unit, the corresponding pause times and pulse times have been defined. Now, these times have to be used to modulate the frame which will be emitted by the illumination unit. Therefore, a buffer of size 32 is filled with all encoded pause times and another buffer of size 32 is filled with all pulse times. Then, the content of the two buffers are written into the corresponding configuration registers of the ToF camera.

4.6 Coding

This section shows excerpts of the permutation tables CW that form the sets of codewords for PLQPSK and DPPM.

4.6.1 PLQPSK

Table 4.3 shows the set of codewords CW for PLQPSK. As already defined, the number of codewords M is 64, four symbols are used ($\{0°, 90°, 180°, 270°\}$) and thus three symbols are required to form a codeword. It was further explained that PLQPSK needs two carriers to transmit a codeword, hence two phases shifted by 90° are necessary to transmit one symbol. Table 4.3 illustrates an excerpt of the permutations in logical representation as well as expressed by their real phase representations.

codeword	logical representation			phase representation						information
	s_1	s_2	s_3	s_1	s_2	s_3	s_4	s_5	s_6	
1	0	0	0	0°	90°	0°	90°	0°	90°	’0’
2	0	0	1	0°	90°	0°	90°	90°	180°	’1’
3	0	0	2	0°	90°	0°	90°	180°	270°	’2’
⋮	⋮	⋮	⋮	⋮	⋮		⋮	⋮	⋮	⋮
11	0	2	2	0°	90°	180°	270°	180°	270°	’a’
12	0	2	3	0°	90°	180°	270°	270°	0°	’b’
⋮	⋮	⋮	⋮	⋮	⋮		⋮	⋮	⋮	⋮
36	2	0	3	180°	270°	0°	90°	270°	0°	’z’
37	2	1	0	180°	270°	90°	180°	0°	90°	’stop config phase’
⋮	⋮	⋮	⋮	⋮	⋮		⋮	⋮	⋮	⋮

Table 4.3: Excerpt of the codeword set CW for PLQPSK. The corresponding permutations of the symbols are illustrated in their logical representation as well as in their real phase representation.

4.6.2 DPPM

Along with DPPM, eight symbols are used($\{126\mu s$, $134\mu s$, $142\mu s$, $150\mu s$, $158\mu s$, $166\mu s$, $174\mu s$, $182\mu s\}$) and two symbols are required for one codeword. Table 4.4 shows an excerpt of the permutations and thus the codewords.

codeword	logical representation		phase representation		information
	s_1	s_2	s_1	s_2	
1	0	0	$126\mu s$	126 μs	’0’
2	0	1	$126\mu s$	134 μs	’1’
⋮	⋮	⋮	⋮	⋮	⋮
11	1	2	$126\mu s$	134 μs	’a’
12	1	3	$126\mu s$	142 μs	’b’
⋮	⋮	⋮	⋮	⋮	⋮
36	4	3	$150\mu s$	142 μs	’z’

Table 4.4: Excerpt of the codeword set CW for DPPM. The corresponding permutations of the symbols are illustrated in their logical representation as well as in their real pause duration representation.

Chapter 5

Results

This Chapter presents the results regarding the proposed ToF based communication system. This includes an introduction of the evaluation setup, discussion of the observed effects resulting from the frequency difference $\mathcal{F}_{error}$ between ToF camera and Optical Beacon and the data and bit error rates for both communication links. Moreover, the limits of the system are tested regarding distance between sender and receiver.

5.1 Demonstrator

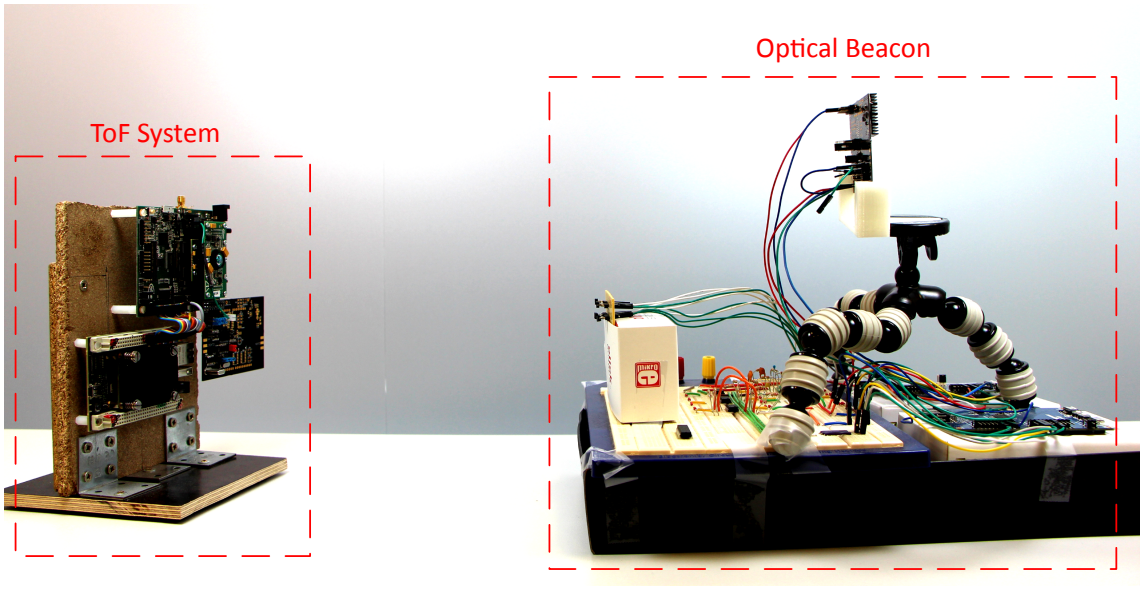

Figure 5.1: Evaluation setup.

Figure 5.1 illustrates the evaluation setup. The two microcontrollers and the sending circuit for the Optical Beacon are supplied with 5 V over USB, the ToF camera via socket outlet and transformer down to 5 V. The sender unit of the Optical Beacon is powered

with 3.3 V from one of the two microcontrollers. The PC is connected to the Zync 7000 via micro USB. The software for the ToF system can be implemented onto the Zync via this connection. The communication between Zync 7000 and PC works via UART interface. On PC side, the data from the ToF camera is read with Matlab. In order to read the output of the two microcontrollers of the Optical Beacon, Putty shell is used also with an UART interface. The system is tested with different distances between ToF camera and Optical Beacon to determine the robustness and limits. Therefore, the data rate and bit error ratio are measured for distances of 20 cm, 1 m, 3 m and 5 m.

5.2 Side-Effects of Frequency Difference $\mathcal{F}_{error}$

This section compares the results for demodulation at ToF side which are obtained with and without frequency synchronization. Additionally, it depicts the occurring effects of the frequency difference $\mathcal{F}_{error}$ between ToF camera and Optical Beacon.

5.2.1 Modulation Frequency Synchronization

This section shows the impact of the frequency synchronization as it was explained in Section 3.5.1. If the Optical Beacon continuously emits pulsed light, the ToF camera should ideally measure a constant phase value. Due to the frequency difference, the ToF camera measures oscillating phase_{tof} values. This is illustrated in Figure 5.2, where 1000 raw images are captured and the averaged phase_{tof} values are plotted. The measured phase signal oscillates with a frequency of 127 Hz.

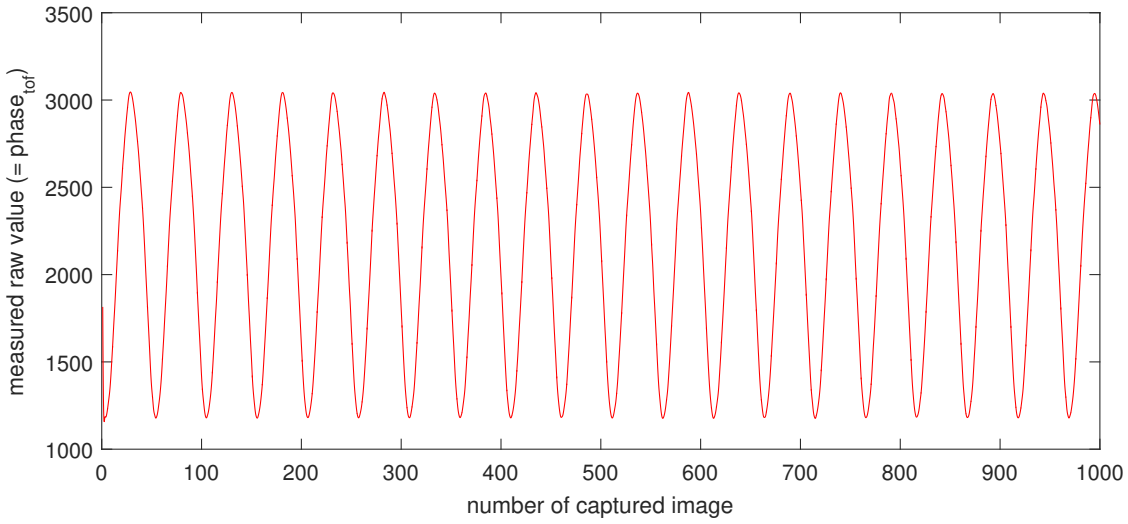

Figure 5.2: Phase signal resulting from the frequency difference between ToF camera and Optical Beacon. The frequency difference is 127 Hz.

Figure 5.3 illustrates the same scenario, but after the frequency synchronization which is conducted during the *INIT* phase. The system determines that the frequency difference

amounts 127 Hz and thus the modulation frequency of the ToF camera has been adjusted to match the frequency of the Optical Beacon. As Figure 5.3 shows, the modulation frequency difference could be corrected enormously, but does not disappear completely. The consequences of this remaining synchronization error are further discussed in Section 5.2.3.

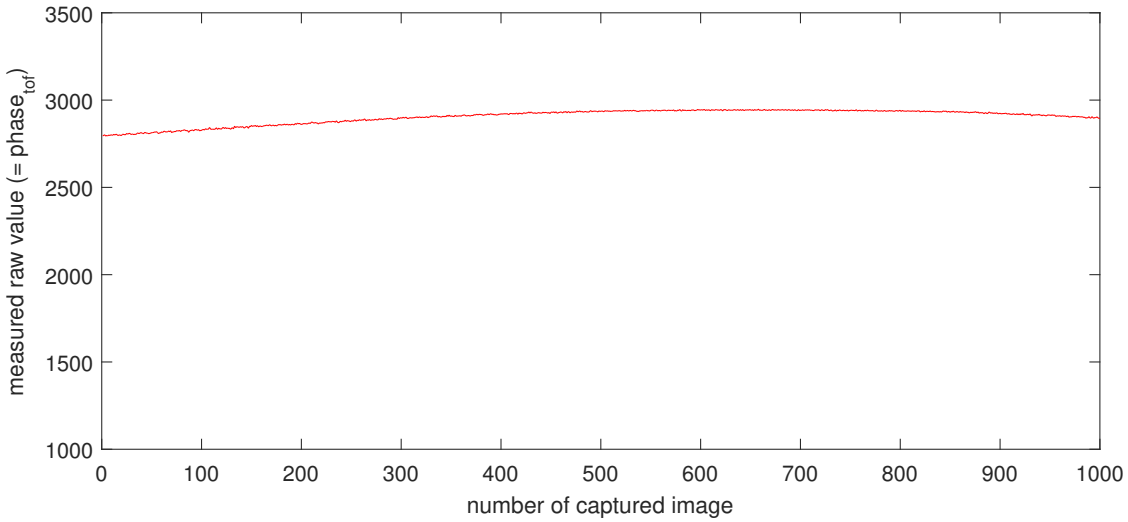

Figure 5.3: Phase signal after frequency synchronization.

5.2.2 Range of Quadrants

In Section 4.5.2, it is assumed that each quadrant has a range of 90°. Thus, the first demodulated point p_{q1} is defined as the midpoint of the first quadrant. Then, the other three quadrants are determined, under the assumption that each midpoint of a quadrant has an angle of 90° to the midpoints of the previous and the following quadrant. This is illustrated in Figure 5.4a. p_{q1} is demodulated at 45°. Thus, the first quadrant ranges from 0° to 90°, the second from 90° to 180°, the third from 180° to 270°, and the last quadrant ranges from 270° to 360°. Figure 5.4b shows four transmitted and demodulated phases_{plqpsk} without frequency synchronization. Each of the four phases_{plqpsk} transmitted by the Optical Beacon should correspond to the first, second, third and fourth quadrant. But without frequency synchronization, the phase distance between these four demodulated points is not 90° as it should be. If now the same definition for the four quadrants is used as in Figure 5.4a, only p_{q1} and p_{q2} are demodulated correctly. The third point, p_{q3}, is classified to the second quadrant, although p_{q3} should be in the third quadrant. p_{q4}, which should be matched rightly to the fourth quadrant, is placed in the third one.

With frequency synchronization, this effect will be mitigated, but no completely eliminated. Hence, another definition for the four quadrants is tested. Instead of assuming that the distance between all midpoints amounts 90°, it is assumed that of the first four symbols transmitted, each belongs to the first, second, third and fourth quadrant. Then, half of the angle between two points p_{qi} forms the limit between two quadrants. This is

also illustrated in Figure 5.4b, where the green area forms the first, yellow the second, blue the third and the red forms the fourth quadrant. With this solution, p_{q1} to p_{q4} are matched to the correct quadrant.

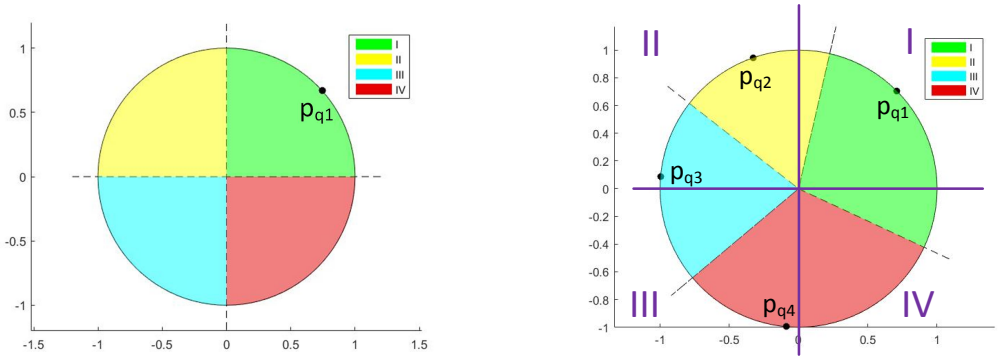

(a) (b)

Figure 5.4: Two different definitions of the four quadrants. a) Each quadrant has a range of 90°. b) The limit of each range is in the middle between two adjacent midpoints.

5.2.3 Impact of remaining Synchronization Error

As outlined in Section 4.5.2, a remaining synchronization error yields in a rotating demodulated φ with respect to the constellation diagram. This effect is illustrated in Figure 5.5. All subfigures in the left column show the phase drift with frequency synchronization, and the right side shows the drift without synchronization. If the three illustrations on the left side are compared, it can be seen that the range of each quadrant amounts to nearly 90°, while the ranges of the quadrants without frequency synchronization differ strongly. Without frequency synchronization, the first and second quadrants have a range of about only 65°, while the third and fourth quadrants have about 115°. Moreover, Figure 5.5 illustrates that the phase drift is smaller by a multiple if the frequency of the ToF camera is adjusted. In Subfigure 5.5c, the quadrant has rotated about 35° after 22 transmissions. Only after the 207^{th} transmitted symbol, it has rotated about 360°. Hence, the average drift of φ between two transmissions amounts 1.7°. In comparison, without frequency synchronization, the first quadrant has already rotated about 70° after only five transmissions. After 22 transmitted symbols, the rotation of the quadrant amounts 351° (Subfigure 5.5f). Here, the average drift between two rotations is about 16°. However, some outliers have a higher rotation and so it may happen that a modulated φ is classified to a wrong quadrant. This can be seen in Subfigure 5.5f, where φ is placed in the range of the second quadrant instead of the first.

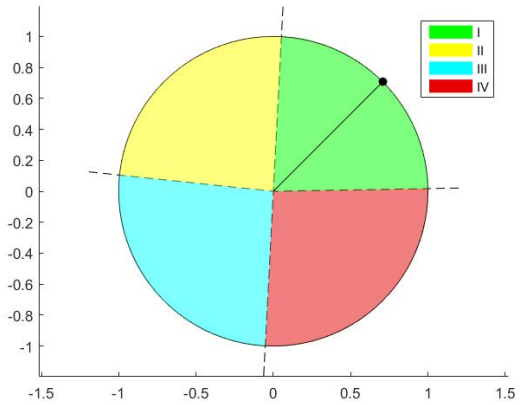

(a) 1^{st} symbol φ with frequency synchronization

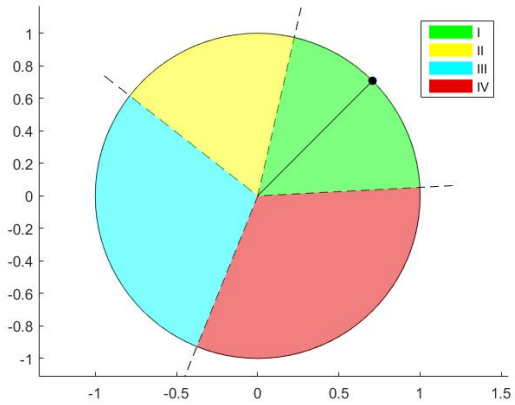

(b) 1^{st} φ without frequency synchronization

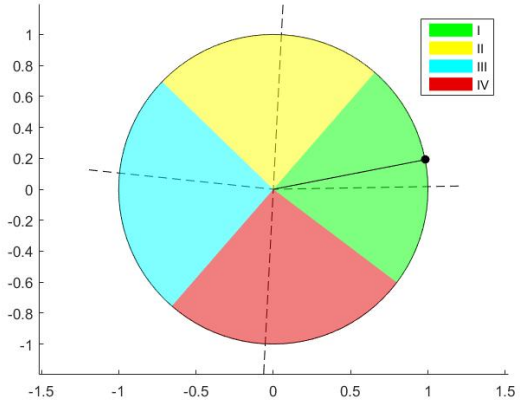

(c) 22^{nd} φ with frequency synchronization

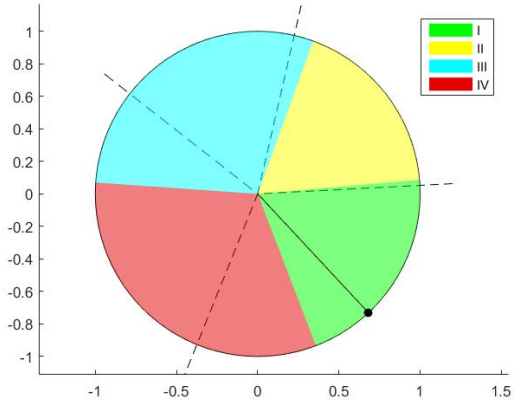

(d) 5^{th} φ without frequency synchronization

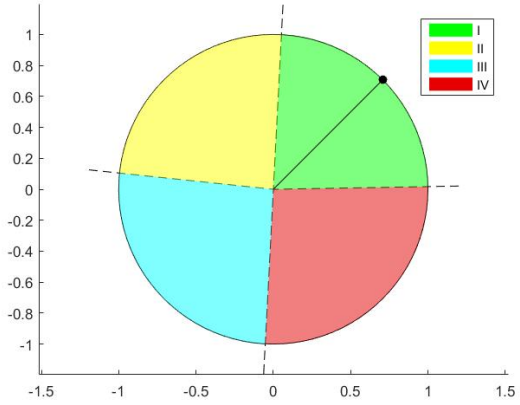

(e) 207^{th} φ with frequency synchronization

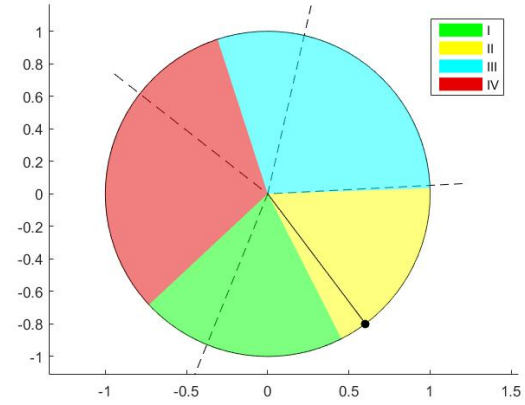

(f) 30^{th} φ without frequency synchronization

Figure 5.5: The demodulated angle φ (= symbol) varies although the embedded device emits light with a constant phase. Thus, the quadrants for classification rotate in circle along with φ_{error} in order to allow correct demodulation. The images (a, c, e) on the left side show the impact of φ_{error} with frequency synchronization and the images on the right (b, d, f) without frequency synchronization.

5.3 Communication Link - ToF Camera to Optical Beacon

As mentioned in Section 3.9.2, the ToF camera has to be reconfigured between the transmission of two successive frames, where a frame consists of 32 pauses and 32 pulses. In the current system implementation, a reconfiguration takes about 7 ms. Thus, the camera can be reconfigured 142 times per second in the best case. This means, that maximally 142 frames can be transmitted per second. Since future optical communication will likely be able to configure the sensor during operation, this evaluation does not consider the reconfiguration time. Instead, the same frame is sent for ten seconds without a reconfiguration of the ToF camera. With this setup, the maximum possible data rate can be estimated in view of the fact that new generations of the ToF sensor can change the modulation of pulses and pauses at runtime. This means, that reconfiguration might become unnecessary which will increase the number of frames per second.

In the proof-of-concept setup, the distance between ToF camera and the receiver of the Optical Beacon is about 20 cm to test the feasibility under ideal conditions. The test frame consists of eight different codewords that are repeated two times. Then, the frame is transmitted repeatedly for ten seconds. In this time, the number of decoded codewords is measured as well as the number of codewords which could not be decoded. Additionally, it is checked if a codeword is decoded correctly. Since the codewords are arranged in a certain pattern, the correctness of the transmission can be verified. The test pattern is { ’0’, ’1’, ’2’, ’3’, ’4’, ’5’, ’6’, ’7’, ’0’, ’1’, ’2’, ’3’, ’4’, ’5’, ’6’, ’7’ }. If now for example a ’5’ is received after a ’3’, the codeword was decoded incorrectly since a ’4’ is expected after a ’3’.

Within the ten seconds of transmission, each of the eight different codewords is decoded 4130 times. Summed up, 33040 codewords are received in ten seconds resulting in 3304 codewords per second. So, the data rate is 3304 codewords per second. This leads to a baud rate of 6608 baud since a codeword consists of two symbols. For this evaluation setup, four different symbols are used. This means, that one symbol can represent four different states and can hence encode two bits. Since a codeword consists of two symbols, a codeword represents four bits. As a result, a data rate of 13216 bits per second can be derived by multiplying the number of transmitted codewords per second by four. In this ten seconds, all received pulses and pauses could be potentially decoded and all codewords arrived in the correct order. Thus, there were no transmission errors. Table 5.1 illustrates these results.

# codewords / 10 seconds	data rate [cps]	baud rate [Bd]	bit rate [bps]	# codewords incorr. decoded	# codewords not decodable
33040	3304	6608	13216	0	0

Table 5.1: Results for the evaluation of the transmission from the ToF camera to the Optical Beacon at a distance of 20 cm.

5.3.1 Robustness Check with different Distances

In order to determine the robustness of the system, a set of measurements is performed at different distances. Again, a frame consists of 8 different codewords repeated two times and sent for 10 seconds. Table 5.2 shows the results for distances of 1 m, 3 m and 5 m. For comparison, the results from the previous section for a distance of 20 cm are listed too. The results for 1 m and 3 m show a data rate of 13220 bit per second with no errors. For measurements at a distance of 5 m, the cut-off frequency of the first high-pass filter has to be increased as well as the gain of the last amplifier. The results for the first measurement with 5 m show a data rate of 12220 bit per second. The shortest pause time has to be increased by $x_{pause} = 2$ and thus the data rate is lower compared to the results at 1 m and 3 m. Further, 36 codewords are unable to be decoded while 257 codewords are incorrectly decoded, leading to a bit error ratio (BER) of 0.009 according to Formula 5.1. The number of transmission errors is divided by 10 to receive the number of transmission errors per second. Then, the number of transmission errors per second is multiplied by four to obtain the number of bit errors per second. Finally, this number is divided by the number of transmitted bits per second.

$$ber = \frac{\#\ \ transmission\ \ \ errors}{10} \cdot \frac{4}{\#\ \ transmitted\ \ \ bits\ \ \ per\ \ \ second} \tag{5.1}$$

For the second measurement at a distance of 5* m, two parameters are changed in order to decrease the error rate. First, the shortest pause time is again increased by further $x_{pause} = 4$. Moreover, the difference between two symbols is increased from $x_{pause} = 1$ to $x_{pause} = 3$. Thus, two pause times have a higher temporal distance and can be distinguished more reliably. This decreases the data rate to 9220 bit per second. However, the error rate is decreased too. Only four codewords are not able to be decoded and five codewords are incorrectly decoded resulting in a bit error ratio of 0.0003. Compared to the previous measurement at 5 m, the bit rate decreases by a factor of 1.3, while the bit error ratio decreases by a factor of 31.

distance [m]	data rate [cps]	baud rate [Bd]	bit rate [bps]	# codewords incorr. decoded	# codewords not decodable	BER
0.2	3304	6608	13216	0	0	0.0
1	3305	6610	13220	0	0	0.0
3	3305	6610	13220	0	0	0.0
5	3055	6110	12220	257	36	0.0095
5*	2305	4610	9220	3	4	0.0003

Table 5.2: Results for the evaluation of the transmission from ToF camera to the Optical Beacon at different distances.

5.4 Communication Link - Optical Beacon to ToF Camera

As explained in Section 4.5.1, it is not possible to process received data at runtime in the current system. The process for demodulation and decoding of measured phase_{tof} values takes longer than a capturing time of an image. This means, that the callback of subsequent images will be missed while received data is processed. Hence, received data is stored into a buffer and processed after the last transmitted phase. In this test setup, 1000 phase_{tof} values are measured, stored and evaluated. This measurement process is repeated 100 times.

Table 5.3 shows the results. t_{1000} is the time it take to measure 1000 phase_{tof} values and is 156 ms in average. Thus, the averaged number of decoded codewords is multiplied by $\frac{1}{156ms} = 6.4$ in order to obtain the number of codewords per second. The camera decodes 1044 codewords per second resulting in a baud rate of 3132 baud since a codeword is formed by three symbols. Since four different symbols exist for PLQPSK, a symbol represents two bit. With regard to the fact that a codeword is formed by three symbols, it can be said that a codeword represents six bit. Thus, a data rate of 1044 codewords per second yields in a data rate of 6264 bits per second. During the measurement, 149 transmission errors occurred. 140 received codewords are not decodable which means that at least one of the three symbols is demodulated incorrectly. Furthermore, 9 codewords are decoded incorrectly implying that the codeword is decodable, but regarding the order of the received codewords, it was not the expected one. The bit error ratio is calculated with Formula 5.2. The number of transmission errors is first divided by 100 to get the average and then multiplied by $\frac{1}{t_{1000}}$ to get the number of transmission errors per second. A further multiplication by 6 yields in bit errors per second. This number is finally divided by the number of transmitted bits and results in a bit error ratio of 0.009.

$$ber = \frac{\#\ transmission\ \ errors}{100} \cdot \frac{1}{t_{1000}} \cdot \frac{6}{\#\ \ transmitted\ \ bits\ \ per\ \ second} \tag{5.2}$$

t_{1000} [s]	data rate [cps]	baud rate [Bd]	bit rate [bps]	# codewords incorr. decoded	# codewords not decodable	BER
0.156	1044	3132	6264	140	9	0.009

Table 5.3: Results for the evaluation of the transmission from the Optical Beacon to the ToF camera at a distance of 20 cm.

5.4.1 Robustness Check with different Distances

The same test setup as described in Section 5.4 is now tested at different distances. Table 5.4 shows the results for 20 cm, 1 m, 3 m and 5 m. If the distance increases, the exposure time has to be increased to be able to sample the light source of the Optical Beacon. However, increasing the exposure time decreases the number of images that can be captured

dist. [m]	t_{1000} [s]	data rate [cps]	baud rate [Bd]	bit rate [bps]	# codewords incorr. decoded	# codewords not decodable	BER
0.2	0.156	1044	3132	6264	140	9	0.009
1	0.167	955	2865	5712	287	13	0.019
3	0.278	571	1713	3426	274	45	0.020
5	0.523	304	912	1824	273	18	0.018

Table 5.4: Results for the evaluation of the transmission from Optical Beacon to ToF camera at different distances.

per second. This decreases the data rate as is can be seen in Table 5.4. Moreover, the results show that the bit error ratio is the lowest for a distance of 20 cm, while being fairly constant for the distances of 1 m, 3 m and 5 m.

As the results show, the proposed communication system between Time-of-Flight cameras and Optical Beacons is feasible. In both communication directions, suitable data rates with acceptable bit error ratios are observed.

Chapter 6

Conclusion and Future Work

6.1 Conclusion

In this thesis, a communication system based on Time-of-Flight technology is proposed. The communication partners are formed by a Time-of-Flight camera on the one side, and a physical device called *Optical Beacon* on the other side. This opens the path for a location-aware communication link, where the ToF system is able to localize its communication partners in 3D. An asymmetric communication link is established, using differential pulse position keying (DPPK) and the novel method of quadrature phase shift keying of pulsed light (PLQPSK). Finally, the system is evaluated by determining the possible data rate for both communication links as well as the error rate.

For the realization of the Optical Beacon, a circuit is designed which is capable of receiving modulated light pulses (DPPM) emitted by the ToF camera and emitting quadrature phase-shifted light pulses (PLQPSK) which can be efficiently decoded by the ToF camera. Two microcontrollers are used in order to control the sending and receiving unit of the circuit and process the received data. The incoming signal is demodulated and decoded by an embedded software application. A transmission unit is able to transmit data to Time-of-Flight systems. A synchronization method ensures proper sampling on the ToF side. Future applications can implement custom logic on the Optical Beacon system.

On the ToF system, the work accomplished in the OptiSec3D project is extended to make the ToF system capable of exchanging data with the proposed Optical Beacon platform. A ToF camera measures distances based on the phase shift between emitted signals and the signals reflected by the scene. This means that a phase value is obtained for every captured pixel. Thus, a modulation technique based on phase shift keying (PLQPSK) is used for the communication link from the Optical Beacon to the ToF camera. For the other communication link, DPPM is applied. This method exploits the fact that the pause and pulse durations of the emitted light are parameters freely set at the ToF camera.

In order to show the feasibility of the introduced communication system, an evaluation system is implemented. The behavior of the communication channel is observed in both

directions and the error rate is recorded. Finally, the achievable data rate is measured for both communication links. For the communication link from the Optical Beacon to the ToF camera, a maximum data rate of 6264 bits per second is reached. The other communication link accomplishes a data rate of 13216 bits per second. The robustness of the proposed system is tested by capturing a measurement series with varying distances between ToF camera and Optical Beacon. As the results show, the proposed modulation methods can fulfill the demanding requirements of future location-aware ToF based communication systems.

6.2 Future Work

This section presents areas which offer room for improvement regarding stability, data rate and applicability.

- **Hardware Miniaturization of the Optical Beacon Platform**

  At the moment, the Optical Beacon consists of a PCB for the sending unit, while the receiving unit is implemented with through-hole assembly devices on a breadboard. The two microcontrollers are placed on evaluation kits. In future work, the hardware for the receiving unit should be simplified and integrated in a single PCB in combination with the sending and the processing unit.

- **System Optimization**

  The receiving unit uses two microcontrollers at the moment, one for controlling the threshold of the comparator and one for receiving and processing data from the ToF camera. All operations are executed in the event of a rising or falling edge. The operations need to be executed before the next interrupt of a rising or falling edge occurs, otherwise an interrupt is missed and thus information is lost. That is the reason why two microcontrollers are used at the moment. In continuing work, the code of the two microcontrollers could be simplified and hastened in order to allow using just one microcontroller.

- **Dynamic Adjustment of Cut-off Frequency for Filtering System**

  In Section 4.3.1 it was explained why a compromise between a high or a low cut-off frequency f_c has to be made. For this thesis, a middle f_c is chosen in order to handle both types of described light disturbances fairly satisfactorily. For future work, the type of disturbance could be determined at runtime and hence an appropriate f_c could be set. For determination, the ambient light could be identified by measuring the voltage level between two pulses with the ADC of the microcontroller. If this voltage level increases, the light disturbance results from an increasing ambient light. Otherwise, if the signal strength of the pulse shrinks while the voltage level between two pulses remains at the same level, an obstacle in the line of sight causes the disturbance.

- **Communication with Multiple Optical Beacons**

  The purpose of this thesis is to show the feasibility of the proposed communication system. Thus, the prototype system is designed to evaluate a communication link with only one Optical Beacon. For future applications, it is desirable to allow simultaneous communication between a ToF camera and several Optical Beacons. This enables a range of applications, where a ToF sensor requires high-performance localization and simultaneous data transfer to a manifold of devices.

- **ToF Signal Processing Synthesized in IP Block**

  In the current evaluation sysem, the code for the ToF camera is implemented in C++ and executed on the ARM processor of the Zync 7000. Currently, no extensive image processing operations are possible on the Zynq platform, due to the limited processing power of the ARM processor. This problem could be tackled if the C++ implementation of the demodulation unit was synthesized and processed by the hardware.

Bibliography

[1] *Tango*. URL: http://get.google.com/tango/ (visited on June 6, 2017).

[2] Hannes Plank, Theresa Egger, Christoph Steffan, Christian Steger, Gerald Holweg, and Norbert Druml. "High-performance Indoor Positioning and Pose Estimation with Time-of-Flight 3D Imaging". In: *2017 IPIN* (2017).

[3] *Leading 3D chip technology provider — pmdtec.com*. URL: http://www.pmdtec.com/ (visited on June 12, 2017).

[4] Möller Tobias, Kraft Holger, Frey Jochen, Albrecht Martin, and Lange Robert. "Robust 3D Measurement with PMD Sensors". In: *Range Imaging Day, Zürich* 7.Section 5 (2005), p. 8. DOI: ISBN3-906467-57-0.

[5] Anton A. Huurdeman. *The Worldwide History of Telecommunications*. J. Wiley, 2003, p. 638. ISBN: 9780471722243. DOI: 10.1002/0471722243.

[6] Otto Jentsch. "Drahtlose Telephonie mittels Lichtstrahlen". In: *Telegraphie und Telephonie ohne Draht*. Berlin, Heidelberg: Springer Berlin Heidelberg, 1904, pp. 197–201. DOI: 10.1007/978-3-642-51356-5_10.

[7] Murat Uysal and Hatef Nouri. "Optical wireless communications An emerging technology". In: *2014 16th International Conference on Transparent Optical Networks (ICTON)* (2014), pp. 1–7. ISSN: 21627339. DOI: 10.1109/ICTON.2014.6876267.

[8] R Hou, Y Chen, J Wu, and H Zhang. "A Brief Survey of Optical Wireless Communication". In: *13th Australasian Symposium on Parallel and Distributed Computing (AusPDC 2015)* 163.January (2015), pp. 41–50. ISSN: 14451336.

[9] Hany Elgala, Raed Mesleh, and Harald Haas. "Indoor optical wireless communication: Potential and state-of-the-art". In: *IEEE Communications Magazine* 49.9 (2011), pp. 56–62. ISSN: 01636804. DOI: 10.1109/MCOM.2011.6011734.

[10] Joseph M. Kahn and John R. Barry. "Wireless infrared communications". In: *Proceedings of the IEEE* 85.2 (1997), pp. 265–298. ISSN: 00189219. DOI: 10.1109/5.554222.

[11] Nam Tuan Le, Md Shareef Ifthekhar, Yeong Min Jang, and Nirzhar Saha. "Survey on optical camera communications: challenges and opportunities". In: *IET Optoelectronics* 9.5 (2015), pp. 172–183. ISSN: 1751-8768. DOI: 10.1049/iet-opt.2014.0151.

[12] Ozgur Ergul, Ergin Dinc, and Ozgur B. Akan. "Communicate to illuminate: State-of-the-art and research challenges for visible light communications". In: *Physical Communication* 17 (2015), pp. 72–85. ISSN: 18744907. DOI: 10.1016/j.phycom.2015.08.003.

[13] Anurag Sarkar, Shalabh Agarwal, and Asoke Nath. "Li-Fi Technology: Data Transmission through Visible Light". In: 3.6 (2015), pp. 1–10. ISSN: 2321-7782.

[14] Zhengyuan Xu and Brian M. Sadler. "Ultraviolet communications: Potential and state-of-the-art". In: *IEEE Communications Magazine* 46.5 (2008), pp. 67–73. ISSN: 01636804. DOI: 10.1109/MCOM.2008.4511651.

[15] Renzhi Yuan and Jianshe Ma. "Review of Ultraviolet Non-Line-of-Sight Communication". In: June (2016), pp. 63–75.

[16] Da shan Shiu and Joseph M. Kahn. "Differential pulse-position modulation for power-efficient optical communication". In: *IEEE Transactions on Communications* 47.8 (1999), pp. 1201–1210. ISSN: 00906778. DOI: 10.1109/26.780456.

[17] J.B. Carruthers and J.M. Kahn. "Multiple-subcarrier modulation for non-directed wireless infrared". In: *1994 IEEE GLOBECOM. Communications: The Global Bridge* 2.3 (1994), pp. 1055–1059. ISSN: 0733-8716. DOI: 10.1109/GLOCOM.1994.512819.

[18] Isamu Takai, Tomohisa Harada, Michinori Andoh, Keita Yasutomi, Keiichiro Kagawa, and Shoji Kawahito. "Optical Vehicle-to-Vehicle Communication System Using LED Transmitter and Camera Receiver". In: *IEEE Photonics Journal* 6.5 (2014), pp. 1–14. ISSN: 1943-0655. DOI: 10.1109/JPHOT.2014.2352620.

[19] Willy Anugrah Cahyadi, Yong-hyeon Kim, and Yeon-ho Chung. "Dual camera-based split shutter for high-rate and long-distance optical camera communications". In: *Optical Engineering* 55.11 (2016), p. 110504. ISSN: 0091-3286. DOI: 10.1117/1.OE.55.11.110504.

[20] Pengfei Luo, Min Zhang, Zabih Ghassemlooy, Hoa Le Minh, Hsin Mu Tsai, Xuan Tang, and Dahai Han. "Experimental demonstration of a 1024-QAM optical camera communication system". In: *IEEE Photonics Technology Letters* 28.2 (2016), pp. 139–142. ISSN: 10411135. DOI: 10.1109/LPT.2015.2487544.

[21] Thai-chien Bui and Suwit Kiravittaya. "Demonstration of Using Camera Communication Based Infrared LED for Uplink in Indoor Visible Light Communication". In: *2016 IEEE Sixth International Conference on Communications and Electronics (ICCE)*. IEEE, 2016, pp. 71–76. ISBN: 9781509018017. DOI: 10.1109/CCE.2016.7562615.

[22] Wenjia Yuan, Richard E. Howard, Kristin J. Dana, Ramesh Raskar, Ashwin Ashok, Marco Gruteser, and Narayan Mandayam. "Phase messaging method for time-of-flight cameras". In: *2014 IEEE International Conference on Computational Photography, ICCP 2014* (2014). DOI: 10.1109/ICCPHOT.2014.6831812.

[23] Christos Danakis, Mostafa Afgani, Gordon Povey, Ian Underwood, and Harald Haas. "Using a CMOS camera sensor for visible light communication". In: *2012 IEEE Globecom Workshops, GC Wkshps 2012* (2012), pp. 1244–1248. DOI: 10.1109/GLOCOMW.2012.6477759.

[24] Trang Nguyen, Nam Tuan Le, and Yeong Min Jang. "Practical design of Screen-to-Camera based Optical Camera Communication". In: *International Conference on Information Networking* 2015-Janua (2015), pp. 369–374. ISSN: 19767684. DOI: 10.1109/ICOIN.2015.7057916.

[25] Thilo Fath, Falk Schubert, and Harald Haas. "Wireless data transmission using visual codes". In: 2.5 (2014), pp. 150–160.

[26] Richard D. Roberts. "A MIMO protocol for camera communications (CamCom) using undersampled frequency shift ON-OFF keying (UFSOOK)". In: *2013 IEEE Globecom Workshops, GC Wkshps 2013*. IEEE, 2013, pp. 1052–1057. ISBN: 9781479928514. DOI: 10.1109/GLOCOMW.2013.6825131.

[27] Zabih Ghassemlooy, Pengfei Luo, and Stanislav Zvanovec. "Optical Camera Communications". In: 2016, pp. 547–568. DOI: 10.1007/978-3-319-30201-0_25.

[28] Alin Cailean and Mihai Dimian. "Current Challenges for Visible Light Communications Usage in Vehicle Applications: A Survey". In: *IEEE Communications Surveys Tutorials* (2017), pp. 1–1. ISSN: 1553-877X. DOI: 10.1109/COMST.2017.2706940.

[29] Trang Nguyen, Chang Hyun Hong, Nam Tuan Le, and Yeong Min Jang. "High-speed asynchronous Optical Camera Communication using LED and rolling shutter camera". In: *International Conference on Ubiquitous and Future Networks, ICUFN* 2015-Augus (2015), pp. 214–219. ISSN: 21658536. DOI: 10.1109/ICUFN.2015.7182536.

[30] Wenjia Yuan, Kristin Dana, Ashwin Ashok, Marco Gruteser, and Narayan Mandayam. "Dynamic and invisible messaging for visual MIMO". In: *Proceedings of IEEE Workshop on Applications of Computer Vision*. IEEE, 2012, pp. 345–352. ISBN: 9781467302333. DOI: 10.1109/WACV.2012.6162992.

[31] Isamu Takai, Tomohisa Harada, Michinori Andoh, Keita Yasutomi, Keiichiro Kagawa, and Shoji Kawahito. "Optical vehicle-to-vehicle communication system using LED transmitter and camera receiver". In: *IEEE Photonics Journal* 6.5 (2014), pp. 1–14. ISSN: 19430655. DOI: 10.1109/JPHOT.2014.2352620.

[32] Hannes Plank, Matthias Almer, Robert Lobnik, Christian Steger, Thomas Ruprechter, Holger Bock, Josef Haid, Gerald Holweg, and Norbert Druml. "OptiSec3D - A New Paradigm in Secure Communication and Authentication Featuring Time-of-Flight". In: *Proceedings of the 2016 International Conference on Embedded Wireless Systems and Networks* (2016), pp. 335–340.

[33] Hannes Plank, Christian Steger, Thomas Ruprechter, Gerald Holweg, and Norbert Druml. "Survey on Camera based Communication for Location-Aware Secure Authentication and Communication". In: *EMC2 summit, CPS Week 2016* ().

[34] Hannes Plank, Armin Schoenlieb, Christoph Ehrenhoefer, Christian Steger, Gerald Holweg, and Norbert Druml. "Synchronization of time-of-flight 3D sensors for optical communication". In: *IEEE International Conference on Communications* (2017). ISSN: 15503607. DOI: 10.1109/ICC.2017.7996373.

[35] Hannes Plank, Josef Steinbaeck, Norbert Druml, Christian Steger, and Gerald Holweg. "Localization and Context Determination for Cyber-physical Systems based on 3D Imaging". In: *Handbook of Research on Solutions for Cyber-Physical Systems Ubiquity*.

[36] Hannes Plank, Gerald Holweg, Christian Steger, and Norbert Druml. "Time-of-Flight Based Optical Communication for Safety-Critical Applications in Autonomous Driving". In: Springer, Cham, 2016, pp. 183–194. DOI: 10.1007/978-3-319-45480-1_15.

[37] Trong-Hop Do and Myungsik Yoo. "An in-Depth Survey of Visible Light Communication Based Positioning Systems". In: *Sensors* 16.5 (2016), p. 678. ISSN: 1424-8220. DOI: 10.3390/s16050678.

[38] Chinnapat Sertthin, Takeo Fujii, Osamu Takyu, Yohtaro Umeda, and Tomoaki Ohtsuki. "On physical layer simulation model for 6-axis sensor assisted VLC based positioning system". In: *GLOBECOM - IEEE Global Telecommunications Conference*. IEEE, 2011, pp. 1–5. ISBN: 9781424492688. DOI: 10.1109/GLOCOM.2011.6134119.

[39] Ming Liu, Kejie Qiu, Fengyu Che, Shaohua Li, Babar Hussain, Liang Wu, and C. Patrick Yue. "Towards indoor localization using Visible Light Communication for consumer electronic devices". In: *2014 IEEE/RSJ International Conference on Intelligent Robots and Systems* Iros (2014), pp. 143–148. ISSN: 21530866. DOI: 10.1109/IROS.2014.6942553.

[40] Soo Yong Jung, Swook Hann, and Chang Soo Park. "TDOA-based optical wireless indoor localization using LED ceiling lamps". In: *IEEE Transactions on Consumer Electronics* 57.4 (2011), pp. 1592–1597. ISSN: 00983063. DOI: 10.1109/TCE.2011.6131130.

[41] Tuan Nguyen and Yeong Min Jang. "Highly Accurate Indoor Three-Dimensional Localization Technique in Visible Light Communication Systems". In: *The Journal of Korean Institute of Communications and Information Sciences* 38C.9 (2013), pp. 775–780. ISSN: 1226-4717. DOI: 10.7840/kics.2013.38C.9.775.

[42] M.A. Pasha, C. Yuen, N.U. Hassan, and U. Nadeem. "Indoor positioning system designs using visible LED lights: performance comparison of TDM and FDM protocols". In: *Electronics Letters* 51.1 (2015), pp. 72–74. ISSN: 0013-5194. DOI: 10.1049/el.2014.1668.

[43] *LED Based Indoor Positioning System — Philips Lighting*. URL: http://www.lighting.philips.com/main/systems/themes/led-based-indoor-positioning (visited on Oct. 18, 2017).

[44] Armin Schoenlieb. "Design and Implementation of a ToF-based Data Transmission System". Master's Thesis. FH Joanneum, 2016.

[45] *Atmel® Studio 7 Easier to Use and More Powerful than Ever - Overview*. URL: http://www.atmel.com/microsite/atmel-studio/ (visited on Sept. 19, 2017).

[46] *MATLAB - MathWorks*. URL: https://de.mathworks.com/products/matlab.html?s_tid=hp_products_matlab (visited on Sept. 19, 2017).

[47] *Xilinx Software Development Kit (XSDK)*. URL: https://www.xilinx.com/products/design-tools/embedded-software/sdk.html (visited on Sept. 19, 2017).

[48] Christoph Ehrenhoefer. "Design and Implementation of an FPGA-based Time-of-Flight Processing System". Master's Thesis. University of Technology Graz, 2016.